Forschungszentrum Karlsruhe
Technik und Umwelt

Wissenschaftliche Berichte
FZKA 5522

The WECHSL-Mod3 Code: A Computer Program for the Interaction of a Core Melt with Concrete Including the Long Term Behavior

Model Description and User's Manual

J. J. Foit, M. Reimann, B. Adroguer, G. Cenerino, S. Stiefel

Institut für Angewandte Thermo- und Fluiddynamik

Februar 1995

Forschungszentrum Karlsruhe
Technik und Umwelt
Wissenschaftliche Berichte
FZKA 5522

The WECHSL-Mod3 Code: A Computer Program for the Interaction of a Core Melt with Concrete Including the Long Term Behavior

Model Description and User´s Manual

J.J. Foit, M. Reimann*, B. Adroguer**, G.Cenerino***, S. Stiefel

Institut für Angewandte Thermo- und Fluiddynamik

* Fachhochschule des Saarlandes, Saarbrücken
* CEA, Centre d´Etudes de Cadarache, Saint Paul Lez Durance, France
* CEA, Institut de Protection et de Surete Nucleaire, Fontenay aux Roses, France

Forschungszentrum Karlsruhe GmbH, Karlsruhe
1995

Als Manuskript gedruckt

Forschungszentrum Karlsruhe GmbH
Postfach 3640, 76021 Karlsruhe

ISSN 0947-8620

Abstract

The WECHSL-Mod3 code is a mechanistic computer code developed for the analysis of the thermal and chemical interaction of initially molten reactor materials with concrete in a two-dimensional as well as in a one-dimensional, axisymmetrical concrete cavity. The code performs calculations from the time of initial contact of a hot molten pool over start of solidification processes until long term basemat erosion over several days with the possibility of basemat penetration.

It is assumed that an underlying metallic layer exists covered by an oxidic layer or that only one oxidic layer is present which can contain a homogeneously dispersed metallic phase. Heat generation in the melt is by decay heat and chemical reactions from metal oxidation. Energy is lost to the melting concrete and to the upper containment by radiation or evaporation of sumpwater possibly flooding the surface of the melt.

Thermodynamic and transport properties as well as criteria for heat transfer and solidification processes are internally calculated for each time step. Heat transfer is modelled taking into account the high gas flux from the decomposing concrete and the heat conduction in the crusts possibly forming in the long term at the melt/concrete interface.

The CALTHER code (developed at CEA, France) which models the radiative heat transfer from the upper surface of the corium melt to the surrounding cavity is implemented in the present WECHSL version.

The WECHSL code in its present version was validated by the BETA, ACE and SURC experiments. The test samples include a BETA and the SURC2 post test calculations and a WECHSL application to a reactor accident.

Der WECHSL-Mod3 Code: Ein Rechenprogramm für die Wechselwirkung einer Kernschmelze mit Beton mit Einschluß des Langzeit-Verhaltens

Zusammenfassung

Der WECHSL-Mod3 Computer Code ist ein mechanistisches Rechenprogramm, das zur Analyse der thermischen und chemischen Wechselwirkung einer zu Beginn flüssigen Kernschmelze mit Beton in zweidimensionaler wie auch in eindimensionaler achsensymmetrischer Betonkaverne entwickelt wurde. Das Programm kann Rechnungen ausführen vom Beginn des Kontaktes eines heißen flüssigen Schmelzbades über das Einsetzen von Erstarrungsvorgängen bis zur langzeitigen Erosion des Fundaments über mehrere Tage mit der Möglichkeit der Fundamentdurchdringung.

Es wird angenommen, daß der Metallanteil der Schmelze eine Schicht am Boden der Kaverne bildet und von der Oxidschmelze überdeckt ist, oder daß nur eine Oxidschmelze existiert, die homogen eingemischte Metallanteile enthalten kann. Die Wärmeerzeugung in der Schmelze erfolgt durch die nukleare Nachwärme sowie durch chemische Energie infolge Oxidation der Metalle. Die Energie wird abgeführt an den aufschmelzenden Beton und in den oberen Sicherheitsbehälter. Für letzteres sind die thermische Strahlung oder das Verdampfen von Sumpfwasser, das die Schmelzenoberfläche möglicherweise fluten kann, von Bedeutung.

Die thermodynamischen und die Transport-Größen sowie die Kriterien für Wärmetransport und Erstarrung werden für jeden Zeitpunkt berechnet. Die Wärmeübergangsmodellierung berücksichtigt die hohe Gasfreisetzung aus der Betonzerstörung und die Wärmeleitung in Krusten, die sich möglicherweise langzeitig an der Grenzfläche der Schmelze zum Beton ausbilden.

Die vorliegende WECHSL-Version enthält den CALTHER Code, der bei CEA in Frankreich entwickelt wurde. Dieses Rechenprogramm modelliert den Wärmestrom, der durch thermische Strahlung von der Schmelzbadoberfläche hervorgerufen wird, an die Strukturen im oberen Teil der Reaktorgrube.

Das WECHSL-Programm in seiner derzeitigen Form wurde durch die BETA, ACE und SURC Experimente verifiziert. Die Beispielrechnungen beinhalten Nachrechnungen eines BETA-Experiments, des SURC2-Experiments und eine Anwendung auf einen Reaktorunfall.

Contents

1. Introduction 1

2. Physical Modeling in the WECHSL Code 7

2.1 General Remarks 7
2.2 Melt/Concrete Interface 7
2.2.1 Concrete Decomposition 7
2.2.2 General Features of Heat Transfer From the Melt Bulk to the Concrete 13
2.2.3 Gas Film Model 14
2.2.4 Pool Boundary Layer 24
2.2.5 Discrete Bubble Model 27
2.2.6 Transient Crust Model 28
2.2.7 Application of the Models in the WECHSL Code 31
2.3 Pool Behavior 34
2.3.1 Bubble Size and Velocity of Rise 34
2.3.2 Void Fraction 37
2.3.3 Phase Segregation 37
2.3.4 Heat Transfer between the Molten Layers 38
2.3.5 Heat Transfer from the Top of the Melt 41
2.3.6 Oxidation Reactions 46
2.3.7 Material Properties 49
2.3.8 Freezing Behavior 57
2.4 Supplementary Features of the WECHSL Code 60
2.4.1 Cavity Shape 60
2.4.2 Simplified Calculation Scheme for the Gas Film Model 62
2.4.2.1 Laminar Flow Regime 62
2.4.2.2 Turbulent Flow Regime 64
2.4.3 Energy Balance 68

3. Description of the CALTHER Code 71

3.1 General description and modelling 71
3.2 The radiative heat transfer model of the cavity 73
3.3 The gas-absorption model 74
3.4 Thermal conduction model 75
3.5 Boundary conditions 75
3.6 Gas-release model 76
3.7 Validation of the thermal and gas-release models 76

4. Instructions for the Use of the WECHSL Code 78

4.1 WECHSL Code Characteristics 78
4.2 Input Description 80
4.2.1 Control Parameters 80
4.2.2 Initial Input Data 81
4.3 Cleaned Data File 92
4.4 Restart Files 92
4.5 Output Description 93
4.5.1 Detailed Printout 93
4.5.2 Table Printout 95
4.5.3 Diagram Plot File 97
4.5.4 Cavity Plot File 102

4.6 Compilation of the Subroutines and Functions Used in the WECHSL Code 104
4.7 Installation of the WECHSL-Mod3 Code on IBM Compatible Personal Computer 114

5. Instructions for Use of the CALTHER Code 116

5.1 Linking between WECHSL Mod3 and CALTHER 116
5.2 Description of Input Data 116
5.3 List of the Subroutines and Input Data 129

6. Literature 130

Appendix A: Sample Calculations with WECHSL 135

A.1 BETA Test 135
A.1.1 Input Data 136
A.1.2 Results 139
A.1.2.1 Print Output Example 139
A.1.2.2 Cavity Shape 142
A.1.2.3 Selected Diagrams 143
A.2 SURC Test 145
A.2.1 Input Data 146
A.2.2 Results 149
A.2.2.1 Print Output Example 149
A.2.2.2 Cavity Shape 152
A.2.2.3 Selected Diagrams 153
A.3 Reactor Calculation 155
A.3.1 Input Data 156
A.3.2 Results 159
A.3.2.1 Print Output Example 159
A.3.2.2 Cavity Shape 163
A.3.2.3 Selected Diagrams 164

Appendix B: Sample Calculation with WECHSL + CALTHER 166

B.1 Input Data 167
B.2 Print Output Example 174

1. INTRODUCTION

Light water reactors are designed and constructed with great attention paid to safety. As a result, it is highly improbable that an accident leading to meltdown of the nuclear core will occur. However, in the unlikely event of the simultaneous failure of a number of safety systems, it is possible that cooling of the core could be completely lost. If this occurred, decay heat would cause the reactor core to melt. In the course of such a core meltdown accident, molten fuel together with cladding and structural materials would accumulate in the lower plenum of the reactor pressure vessel. This molten material would melt through the pressure vessel within 20-160 min. after initiation of the accident, depending on the type and the course of the accident. Following reactor pressure vessel meltthrough, the molten core would drop onto the concrete base structure of the reactor building. The interaction of the core melt with concrete would continue for a long period of time.

During this interaction, a number of phenomena have an important bearing on the subsequent course of the accident [40]. These include:

- concrete decomposition,
- release of steam and gases from the decomposing concrete,
- chemical reactions of these gases and of the molten concrete constituents with metallic constituents of the melt and within the containment atmosphere,
- dilution of the molten fuel materials by molten concrete constituents and alteration of the freezing behavior of the molten pool.

The phenomena above have a decisive influence on the basic safety related questions, i.e.:

Can the containment fail by overpressurization?
Can the conrete basemat melt through?
Can building structures inside the containment collapse?

Even though a core melt accident is very unlikely, the potential health consequences on the public require that best-estimate answers are given to these questions. In the early risk studies [1, 2], conservative assumptions were formulated to estimate the source term. Better understanding of the physical background of the molten core/concrete interaction would provide a more realistic basis for an advanced risk study. Furthermore, good understanding of this part of the accident sequence could lead to design measures which would help reducing the risk of a core meltdown accident.

It is impossible to completely simulate the interaction in experiments because of the materials, masses, time scales, and dimensions involved. Recourse must be made to mathematical models or computer codes in order to extrapolate the limited tests which can be performed with the expected materials, masses, and dimensions involved in a meltdown accident. In this context, simulation experiments characteristic of the different situations occuring during the sequence of a core melt/concrete interaction are of special importance.

Therefore, the Nuclear Safety Project (PNS) in February 1977 suggested a multistage concept to simulate experiments allowing a number of experiments to be performed on the 100 kg scale, with variation of such characteristic parameters as the composition and the temperature of the molten pool, the heat flow, and the amount of decay heat to be simulated by inductive heating. The BETA test facility [3] was started up in early 1984 and the experimental program including a series of high power and low power experiments was executed within two years. Since February 1986, all experimental results have been available [4]. The visual observations as well as the measured data in the BETA tests were extremely helpful in acquiring a deeper understanding of separate effects and improving modeling in the WECHSL code. Recently, a new series of BETA experiments [56] were performed in order to investigate the Zr/SiO_2 condensed phase chemistry and the influence of the B_4C on the melt properties. But, above all, the BETA tests as well as the ACE [57] and SURC [58] tests served for integral validation of the WECHSL code [59,60].

This assessment has shown that the code has a wide range of applicability with respect to corium composition, concrete type and level of the internal power. For the metallic melt experiments (BETA) the WECHSL results are in quite good agreement with the finding of the experiments. Particularly, the model used in WECHSL according to which the heat transfer is determined by gas superficial velocity and crust formation was found to be adequate to represent a large variety of physical conditions ranging from liquid metal attack to crust-dominated ablation. The WECHSL code was also used to analyse oxidic experiments (SURC, ACE) to assess predictions for plant applications in an intermediate time period. Some serious discrepancies were observed between the behaviour of complex oxidic melts in the experiment and that predicted by the WECHSL code. However, there are still open questions concerning the reliability of the experimental data and the understanding of the physics of this type of melts.

The WECHSL code is a mechanistic code based on the current understanding of the phenomena occurring during the interaction of a molten pool with concrete. As far as possible, the code is capable of treating both the simulation experiments with non-radioactive materials and melt masses between 100 and 600 kg and, in addition, hypothetical core meltdown accidents with real, full scale reactor dimensions. The code was originally based on the INTER code [5] developed in 1977. However, in the meantime so many improvements and changes have been made that the WECHSL code now bears nearly no resemblance to the INTER code.

WECHSL served for dimensioning the BETA test facility and for precalculations of the BETA tests. The former documentation of the WECHSL code representing this early status was written in 1981 [6a]. The documentation of the WECHSL-Mod2 version [6b] is the basis for the present report.

WECHSL considers either one oxidic layer which can contain a homogeneously dispersed metallic phase or the separation of the molten pool into metal and oxide layers. The mixed melt configuration can be used to describe the early stage of interaction or for the analysis of the ACE [57] and SURC [58] series of experiments which were performed with a pure oxidic melt or an oxidic melt containing metallic zirconium. In the late period of melt/concrete interaction a segregation of the metallic and the oxidic phase will occur as shown in numerous experiments with simulant materials [7, 8]. The heavier metal will be situated at the bottom of the concrete cavity.

WECHSL is directly applicable only to deep melt pools. For shallow layers additional considerations are necessary before the WECHSL code can be used.

Energy can be produced internally by decay heat or by exothermic reactions. Energy is lost to the conrete and to the overlying environment by a variety of mechanisms. Moreover, energy can be exchanged between the molten layers.

The thermal attack on concrete gives rise to a vigorous evolution of gases. Much of these gases pass through the melt. During their passage, the melt is thoroughly stirred, so that each layer is nearly isothermal. Water vapor and carbon dioxide are reduced as they pass through the metallic layer. Liquid concrete decomposition products dilute the oxide layer. Thus, composition and, consequently, the material properties of the layers are continuously changing.

From the top of the melt heat is transferred to the upper containment by thermal radiation or - if the melt pool is flooded by sump water - by evaporation. All these phenomena suggest a conceptual model as shown schematically in Fig. 1.

In addition the CALTHER subroutine package can be activated as an option in WECHSL-MOD3. It allows to calculate the radiative heat transfer from the corium to the walls and bottom of the dry reactor vessel cavity. The bottom can be considered to consist of steel (it could represent the non-molten part of the RPV) or concrete. Under radiative heat transfer, the walls heat up and are allowed to melt. The molten products are then added to the corium mass, and the resulting gases to the gases originating from the corium.

Because of the high rate of heat extracted from the melt pool, the temperatures of the melt layers drop continuously. Crust formation sets in, if the temperature of the relevant melt surface drops below the freezing temperature. Figure 2 shows schematically the possibilities of crust formation as handled in the WECHSL code. On the metal layer surfaces crusts start to be formed in the bottom region and at the side walls. If the melt bulk temperature is higher than that of the oxide, metal crust growth at the interface between the metal and the oxide melt layers is possible, too. In the oxide layer crust growth may occur at the top of the layer and in the side wall region. If the oxide bulk temperature is higher than that of the metal bulk, an oxide crust may build up at the oxide/metal interface.

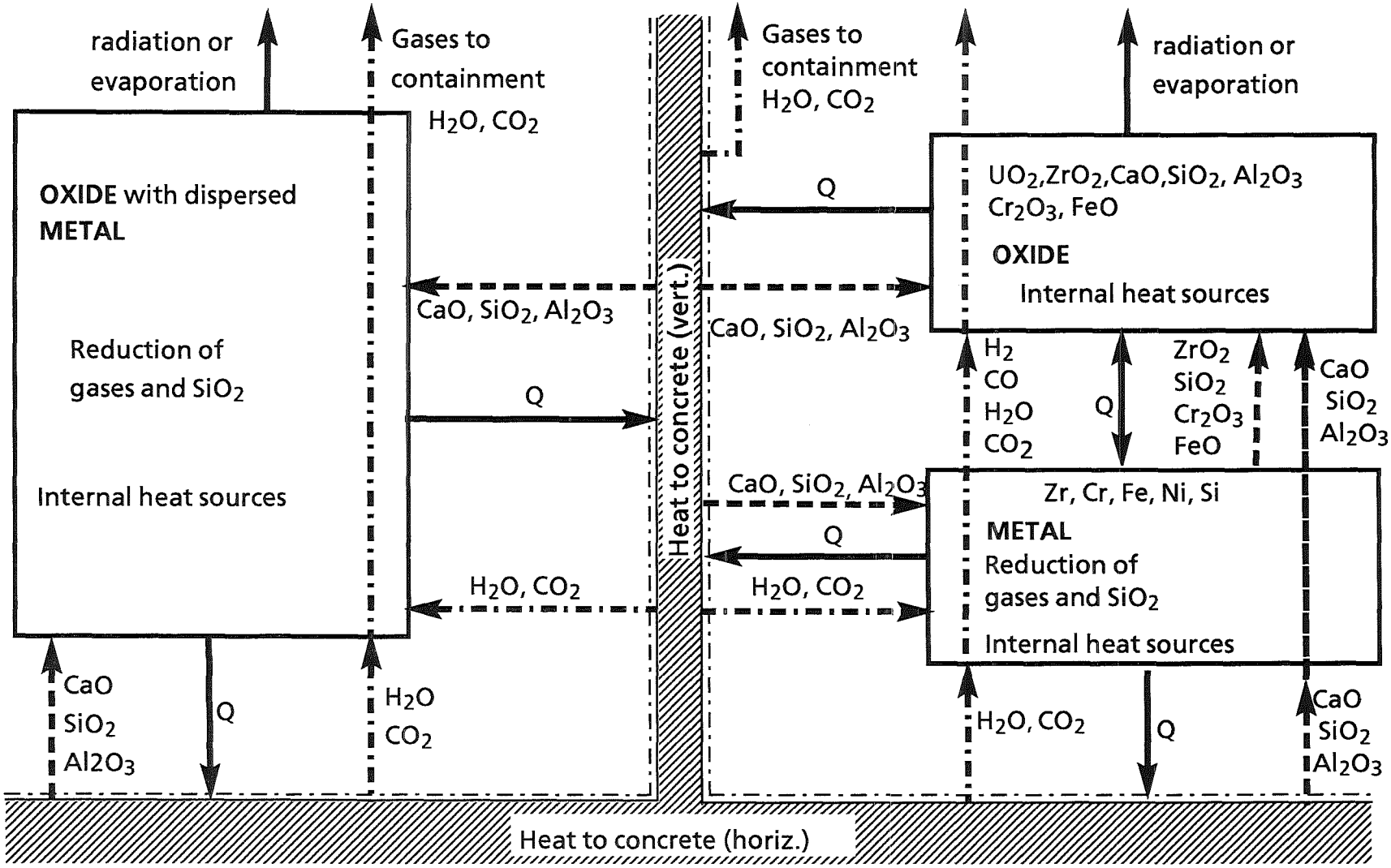

Figure 1: Flows of energy and meterial in WECHSL

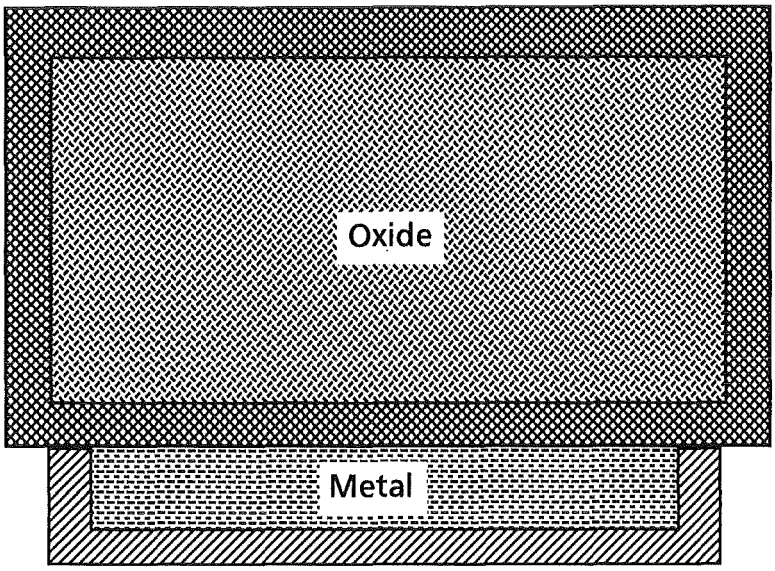

Fig. 2 Schematic representation of the crust formation in WECHSL

Crust formation reduces considerably the heat extraction from the bulk of the melt. Consequently, the long term behavior of a core melt in the basemat of a reactor building will be governed by encrusted melt layers, with the decay heat released inside the layers balanced by the heat transmission through crusts to the concrete and to the upper structures and the atmosphere of the containment building.

In the late phase of a core melt accident, the temperature of the metal bulk may drop below the solidification temperature. Then, a block of frozen metal will attack the conrete basemat. This situation is also considered in WECHSL in case the stratified melt is used. Liquid decomposition products of the concrete dilute the oxidic phase. This changes continuously the properties of the oxide bulk. Above all, the solidification temperature is reduced. In the late phase of a core melt accident, the freezing temperature of the oxide bulk may drop to values near or even below the ablation temperature of the concrete. This is due to the formation of eutectic mixtures with solidification temperatures as low as 1200°C [9]. Because the decay heat can only be removed by concrete ablation or via the top of the melt, while the heat conduction in the basemat is not effective in heat removal for many days after attack on the concrete starts, it is not possible that the whole oxide bulk solidifies. Therefore, only a completely liquid or encrusted oxide bulk with increasing viscosity must be considered in WECHSL. To estimate the final dimension of the melt cavity which is formed after many weeks of erosion and which, indeed, is dominated by heat conduction in the concrete, additional calculations with heat conduction analysis codes are useful [10].

2. Physical Modeling in the WECHSL Code

2.1 General Remarks

The analysis of the core melt/concrete interaction traces the following rationale:

- Identification of the physical phenomena by small scale benchmark experiments with simulant materials.
- Establishing of physical separate effect models.
- Linkage of the separate effect models in the WECHSL code.
- Verification of the WECHSL code by integral experiments with hot, non-radioactive melts with simulation of the decay heat (BETA, ACE and SURC tests).
- Upgrading to full reactor dimensions by computations with the validated computer code.

Consequently, each of the phenomena modeled in the code has been included in such a way as to permit experimental verification. In some models, empirical constants have been fixed to represent adequately the sufficient representation of the BETA test results.

Each of the important models contained in the code will be described in detail in the following sections. Also the sources from which the submodels have been built will be given.

2.2 Melt/Concrete Interface

2.2.1 Concrete Decomposition

The decomposition of concrete is a highly complex process. Differential thermal analyses of conrete with different aggregates [11] yield the consecutive steps of dehydration, $CaCO_3$ decomposition, and the range of melting with increasing temperature. Each of these decomposition steps takes place in a certain temperature range. Furthermore, as indicated by Powers [12], chemical kinetics can alter each range of effective decomposition temperature. The released gases flow through the residual porous concrete matrix and are transporting energy. Moreover, energy is transferred in this matrix of changing porosity by transient heat conduction.

In the WECHSL code a strongly simplified model is applied. It is assumed that under the impact of a high heat flux the decomposition process of concrete can be treated as one-dimensional heat conduction in a semi-infinite body. At the melting surface, the molten material is continuously being removed. The gas release and

other chemical reactions are assumed to occur at definite temperatures during the process of concrete heatup. The higher the heat flux density is, the smaller is the zone in the conrete where the temperature drops from the melting point of the silicates to the ambient temperature. This means that a quasi-stationary temperature profile will be established in the concrete shortly after the surface is exposed to a high temperature melt.

The model for the decomposition process is formulated for n different layers [13]. In the layer i, the porosity of the concrete is Φ_{gi} and the weight percentage of the released gases escaping through this layer is Ψ_{gi}. By assuming perfect temperature exchange between the solid and the gases, coupling of the two relevant energy equations by source and sink terms results in a quasi-stationary energy equation for the whole system. Between the layers of the concrete, heat is absorbed by chemical or physical reactions. One set of boundary conditions is given by the melting temperature at the surface and the decomposition temperatures between the layers. Another set of boundary conditions can be established by energy balances at the boundaries between the layers.

The quasi-stationary energy equation can be described by an exponential temperature distribution. Applying the boundary conditions to this solution, we obtain the decomposition velocity, ζ, according to [14] as

$$\zeta = \frac{(Q/A)}{\rho_c \Delta H_c}. \qquad (2.2.1\text{-}1)$$

This equation indicates that the rate of quasi-stationary decomposition depends only on the heat flux imposed . The enthalpy of concrete decomposition

$$\Delta H_c = (1-\Psi_{g0})h_{d0} + \left((\rho c)_{eff\,0} / \rho \right)_c \quad (T_{d0} - T_{00}) \qquad (2.2.1\text{-}2)$$

is a material property. The effective volumetric heat capacity, ρc, and the effective thermal conductivity, k, are given by

$$(\rho c)_{eff\,i} = \rho_{gi} c_{p\,gi} \Phi_{gi} \left(1 + \frac{\Psi_{gi} \rho_c}{\Phi_{gi} \rho_{gi}} \right) + (1-\Phi_{gi}) \rho_{si}\, c_{si}, \qquad (2.2.1\text{-}3)$$

and

$$k_{eff\,i} = \Phi_{gi} k_{gi} + (1-\Phi_{gi}) k_{si}. \qquad (2.2.1\text{-}4)$$

Equations (2.2.1-3 and 4) can be evaluated by applying averaged solid (subscript s) and gaseous (subscript g) properties of the relevant concrete components. The unknown temperature difference (T_{d0}-T_{00}) in Eq. (2.2.1-2) is determined by regression from

$$T_{di-1} - T_{d0\,i-1} = T_{di-1} - T_{di} + \frac{\Psi_i \rho_c h_{di} + (T_{di} - T_{0i})(\rho c)_{effi}}{(\rho c)_{effi-1}}. \qquad (2.2.1\text{-}5)$$

The decomposition reactions as considered in the model are given in Table 1. The exothermal formation of wollastonite ($CaSiO_3$) can be optionally included. A comparison between calculated and measured values for the decomposition enthalpies of different types of concrete is made in [11] and [15].

Decomposition Temperature (K)	Decomposition Reaction	Heat of Decomposition (kJ/mole)
1573	$SiO_{2s} \rightarrow SiO_{2l}$	-8.53
	$CaO + SiO_2 \rightarrow CaSiO_3$	+88.5
	$CaSiO_{3s} \rightarrow CaSiO_{3l}$	-46.5
1167	$CaCO_3 \rightarrow CaO + CO_{2g}$	-165.5
796	$Ca(OH)_2 \rightarrow CaO + H_2O_g$	-99.5
400	$H_2O_l \rightarrow H_2O_g$	-39.4

Table 1: Characteristics of the concrete decomposition.

By applying this model in the WECHSL-code, the decomposition process is characterized by a surface temperature T_{d0} and by a unique concrete property, the volumetric decomposition enthalpy $\rho_c \Delta H_c$.

The assumption of a quasi-stationary decomposition velocity as given in Eq. (2.2.1-1) introduces two principal errors; the first results from the time dependence of the heat flux imposed on the surface, and, consequently, the transient nature of the heat conduction process, and the second from chemical kinetics. Although these two components are actually coupled, an idea of their magnitude can be obtained by considering them separately.

The transient problem of heat conduction with simultaneous melting in a homogeneous solid has been solved by Landau [14]. Although concrete is certainly far from being homogeneous, it is instructive to apply the method of Landau to get a feeling of the magnitude of the error involved.

At time $\tau = 0$, the semi-infinite homogeneous concrete layer is at ambient temperature T_∞ and a constant heat flux density Q/A is imposed at the surface. The transient temperature distribution can be found analytically. From the time-dependent temperature profile, the time at which the surface reaches the melting temperature is evaluated as

$$\tau_m = \frac{\pi (T_m - T_\infty)^2}{4(Q/A)^2} k\rho c \qquad (2.2.1\text{-}6)$$

or, after introducing the parameter

$$\theta = \frac{\pi^{1/2}}{2} \frac{c(T_m - T_\infty)}{h_{d0}}; \qquad (2.2.1\text{-}7)$$

$$\tau_m = \left(\rho \frac{h_{d0}}{(Q/A)} \frac{k}{\rho c} \theta \right)^2 . \qquad (2.2.1\text{-}8)$$

After the surface has reached the melting temperature, the melt front starts moving. The subsequent heatup process with simultaneous melting was treated numerically in [14]. In Figure 3, the ratio of the actual melt front velocity to the quasi-stationary melt front velocity resulting from Eq. (2.2.1-1) is plotted over the dimensionless time τ/τ_m with the material property θ as the parameter. For a typical siliceous concrete, this property yields $\theta = 16.9$. By integration of the relevant curve in Figure 3, it follows that for this type of concrete the acceleration phase of

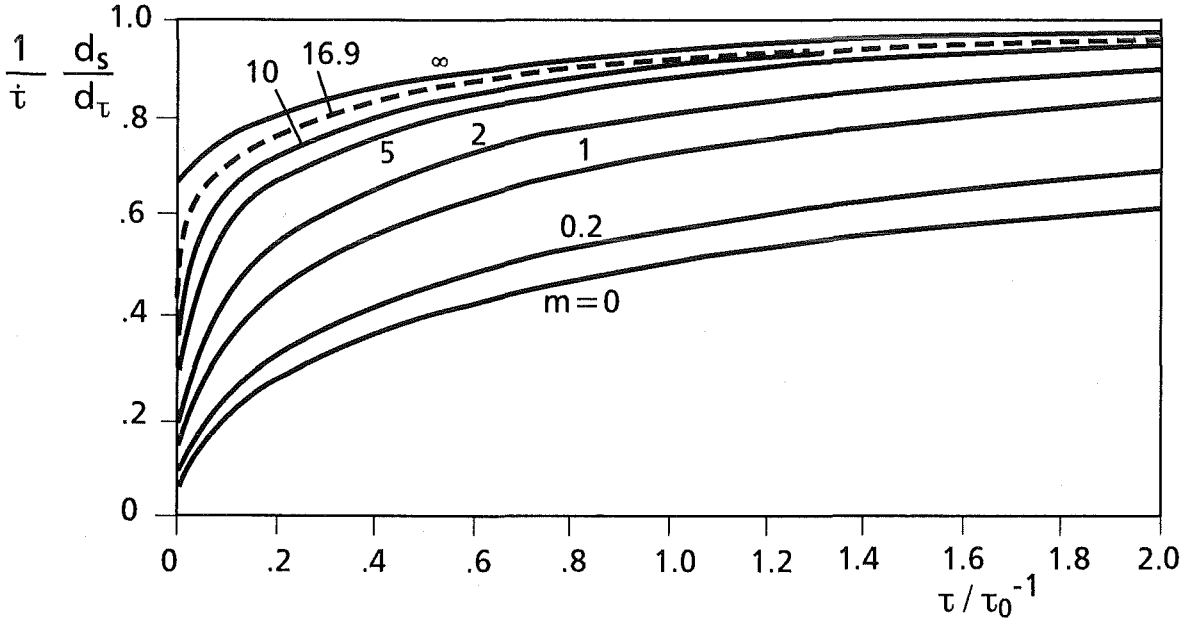

Figure 3: Melt front accelleration phase.

the melt front can be substituted by a displacement of the time ordinate as

$$\tau_{q,st} = 1.26\,\tau_m . \qquad (2.2.1\text{-}9)$$

By evaluating Eqs. (2.2.1-8, 9) the results given in Table 2 are obtained:

$\tau_{q,st}$ s	Q/A 10^4 W/m^2
1	377.2
10	119.3
100	37.7

Table 2: Time ordinate displacement substituting the initial heatup process

The error due to chemical reactions is not as easily assessed. An approximate magnitude of the error can be obtained by assuming that the concrete is heated at a constant rate from room temperature to the decomposition temperature for each decomposition step in the time $\tau_{q,st}$. When the resulting temperature rate is substituted into the kinetic decomposition model proposed by Powers [12], it is found that the time required to decompose 90% of the concrete constituents is of the order of the required displacement of the time axis, but generally shorter.

As mentioned above, the quasi-stationary concrete ablation model is characterized by two parameters:

- the surface ablation temperature of the concrete T_{do}, and
- the volumetric decomposition enthalpy $\rho_c \Delta H_c$.

Consequently, the properties T_{do} in K, ρ_c in kg/m^3 and ΔH_c in J/kg, must be specified as input to the WECHSL code. For the computation of the specific decomposition enthalpy ΔH_c, a separate computer program BEZENT based on equations (2.2.1-2) to (2.2.1-5) is available.

The applicability of the quasi-stationary concrete ablation model could always be derived from the BETA tests in which thermocouples had been embedded at different locations in the concrete crucible. Due to the poor thermal conductivity of the concrete, the penetration depth of the temperature front into the concrete structure is low, on the order of some centimeters only, as long as melting of the concrete surface proceeds. It is the lower, the higher the heat flux density (Q/A) imposed at the concrete surface is. Consequently, thermocouples in the concrete in front of the melting surface generally give the ambient temperature. Only upon

direct arrival of the melt front, there is a sharp increase in the temperature reading and, finally, the thermocouple fails. This behavior is an indication of the limited range of temperature penetration. A long-range temperature distribution in the concrete crucible was only established after switching off inductive heating simulating the decay heat, when the interface temperature between the frozen slug and the concrete had dropped below the ablation temperature of the concrete and thus the melt front stopped propagating.

It should be noted that the quasi-steady-state concept holds even in the case of very low heat flux densities acting for a sufficiently long period of time on the concrete structure. In experiments carried out at Sandia Labs [16], solid blocks of metal or oxide were heated with very low power density. In these tests, the transient phase in which the relevant quasi-stationary temperature profile established took a comparatively long time on the order of several ten minutes, but, finally, the block started to move downwards attaining a slow, but constant velocity of propagation.

In a core melt accident as well as in the BETA experiments the melt is poured onto the conrete surface at high temperatures which results in very high initial heat flux densities so that the period of establishing the quasi-stationary temperature profile in the concrete may be neglected. However, the heat flux density is not constant so that the temperature profile in the concrete changes with time. By applying always the quasi steady-state concept, the transient storage of heat in the concrete structure is neglected and, consequently, the concrete ablation will be slightly overpredicted. Only in such tests whose duration - i.e. the time needed to solidify the melt - is less than several minutes and the transferred heat fluxes are mainly transient, the experimental results may deviate from the calculations. However, in the BETA tests with sustained induction heating and, with better justification, in a core melt accident, the period of interaction and concrete ablation is long enough to justify the application of the quasi-steady-state concept.

2.2.2 General Features of Heat Transfer From the Melt Bulk to the Concrete

The heat transfer from the melt bulk to the concrete is characterized by processes forming boundary layers at the melt pool surface facing the concrete. The most important process is the release of large volume fluxes of gases from the concrete, which govern the heat transfer phenomena.

Due to the heat flux density (Q/A), the concrete is decomposed into gaseous weight fraction Ψ_g and into liquid (weight fraction $1-\Psi_g$) decomposition products. From the quasi-stationary heat transport model discussed above, the mass flux density of the released gases is given by

$$\left(\frac{\dot{m}}{A}\right) = \frac{\Psi_g}{\Delta H_c}\left(\frac{Q}{A}\right)_{tot} . \qquad (2.2.2\text{-}1)$$

In Figure 4, the possible combinations at the core melt/concrete interface are shown schematically. When the melt layer is completely liquid, the concrete surface is passed by a large volume gasflow (H_2O, CO_2) exceeding the volume flows of liquid decomposition products (SiO_2, CaO, Al_2O_3) by some orders of magnitude. If the superficial velocity of the gases being released from the concrete is sufficiently high, a stable gas film is formed between the melt and concrete (Fig.4a). If the superficial gas velocity drops below a limiting value, the heat transfer will be governed by a nucleate boling type of discrete bubble gas release (Figure 4b). Due to cooldown of the melt, the temperature in the melt boundary layer facing the concrete may drop below the freezing temperature, which characterizes the onset of crust formation. The crusts are intially thin skins, which follow the movements of the meltpool interface. With crust growth stabilization can be observed to increase. Finally, the crust has reached a thickness which is sufficient to form a stable layer. There is an adequate number of holes in the stable crust which allow passage of the gases released from the concrete (Figure 4c). Between the crust and the concrete a gas film exists. The heat transfer between the melt bulk and the inside of the crust is determined by a discrete bubble type heat transfer mechanism, with the driving temperature difference determined by the bulk temperature and the freezing temperature of the melt layer at the crust interface.

Crusts or even solidified metal reguli have always been observed to be completely gas permeable in the BETA tests. Consequently, the convection processes inside the encrusted melt slug are always gas driven. Single-phase natural convection inside the melt slug, as shown in Figure 4d, has not to be considered.

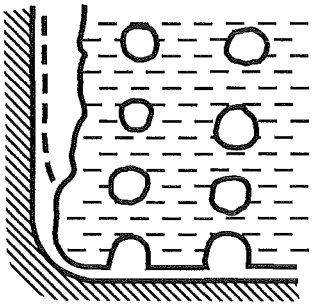

a) Gas film with adjacent boundary layer in the melt

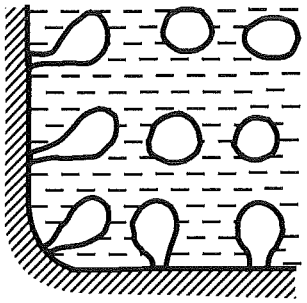

b) Discrete bubble model

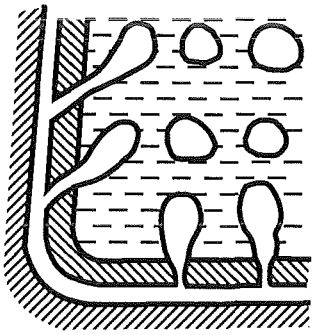

c) Transient growing gas permeable crust with film (outside) and discrete bubble model (inside)

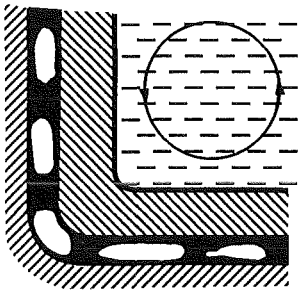

d) Gas tight crust with two-phase (outside) and natural convection heat transfer (inside)

Figure 4: Schematic representation of the possible combinations of heat transfer models.

In the following sections, the relevant physical heat transfer models are given in detail.

2.2.3 Gas Film Model

The ratio of the released gas volume to the volume of liquid decomposition products from the concrete is on the order of 1000:1. Because of the dominance of the gaseous phase at very high heat flux densities, a gas film of thickness δ is likely to be present between the core melt and the concrete. Through this gas film, heat will be transferred by conduction and radiation. So, the total heat flux density is

$$(Q/A)_{tot} = (Q/A)_{cond} + (Q/A)_{rad} \qquad (2.2.3\text{-}1)$$

with

$$(Q/A)_{cond} = \frac{A_{eff}}{A_{tot}} \frac{k_g (T_i - T_{d0})}{\delta} \qquad (2.2.3\text{-}2)$$

and

$$(Q/A)_{rad} = \varepsilon_{id} c_0 (T_i^4 - T_{d0}^4) \qquad (2.2.3\text{-}3)$$

where

$$\varepsilon_{id} = \frac{1}{1/\varepsilon_i + 1/\varepsilon_d - 1}. \qquad (2.2.3\text{-}4)$$

As the heat is transferred from a molten pool to a gas liberating wall, the process can be considered as inverse film boiling. Consequently, the derivation of the heat transfer correlations follows closely the ideas of Berenson [17], Bromley [18], and Hsu, Westwater [19] with the heat transfer by radiation taken into account in addition.

Model experiments with dry ice slabs in a water pool are helpful to study the principles of an inverse film boiling process. As shown in [13], the carbon dioxide gas film which covers a horizontal sublimating dry ice slab gives rise to the formation of a square grid of bubble release sites. Similar experiments were carried out by Dhir et al. [20] who also proposed the Berenson model for this process. By passing over to strongly inclined or vertical walls, bubbles do not break away any longer and a continuous laminar gas layer streaming upwards separates the pool from the sublimating surface. Having reached a critical film thickness, the flow becomes increasingly turbulent. The different flow regimes as shown in Figure 5 and a model experiment showing the sublimation of a dry ice corner under water have been given in [21].

For the sake of completeness, the models of heat transfer from a hot melt to concrete as derived in [13] for horizontal surfaces and in [22] for inclined and vertical surfaces will be summarized here.

At horizontal or slightly inclined surfaces, the gases give rise to an unstable gas layer at the interface of the decomposing solid with the liquid pool. This unstable gas layer breaks up into a regular pattern of bubble formation sites, where gas bubbles are growing and then leave the film. Due to the theory of stratified layers (Taylor instability), the most probable wavelength between two bubble formation sites

$$\lambda = 2\pi\sqrt{3}\, a \qquad (2.2.3\text{-}5)$$

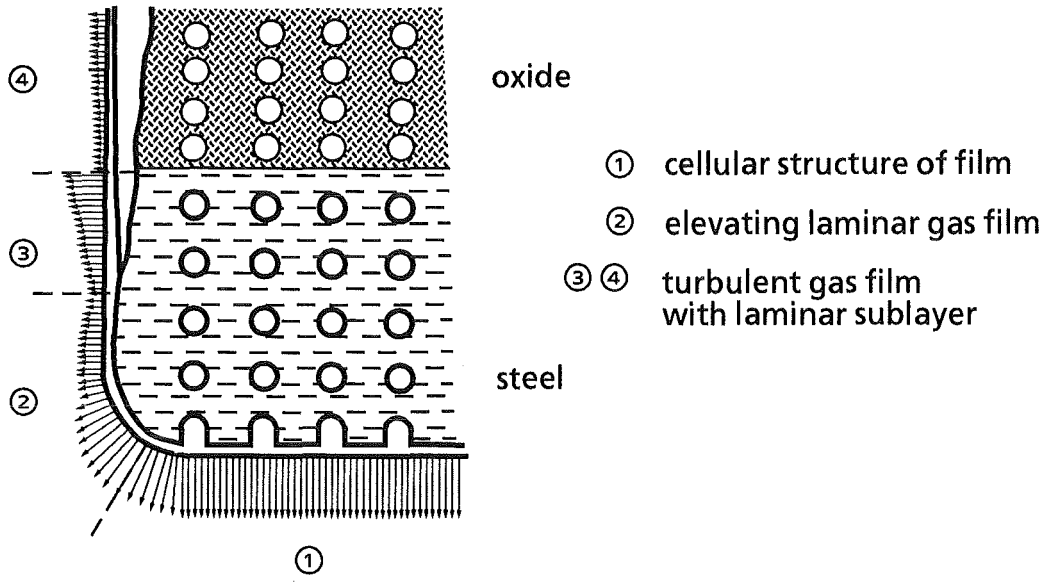

Figure 5: Schematic representation of gas film, bubble rise, and heat transfer coefficient.

depends on the Laplace constant

$$a = \left(\frac{\sigma}{g(\rho_\ell - \rho_g)} \right)^{1/2} . \qquad (2.2.3\text{-}6)$$

In Figure 6 a time averaged rotational symmetric flow cell of the area

$$A_{tot} = \lambda^2 \qquad (2.2.3\text{-}7)$$

around a centre of bubble formation is shown. The quantities r_i and δ^* are connected with the wavelength λ by

$$r_i = \frac{\lambda}{4}; \quad \delta^* = \frac{\lambda}{3} . \qquad (2.2.3\text{-}8)$$

The mean film thickness δ is determined from the balances of mass and momentum under the assumption that the gaseous decomposition products enter the film in z-direction with a constant specific mass flux m/A_{tot}. The mass balance

$$\frac{1}{r}\frac{d}{dr}(r \rho_g w_m \delta) = \left(\frac{m}{A}\right) \qquad (2.2.3\text{-}9)$$

is integrated in radial direction to give

$$w_m = -\frac{1}{2}\left(\frac{\dot{m}}{A}\right)\frac{1}{\rho_g \delta}\left(\frac{r_a^2}{r} - r\right) \tag{2.2.3-10}$$

for the mean velocity of the gas flowing in radial direction.

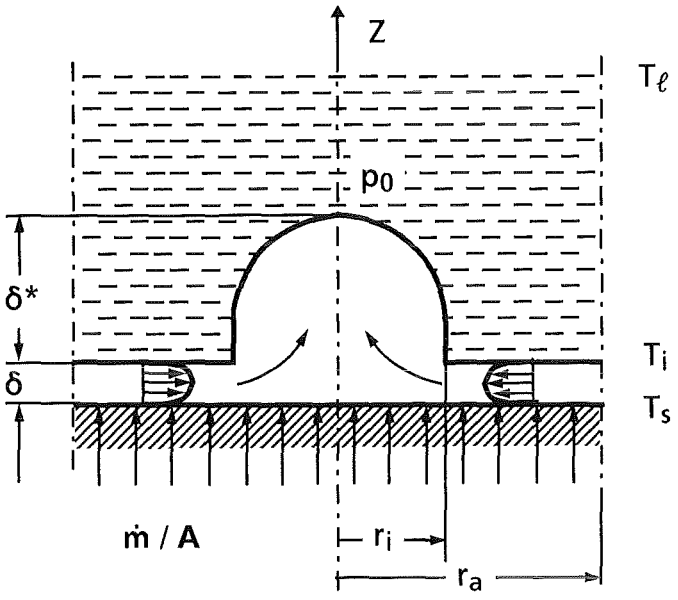

Figure 6: Flow cell on a horizontal wall.

The momentum balance in the radial direction taking into account pressure forces and friction forces reads

$$\frac{\partial p}{\partial r} = \mu_g \frac{\partial^2 w}{\partial z^2}. \tag{2.2.3-11}$$

The integration of this equation results in

$$w_m = -\frac{(3\Phi - 2)\,\delta^2\,\partial p}{12\ \mu_g\,\partial r}. \tag{2.2.3-12}$$

Combining (2.2.2-10, 12) and performing a radial integration one gets

$$p_a - p_i = \frac{6}{(3\Phi - 2)}\frac{\mu_g}{\rho_g \delta^3}\left(r_a^2\,\ell n\frac{r_a}{r_i} - \frac{r_a^2 - r_i^2}{2}\right). \tag{2.2.3-13}$$

In the above equation, the parameter Φ characterizes the boundary condition at the gas/liquid interface. In Eq. (2.2.2-12) $\Phi = 1$ applies to the liquid acting as a sol-

id wall and $\phi=2$ applies to a slip condition. In practice, the boundary condition will lie somewhere between these two conditions.

A hydrostatic pressure balance around the flow cell gives

$$p_a - p_0 = g\,\delta^*\,\rho_\ell\,, \tag{2.2.3-14}$$

$$p_i - p_0 = g\,\delta^*\,\rho_g + \frac{2\sigma}{r_i}. \tag{2.2.3-15}$$

The combination of Eqs. (2.2.2-8, 13, 14, 15) yields

$$\left(\frac{m}{A}\right)_{tot} = 0.3724\,\frac{(3\phi-2)}{12}\,\frac{g\,\rho_g\,\Delta\rho\,\delta^3}{\mu_g\,a} \tag{2.2.3-16}$$

for the specific mass flux of the gases released from the concrete and entering the flow cell.

In the idealized flow cell, the heat transfer by conduction through the gas film of thickness δ is effective on the area given by the ratio

$$A_{eff}/A_{tot} = \left(1-\frac{\pi}{16}\right) = 0.804\,. \tag{2.2.3-17}$$

By combining Eqs. (2.2.2-1, 2.2.3-1, 2, 3 and 16, 17) and by introducing the dimensionless quantities

$$\delta = \delta/L\,,$$

$$Nu = \frac{(Q/A)L}{k_g\,(T_i - T_{d0})}\,,$$

$$Gr = \frac{g\,\rho_g\,\Delta\rho\,L^3}{\mu_g^2}\,, \tag{2.2.3-18}$$

$$Pr\,Ste = \frac{\mu_g\,\Delta H_c}{k_g\,(T_i - T_{d0})}$$

the dimensionless film thickness can be determined from the following equation as

$$\frac{1}{\delta} = 0.825\left\{\frac{3\phi-2}{12}\,\frac{Gr\,Pr\,Ste}{\Psi_g}\,\frac{L}{a}\,\frac{1}{1+1.244\,\delta\,Nu_{rad}}\right\}^{1/4}. \tag{2.2.3-19}$$

The Nusselt number based on the total heat transfer rate for the horizontal surface is obtained as

$$Nu_{tot} = Nu_{rad} + \frac{A_{eff}}{A_{tot}} \frac{1}{\delta} . \qquad (2.2.3\text{-}20)$$

It is now assumed that the wavelength λ is small compared to the radius of curvature while going from a horizontal to a strongly inclined concrete surface. It was seen in model experiments with dry ice slabs that up to an inclination $\alpha = 30^{o}$, the unstable gas film with bubbles breaking away was the governing mechanism of gas release. So, in this intermediate region the heat transfer is assumed to be constant as given by Eqs. (2.2.3-19, 20).
If the inclination goes beyond 30°, a continuous gas layer is formed which flows along the wall. Now, the conductive heat transport across the gas film is effective on the whole surface, i.e.

$$\frac{A_{eff}}{A_{tot}} = 1 . \qquad (2.2.3\text{-}21)$$

With the denotations of Figure 7, the mass balance reads

$$\frac{d}{ds}(\boldsymbol{m}_{ax}) = (\frac{\boldsymbol{m}}{A}) \qquad (2.2.3\text{-}22)$$

with

$$\boldsymbol{m}_{ax} = \rho_g w_m \delta \qquad (2.2.3\text{-}23)$$

and the integration of the simplified momentum equation taking into account friction forces and buoyancy forces yields

$$\mu_g \frac{d^2 w}{dn^2} = -g \Delta\rho \sin\alpha \qquad (2.2.3\text{-}24)$$

or, after integration

$$w_m = \frac{(3\phi - 2)}{12} \delta^2 \frac{g \Delta\rho}{\mu_g} \sin\alpha . \qquad (2.2.3\text{-}25)$$

By introducing the dimensionless variable

$$\zeta = s/L \qquad (2.2.3\text{-}26)$$

and by using the dimensionless groups as defined in Eqs. (2.2.3-18), the combination of Eqs. (2.2.2-1, 2.2.3-1, 2, 3, 22, 23, 26) results in a differential equation for determining the film thickness δ:

$$\frac{d\delta}{d\zeta}=\frac{4}{(3\phi-2)}\frac{\Psi_g}{Gr\,Pr\,Ste\,\sin\alpha}\frac{1+Nu_{rad}\delta}{\delta^3}, \tag{2.2.3-27}$$

and the total heat transfer is evaluated again with Eq. (2.2.3-20).

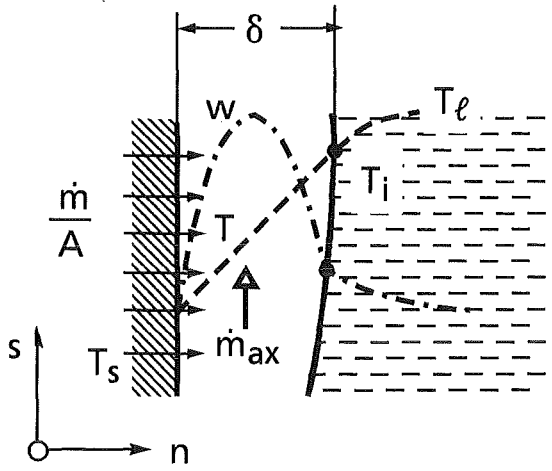

Figure 7: Laminar gas film on an inclined or vertical wall.

The thickness of the laminar gas film increases up to a critical value for which transition to turbulence must be expected and which can be determined from the relations for a single-phase fluid (see i.e. Schlichting [23]). By introducing the wall shear velocity

$$v=(\tau_w/\rho_g)^{1/2}, \tag{2.2.3-28}$$

the dimensionless velocity

$$w^+=w/v, \tag{2.2.3-29}$$

and the dimensionsless distance

$$y^+=n\frac{\rho_g v}{\mu_g} \tag{2.2.3-30}$$

can be defined. Within the framework of a two-layer concept for a single-phase fluid flow, a limiting value for the layer thickness is

$$y^+=10. \tag{2.2.3-31}$$

By assuming a linear velocity profile

$$w^+ = y^+ , \tag{2.2.3-32}$$

the critical Reynolds number is defined as

$$Re^* = \frac{\rho_g w_m \delta}{\mu_g} = w^+ y^+ = 100 . \tag{2.2.3-33}$$

This results in a critical film thickness given by

$$\delta_{crit} = \left\{ \frac{12 \quad Re^*}{(3\Phi - 2) Gr \sin\alpha} \right\}^{1/3} . \tag{2.2.3-34}$$

Above this point, a turbulent core (subscript c) with a laminar sublayer (subscript g) is present as indicated in Figures 5 and 8. The mass flux through the film is

$$m_{ax} = \rho_c w_c \left\{ \delta_c - \delta(1 - \frac{1}{2} \frac{\rho_c}{\rho_g}) \right\} \tag{2.2.3-35}$$

with the velocity w_c in the turbulent core as

$$w_c = y^{+2} \frac{\mu_g}{\rho_g \delta} . \tag{2.2.3-36}$$

Inserting Eqs. (2.2.3-35, 36) in Eq. (2.2.2-22) and combining the result with Eqs. (2.2.2-1, 2.2.3-1, 2) yields

$$\frac{d}{d\zeta} \frac{\delta_c}{\delta} = \frac{\rho_g}{\rho_c} \frac{\Psi_g}{y^{+2} Pr\, Ste} \frac{1}{\delta} (1 + Nu_{rad}\, \delta) . \tag{2.2.3-37}$$

In a second step, a momentum balance is applied to a control element as shown in Figure 9:

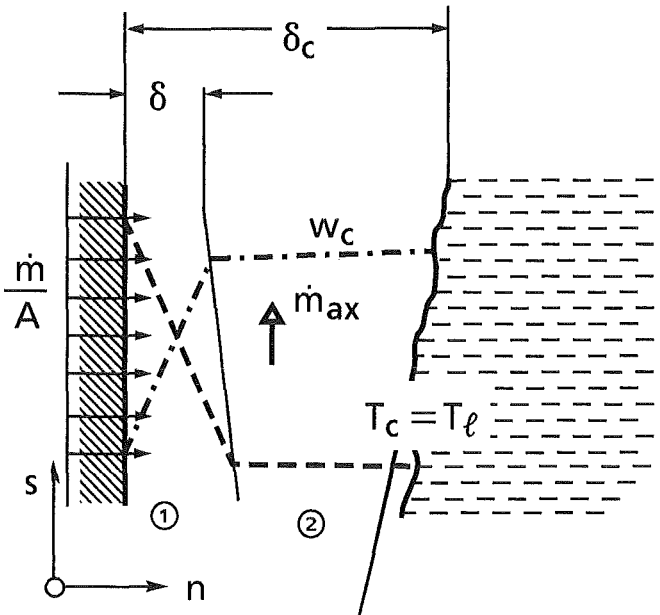

Figure 8: Turbulent gas film on an inclined or vertical wall.

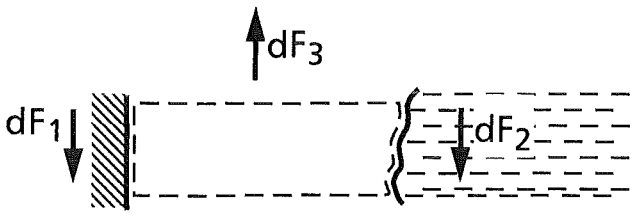

Figure 9: Forces acting on an element of the turbulent gas film.

$$\rho \int_{(K)} w dQ - dF_1 - dF_2 + dF_3 = 0 \,. \tag{2.2.3-38}$$

(Q: volume flux in the film; F: forces)

Evaluating the momentum integral yields

$$\rho \int_{(K)} w dQ = -\frac{\rho_c}{\rho_g} y + 4 \frac{\mu_g^2}{\rho_g} \frac{d}{ds} \left(\frac{1}{\delta} \left\{ \frac{\delta_c}{\delta} - (1 - \frac{1}{3} \frac{\rho_g}{\rho_c}) \right\} \right) ds \,. \tag{2.2.3-39}$$

The forces acting in direction of the flow are the wall friction force

$$dF_1 = \tau_w \, ds = y^{+2} \frac{\mu_g^2}{\rho_g} \frac{1}{\delta^2} ds \,, \tag{2.2.3-40}$$

the interface friction force

$$dF_2 = \tau_i \, ds = \frac{\rho_c}{\rho_g} y^{+4} \frac{\mu_g^2 f_{TP}}{\rho_g} \frac{1}{2} \frac{1}{\delta^2} ds \,, \tag{2.2.3-41}$$

and the buoyancy force

$$dF_3 = g \, \Delta\rho \, \delta_c \, sin\alpha \, ds \tag{2.2.3-42}$$

Combination of Eqs. (2.2.3-38, 39, 40, 41, 42) and use of Eq. (2.2.3-37) results in

$$\frac{d\delta}{d\zeta} = \frac{\dfrac{\rho_g}{\rho_c} \dfrac{\Psi_g}{y^{+2} \, Pr \, Ste} (1 + Nu_{rad} \delta) + \left(\dfrac{f_{TP}}{2} + \dfrac{\rho_g}{\rho_c} \dfrac{1}{y^{+2}} \right) - \dfrac{\rho_g Gr \, sin\alpha}{\rho_c \; y^{+4}} \delta_c \delta^2}{\dfrac{\delta_c}{\delta} - \left(1 - \dfrac{1}{3} \dfrac{\rho_g}{\rho_c} \right)} \,. \tag{2.2.3-43}$$

Eqs. (2.2.3-37, 43) are a system of differential equations for the total layer thickness δ_c and the laminar sublayer thickness δ. This system of differential equations as well as the differential equation (2.2.3-27) for laminar flow may be integrated numerically by means of a Runge-Kutta method.

In the turbulent film model, the heat is assumed to be transferred by conduction through the laminar sublayer of thickness δ and by radiation from the liquid/gas interface to the concrete surface. Consequently, the total heat transfer can again be evaluated by Eq. (2.2.3-20).

As the computation of the heat transmission through the vertical gas film by solving the complete system of differential equations using a Runge-Kutta method is rather time consuming, an approximate solution has been developed by Reinecke [24] which reproduces with sufficient accuracy the results of modeling described above. By this measure, the computer time required by the WECHSL code has been reduced considerably. The relevant approximation equations and sets of constants are given in Section 2.4.2.

2.2.4 Pool Boundary Layer

In all flow regimes of the gas film model, the temperature difference T_i-T_{d0} is decisive for the heat transfer, where T_i is the temperature of the melt at the interface with the gas film and T_{d0} is the surface temperature of the decomposing concrete. In the bottom region of the pool, a thin boundary layer driven by micro-convection between bubble release sites is assumed to exist. Along the inclined walls, a boundary layer is created by drag forces exerted by the gas flowing in the film. Both boundary layers result in a temperature drop of the pool bulk temperature T_m to the interface temperature T_i. Because of the excellent thermal conductivity and the low viscosity of the metals which, normally, occur at the bottom of the pool, this temperature drop across the boundary layer in the metal is only on the order of few degrees. However, in the oxide region (region 4 in Figure 5), the temperature drop across the boundary layer is quite significant because of the low thermal conductivity and the high viscosity of the oxides. This reduces considerably the total heat transfer from the molten pool to the concrete. To describe the attack of a two-phase melt on the concrete properly, a boundary layer analysis, especially for inclined and vertical walls in the oxide region, is important. The results of this approach can also be applied as a first-order approximation on the bottom region where the metallic melt interacts.

In reference [25], the complete analysis is given of the boundary layer formation at a laminar gas film/liquid interface. Boundary layer calculations were carried out for vertical plates of sublimating dry ice in water and water-glycerine mixtures as well as for concrete slabs attacked by metallic or oxidic melts.

In all of these computations, the coefficient ϕ in Eq. (2.2.3-27) which determines the coupling of the gas film with the liquid was found to be almost unity. Consequently, the use of

$$\phi = 1 \tag{2.2.4-1}$$

in Eqs. (2.2.3-19, 22) is appropriate to obtain heat transfer results.

Following a proposal of Lock [26], the ratio of the hydrodynamical boundary layer thickness between two fluids is

$$\frac{\delta_{h1}}{\delta_{h2}} = 0.844 \left(\frac{\mu_1}{\mu_2}\right)^{2/3} \left(\frac{\rho_2}{\rho_1}\right)^{1/3} \tag{2.2.4-2}$$

when fluid 2 is at rest. In the gas film, the thermal boundary layer thickness equals the film thickness, and the hydrodynamic boundary layer thickness can be set as the thickness of the layer where the velocity drops from the maximum to the interface value. This is

$$\frac{\delta_{hg}}{\delta_{tg}}=\frac{1}{2} \tag{2.2.4-3}$$

for $\phi=1$. On the other hand, the ratio of the hydrodynamical and the thermal boundary layer thickness in the liquid is approximated by

$$\frac{\delta_{h\ell}}{\delta_{t\ell}} \sim Pr_{\ell}^{1/2} \; . \tag{2.2.4-4}$$

(see e.g. Schlichting [23]).

With these assumptions made, a good approximation for the heat transfer results of all boundary layer calculations could be found by

$$\frac{\delta_{t\ell}}{\delta_{tg}}=1.236\, Pr_{\ell}^{-1/2}\left(\frac{\mu_{\ell}}{\mu_{g}}\right)^{2/3}\left(\frac{\rho_{g}}{\rho_{\ell}}\right)^{1/3} \; . \tag{2.2.4-5}$$

The comparison of this equation with the results of the boundary layer theory is shown in Figure 10.

The boundary layer analysis was carried out for laminar film flow. However, in the model experiments with dry ice slabs of 25 cm length sublimating in water and water/glycerine mixtures, transition to turbulent gas film flow occurred. As shown in [25], a good representation of the heat transfer results of these model experiments could be found when calculating the interface temperature

$$T_i=\frac{T_{\ell}+\dfrac{\delta_{t\ell}}{\delta_{tg}}\dfrac{k_g}{k_{\ell}}T_{d0}}{1+\dfrac{\delta_{t\ell}}{\delta_{tg}}\dfrac{k_g}{k_{\ell}}} \tag{2.2.4-6}$$

from the laminar analysis (Eq. 2.2.4-5), applying this result also to the turbulent gas film region and setting the friction coefficient f_{TP} in the turbulent film zone as a function of the viscosity ratio (μ_{ℓ}/μ_g) determined at the interface temperature T_i.

$$f_{TP}=3.414\cdot 10^{-4}(\mu_{\ell}/\mu_{g})^{2/3} \; . \tag{2.2.4-7}$$

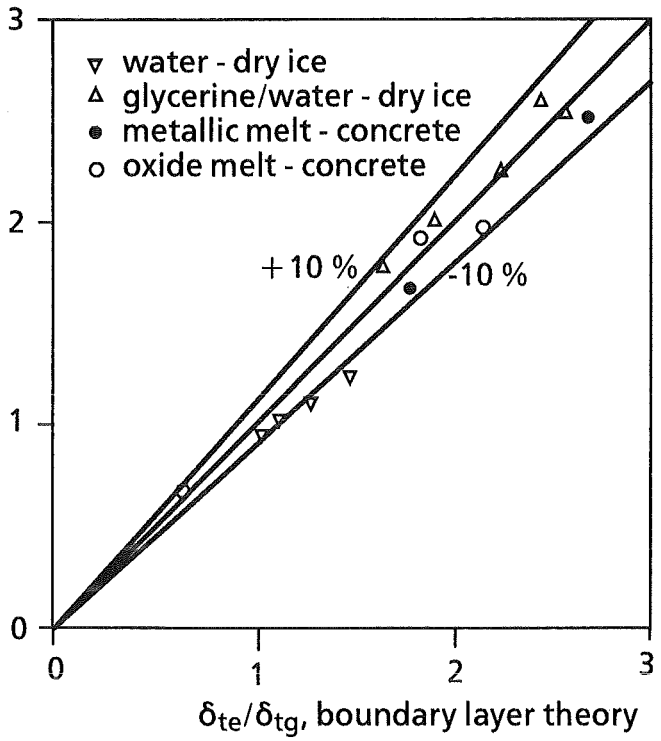

Figure 10: Comparison of Eq. (2.2.4-4) with the results of boundary layer theory.

This comparison is given in Fig. 11.

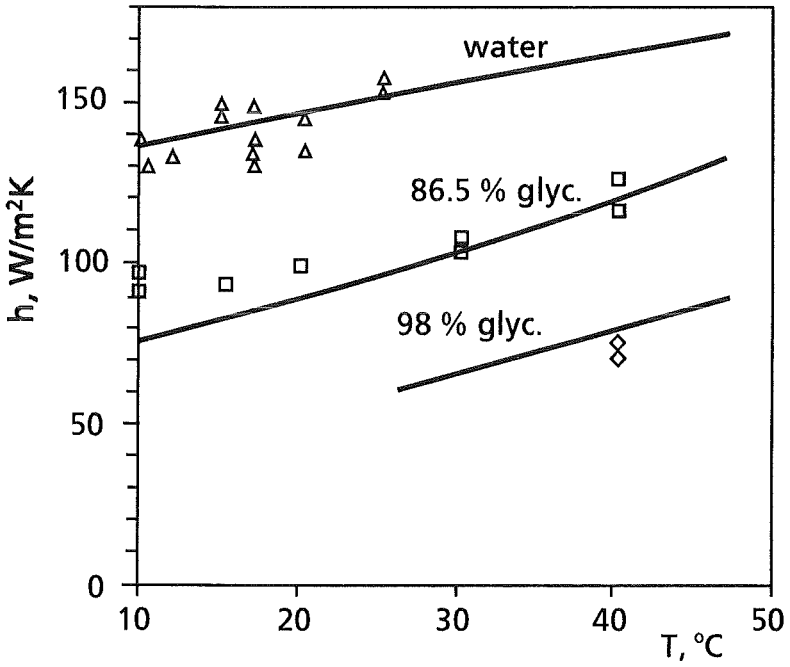

Figure 11: Comparison of experimental and calculated heat transfer results of vertical dry ice slabs sublimating in liquid pools.

2.2.5 Discrete Bubble Model

During the interaction of a core melt with concrete the pool temperature of the melt drops continuously. Moreover, other types of concrete with a lower weight

fraction of gaseous decomposition would release lower gas rates when attacked by the melt. So, the mass flux density of the released gases as defined in Eq. (2.2.2-1) could drop to a value at which a stable gas film can no longer exist. With a Reynolds number based on the mass flux defined by

$$Re = \frac{(m/A)a}{\mu_g} \tag{2.2.5-1}$$

and the approach of Berenson [17] for film boiling on horizontal surfaces followes the minimum Reynolds-number for a stable gas film:

$$Re_{min} = 0.09 \left(Gr \frac{\rho_g}{\rho_\ell + \rho_g} \right)^{1/2} . \tag{2.2.5-2}$$

According to the results of the BETA experiments, this minimum value will be modified in Section 2.2.7. From the Zuber criterion for the maximum gas flow at departure from nucleate boiling (DNB), the maximum Reynolds number yields

$$Re_{max} = 0.09 \left(Gr \frac{\rho_\ell}{\rho_\ell + \rho_g} \right)^{1/2} . \tag{2.2.5-3}$$

After the Reynolds number has dropped below the minimum value, the melt will get into direct contact with the concrete surface and the heat will be transferred through a boundary layer on the melt/concrete interface driven by microconvection between the sites of gas bubble formation. Such a discrete bubble model was derived by Reineke et al. [27] for horizontal surfaces and extended later to include inclined and vertical walls [28].

In terms of the dimensionless quantities based on the properties of the melt

$$Nu_\ell = \frac{(Q/A)a}{k_\ell (T_\ell - T_{d0})} \quad ,$$

$$Pr_\ell = \frac{\mu_\ell \, c_{p\ell}}{k_\ell} \quad , \qquad (2.2.5\text{-}4)$$

$$(Pr\,Ste)_\ell = \frac{\mu_\ell \, \Delta H_c}{k_\ell (T_\ell - T_{d0})}$$

the heat transfer is determined by

$$Nu_{\ell 1} = \frac{C^2(\alpha)}{6^{1/2}} \Psi \frac{Pr_\ell^{0.84}}{g(Pr\,Ste)_\ell} \qquad (2.2.5\text{-}5)$$

with an expression taking into account the angle of inclination α

$$C(\alpha) = 1.65 + 7.47\alpha - 8.77\alpha^{\,2} + 3.65\alpha^{\,3} \, . \qquad (2.2.5\text{-}6)$$

As due to an argument given in [29] the bubble density at the decomposing surface cannot exceed a limiting value, the upper boundary for the Nusselt number is

$$Nu_{\ell 2} = 4.63\, Pr^{\,0.38} \, . \qquad (2.2.5\text{-}7)$$

The governing Nusselt number is evaluated by

$$Nu_\ell = Min\{Nu_{\ell 1} \, , Nu_{\ell 2}\} \quad . \qquad (2.2.5\text{-}8)$$

If the Reynolds number Re_{max} given in Eq. (2.2.5-3) is exceeded, a stable gas film must exist. Between destabilization of the gas film and departure from discrete bubble heat transfer, transition heat transfer is the governing mechanism (see 2.2.7).

2.2.6 Transient Crust Model

Crust formation is governed by the following mechanisms:

- Heat transfer at the crust internal side with the driving temperature difference T_{bulk} - T_{freez}
- Heat conduction through the crust; the bounding temperatures of the crust are T_{freez} and T_i
- Heat transfer at the crust external side with the driving temperature difference T_i and T_{surr}.

Figure 12 illustrates the concept of crust formation with an electrical analogy model.

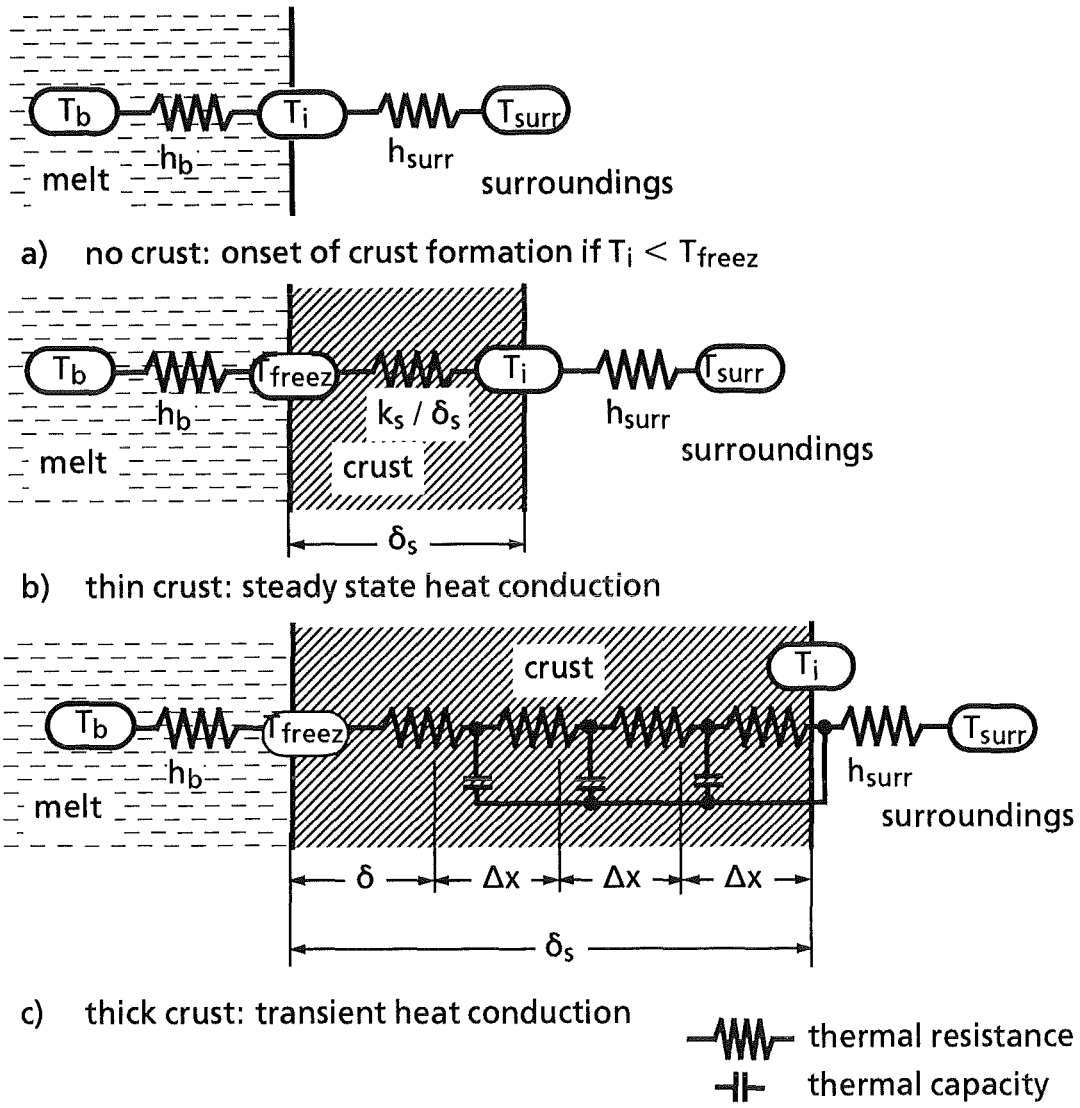

Figure 12: Electrical analogon for crust formation.

In the case of a crust facing the concrete surface, the surrounding temperature T_{surr} is equal to the concrete ablation temperature T_{d0} and the heat transfer coefficient is h_{film}.

After the onset of crust formation, thin solid layers which are formed float with the liquid of the melt bulk. Hence, it is plausible to assume steady-state heat conduction through the crust for this situation . In that case, all three heat flux densities are equal and the situation corresponds to Figure 12b. Thus,

$$h_b(T_b - T_{b,freez}) = \frac{k_s}{\delta_s}(T_{b,freez} - T_i) = h_{surr}(T_i - T_{surr}) . \qquad (2.2.6\text{-}1)$$

From this equation, the unknown quantities

- crust thickness δ_s and
- surface temperature of the crust T_i

can be evaluated.

In the next time step, the mesh width of the relevant bulk material is fixed. If the crust thickness exceeds this value, transient heat conduction is applied in the first complete mesh and the next mesh starts growing. The situation then corresponds to that in Figure 12c (where the effect of internal heat sources is not considered).

The one-dimensional, transient heat conduction inside the crust can be treated with an explicit calculation scheme according to [30] inside the mesh n for the time characterized by j+1, viz,

$$T_{n,j+1} = \bar{p}\,(T_{n+1,j} + T_{n-1,j}) + (1-2\bar{p})\,T_{n,j} + \frac{(\Omega_b/V_b)}{\rho_b c_b} \qquad (2.2.6\text{-}2)$$

where Ω_b/V_b is the heat source density of the bulk, containing nuclear decay, chemical reaction heat, and energy contributions from the liquid and gaseous concrete decomposition products flowing through the solid crust.

The module $\bar{p}$ is defined by

$$\bar{p} = \frac{k_s}{\rho_b c_b}\,\frac{\Delta\tau}{(\Delta x)^2} \qquad (2.2.6\text{-}3)$$

This module is fixed.with the given mesh width Δx and time increment $\Delta\tau$. Care must be taken that the stability criterion

$$\bar{p} < 1/3 \qquad (2.2.6\text{-}4)$$

is fulfilled in the explicit calculation scheme given by Eq. (2.2.6-2).

The temperature of the first fictitious mesh n=1 at the outside of the crust can be evaluated by

$$T_{1,j} = \frac{1-Bi^*}{1+Bi^*}\,T_{2,j} + \frac{2\,Bi^*}{1+Bi^*}\,T_{surr,j} \qquad (2.2.6\text{-}5)$$

with the sourrounding temperature $T_{surr,j}$. The special Biot-number Bi* contains the external boundary condition and is defined by

where h_{surr} is the external heat transfer coefficient.

$$Bi^* = \frac{h_{surr}}{k_s} \frac{\Delta x}{2} \tag{2.2.6-6}$$

At the phase change interface between crust and melt at freezing temperature T_{freez}, the change of the crust thickness δ_s is given by the heat flux balance

$$\rho_b h_{fus} \frac{d\delta_s}{d\tau} = (Q/A)_{out} - (Q/A)_{in} \tag{2.2.6-7}$$

with the specific latent heat of phase change of the bulk material h_{fus}. The heat flux density $(Q/A)_{out}$ is carried away by heat conduction into the last mesh of the crust and

$$(Q/A)_{in} = h_\ell (T_\ell - T_{freez}) \tag{2.2.6-8}$$

is transported by convective mechanisms to the phase change interface. Hence, the crust thickness is changed in a time increment $\Delta\tau$ by

$$\Delta\delta = \frac{\Delta\tau}{\rho_b h_{fus}} \left\{ \frac{T_{freez} - T_{n,j}}{\left(\frac{\Delta x}{2} + \delta^*\right)} k_s - h_\ell (T_\ell - T_{freez}) \right\} . \tag{2.2.6-9}$$

If the residual crust thickness $(\delta^* + \Delta x/2)$ exceeds 1.2 Δx, a further mesh is added to the region of transient heat conduction inside the crust. In the opposite case of crust melting, a mesh is subtracted from the region of transient heat conduction, when the residual crust thickness δ^* drops below 0.3 Δx.

2.2.7 Application of the Models in the WECHSL Code

The BETA high power tests, in which completely liquid layers must be anticipated, showed a strong downward penetration of the metal bulk into the concrete of the crucible and a very limited side-wall erosion. Consequently, an enhanced heat transfer mode must exist in the bottom region of the crucible which leads to the conclusion that at higher superficial gas velocities, as given by the BERENSON criterion Eq. (2.2.5-2), a partial destabilization of the horizontal gas film may occur. Thus, a factor F for multiplication of the BERENSON criterion has been introduced in the post-test calculations.

$$Re_{min\,mod} = F\, Re_{min} \tag{2.2.7-1}$$

which leads to an increase in the minimum superficial gas velocity at which quenching sets in at the bottom of the crucible. The bottom area covered by the gas film is then linearly reduced until the heat transfer is governed completely by the discrete bubble model.

The Reynolds number of the gas film is

$$Re_{film} = \frac{Nu_{film}}{Pr\,Ste} \tag{2.2.7-2}$$

whith Nu_{film} given by Eqs. (2.2.3-19, 20).

If $Re_{film} < Re_{min\ mod}$ (Eq. (2.2.7-1) and $Re_{bubble} < Re_{max}$ Eq. (2.2.5-3)), the Nusselt number based on the gas properties is

$$Nu = f\,Nu_{film} + (1-f)\,Nu_{bubble}\,\frac{k_\ell}{k_g}\,\frac{T_\ell - T_{d0}}{T_i - T_{d0}} \tag{2.2.7-3}$$

where

$$f = \frac{Re_{film} - Re_{min}}{Re_{min\ mod} - Re_{min}} \tag{2.2.7-4}$$

and Nu_{bubble} is given by Eqs. (2.2.5-5, 6, 7, 8) with $\alpha = 0$ in Eq. (2.2.5-6). As in Eq.(2.2.7-2) Re_{bubble} is defined on the basis of liquid properties.

As shown in Figure 13, an earlier destabilization of the gas film is likely to occur, as, in contrast to boiling phenomena, the gases during concrete decomposition are released in the depth of the solid material beneath the ablating concrete surface, while the heat flux causing the gas release has to be transported by thermal conduction through a layer of degassed concrete.

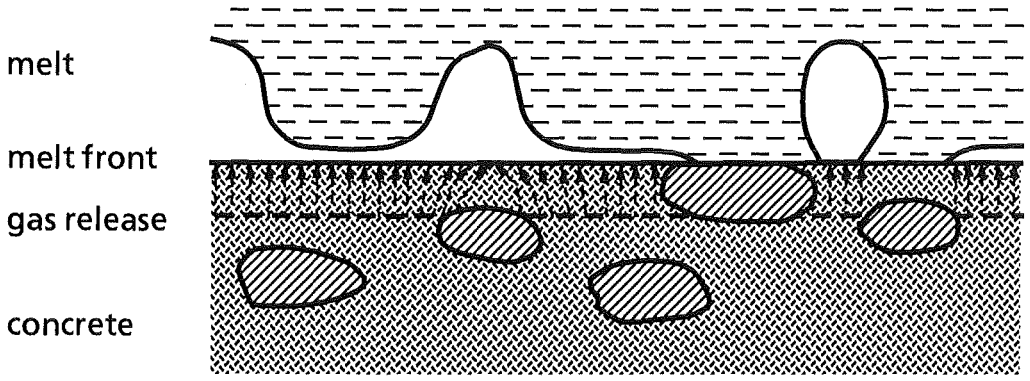

Figure 13: Destabilisation of the gas film.

This may lead to temporal oscillations of gas emission. Moreover, the aggregate stones may form a barrier to the released gases which may lead to local discontinuities in the gas flow. To reproduce the erosion data of the high power BETA tests with WECHSL, a factor

$$F=25 \tag{2.2.7-5}$$

was found to be convenient and was fixed in WECHSL.

If a crust is formed in the bottom region, the quenched regions of the concrete surface are reduced again. At a defined minimum crust thickness δ_{min}, the crust will close completely so that no quenched regions exist any longer. This behavior is taken into account by defining a new factor

$$f^* = (1-f)f_c + f \tag{2.2.7-6}$$

where

$$f_c = \frac{\delta_s}{\delta_{min}}. \tag{2.2.7-7}$$

and by replacing the factor f in Eq. (2.2.7-3) by f*.

At the side walls, the gas film is more stable than in the bottom region of the concrete structure. Consequently, the gas film is retained in WECHSL in all situations occurring .

When the melt layer is completely liquid or has only thin crusts with $\delta_s < \delta_{min}$, the bulk boundary layer heat transfer is calculated as described in Section 2.2.4. When the crust thickness exceeds a defined value δ_{max}, a situation as shown in Figure 3c has established: The gases released from the concrete flow through tubular holes in the crust and form gas bubbles detaching from the inner crust surface. The inside heat transfer from the melt bulk to the crust is then given, in principle, by a discrete bubble type heat transfer relation as recommended in [27]

$$Nu_\ell = C\, Re^{0.5}\, Pr_\ell^{0.42} \tag{2.2.7-8}$$

which is also the basis of Eq. (2.2.5-5). The Reynolds number is defined by Eq. (2.2.5-1) and the Prandtl number by Eq. (2.2.5-4). The constant C was fixed empirically to be

$$C=0.40\,. \tag{2.2.7-9}$$

Between δ_{min} and δ_{max}, the heat transfer is averaged linearly in WECHSL.

When the metal layer has solidified completely, direct contact of the frozen slug with the concrete is assumed. Then, the surface temperature of the metal block facing the concrete is assumed to be at the concrete decomposition temperature T_{d0}.

2.3 Pool Behavior

2.3.1 Bubble Size and Velocity of Rise

Gas bubbles rising through the melt are responsible for melt stirring. They also cause swelling of the melt so that the surface area for heat transfer is effectively increased. The bubble behavior is important because of the large volume fluxes of gas released, and a considerable void fraction may develop in the melt.

It has been assumed in the gas film model that bubbles of uniform size and spacing are formed. This is well confirmed by experiments with simple materials such as water over dry ice. However, also in experiments with water over inhomogeneous materials, i.e. frozen xylene and carbon dioxide snow simulating the liquid and gaseous decomposition products of the concrete [13], it was seen that the gas bubbles have an average diameter similar to that in the experiments with pure materials.

The mean equivalent sphere radius of the bubbles detatching from the gas film has been estimated in Eq. (2.2.3-8) to be

$$r_{eq} = \frac{\lambda}{4} = 2.74a\,. \tag{2.3.1-1}$$

The bubble radius as estimated in the discrete bubble model is of the same order of magnitude.

The Reynolds number of the bubble

$$Re_{\ell} = \frac{\rho_{\ell} r_{eq} u_b}{\mu_{\ell}} \tag{2.3.1-2}$$

is important to the behavior of rising bubbles. For small Reynolds-Numbers, i.e. for small bubble dimensions or for a high kinematic viscosity of the fluid, buoyancy forces are balanced by the friction forces:

$$\frac{4\pi}{3} r_{eq}^3 g \Delta\rho = \zeta \pi r_{eq}^2 \frac{\rho u_b^2}{2} \tag{2.3.1-3}$$

where ζ is the friction coefficient. From this equation, the bubble velocity can be written as

$$u_b = \left(\frac{8\, g\, \Delta\rho\, r_{eq}}{3\, \rho_\ell\, \zeta} \right)^{1/2} . \tag{2.3.1-4}$$

For very small bubbles - which are not of interest here - the friction coefficient for a rigid sphere is applicable (Stokes flow and transition region). For higher Reynolds numbers, the friction coefficient is twice that for Stokes flow around a rigid sphere as proposed by Levich [31]:

$$\zeta = \frac{24}{Re_\ell} \tag{2.3.1-5}$$

and the velocity of bubble rise is obtained as

$$u_{b1} = \frac{1}{9} g \frac{\Delta\rho}{\rho_\ell} r_{eq}^2\, \nu^{-1} . \tag{2.3.1-6}$$

In low viscous fluids, the velocity of rise increases up to a maximum value. Beyond this value, the rise behavior changes completely.

The sperical cap bubbles start oscillating and rise along zig-zag or helical lines. With increasing bubble radius, the rise velocity decreases to a minimum value. Then, the rise velocity increases again. Mendelson [32] formulated this complicated behavior in a single equation by balancing basically the inertia forces with the gravity and capillary forces. By introducing the dimensionless groups

$$We = \frac{r_{eq}\, \rho_\ell\, u_b^2}{\sigma}$$

$$E\ddot{o} = \frac{g\, \rho_\ell\, r_{eq}^2}{\sigma} \tag{2.3.1-7}$$

it results

$$We = E\ddot{o} + 1 , \tag{2.3.1-8}$$

or, for the velocity of bubble rise

$$u_{b2} = \left(g\, r_{eq} + \frac{\sigma}{\rho_\ell\, r e_{eq}} \right)^{1/2} . \tag{2.3.1-9}$$

For large bubbles, the capillary forces can be neglected and the rise velocity approaches

$$u_{b2}^{*}=(g\,r_{eq})^{1/2}\,. \tag{2.3.1-10}$$

In highly viscous fluids, the bubbles rise straight without oscillations. Here, the rise velocity increases continuously with increasing bubble radius and, finally, approaches Eq. (2.3.1-10).

The effective bubble rise velocity is determined by

$$u_b=min(u_{b1},u_{b2})\,. \tag{2.3.1-11}$$

Some data from the experimental work of Habermann and Morton [33] are shown in Figure 14, along with the values computed by Eq. (2.3.1-11).

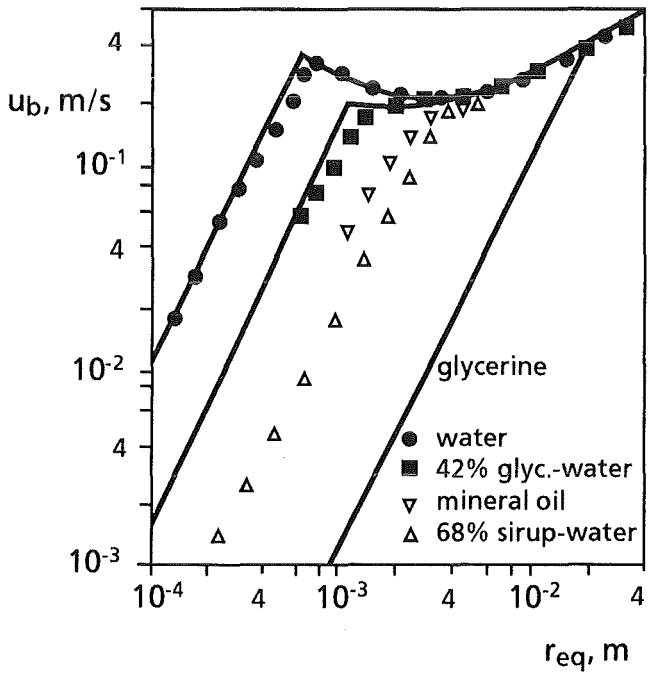

Figure 14: Velocity of rise for air bubbles in a tank of stagnant liquid [33].

The maximum possible equivalent bubble radius is given by Levich [31] to be

$$r_{eq\,max}=\frac{\sigma}{u_b^2}\left(\frac{12}{\rho_g\,\rho_\ell^2}\right)^{1/3}\,. \tag{2.3.1-12}$$

When a bubble exceeds this dimension, it bursts into smaller bubbles.

The formation of a foamy oxide with very small gas bubbles but very high voids, as observed in some of the simulant tests, is not considered in WECHSL because of lack of information about the conditions under which a foamy melt would exist.

2.3.2 Void Fraction

In the foregoing section, the rise behavior of a single bubble in a stagnant liquid was discussed. However, when large numbers of bubbles rise, the rise velocity is reduced to u_{bs}. Le Clair and Hamielec [34] gave a plot of the ratio u_{bs}/u_b over the void fraction ε of the liquid with the single bubble Reynolds number Re_b as the parameter. Their figure can be closely approximated by

$$\frac{u_{bs}}{u_b} = (1-\varepsilon)^n \tag{2.3.2-1}$$

with

$$\begin{aligned} Re_b \leq 50: \; & n = -1.14\, log(Re_b) + 4.11 \;, \\ Re_b > 50: \; & n = -0.52\, log(Re_b) + 3.05 \;. \end{aligned} \tag{2.3.2-2}$$

The values of the exponent n are restricted. By introducing the superficial gas velocity as

$$v_g = \frac{(m/A)}{\rho_g}, \tag{2.3.2-3}$$

the maximum exponent n_{max} is a function of the ratio u_b/v_g. The criterion of estabilishing this function is to avoid numerical overflow in WECHSL.

The void fraction, the artificial gas velocity and the velocity of bubble swarm rise velocity of a bubble swarm are correlated according to Nicklin [35] by

$$\frac{v_g}{\varepsilon} = u_{bs} + v_g \;. \tag{2.3.2-4}$$

By inserting Eq. (2.3.2-1), the void fraction can be evaluated from

$$\varepsilon = \frac{1}{1 + (1-\varepsilon)^n \dfrac{u_b}{v_g}} \;. \tag{2.3.2-5}$$

In WECHSL, the void fraction is arbitrarily limited to $\varepsilon_{max} = 0.85$.

2.3.3 Phase Segregation

It has been experimentally observed [7, 8] that a melt containing metal and lighter oxidic phases may undergo a rapid, density driven phase segregation. The BETA tests [4], however, showed that under certain conditions, mainly characterized

by high viscosity of the oxide phase and by high gas flow, the melt phases may intermix which is likely to occur in the early phase of the melt/concrete interaction. In a core melt, the oxide is initially composed of a mixture of ZrO_2 and UO_2, which, according to Ondracek [36], has a slightly lower density than the metallic phase. This is the maximum possible density for the oxide. The accretion of molten concrete constituents in the oxide layer causes the density to become significantly lower.

WECHSL models either a completely mixed melt where the metallic phase is homogeneously dispersed in the oxide or a separated system with the heavier metal at the bottom covered by the oxidic melt.
In case of pure oxidic or dispered melt the heat transfer between the pool and the concrete is determined from the gas film model.

2.3.4 Heat Transfer between the Molten Layers

Werle [37] studied the heat transfer between liquid layers in the presence of gas percolation using simulant materials. In liquid layers without gas percolation, heat is transferred by natural convection. Haberstroh and Reinders [38] performed an analysis of this case based on the heat transport through a single layer heated from below and they obtained

$$Nu = 0.0535\{Gr\,Pr\}^{1/3}\,Pr^{0.417} \quad . \tag{2.3.4-1}$$

If an odd symmetric temperature profile is assumed to exist in each layer, the heat flux transferred from the high temperature (index h) to the low temperature (index l) layer is

$$\left(\frac{Q}{A}\right)_{i,0} = \left[\left(h^*_h\right)^{-3/4} + \left(h^*_l\right)^{-3/4}\right]^{-4/3} (T_h - T_l)^{4/3} \tag{2.3.4-2}$$

(2.3.4-2)

where T_h and T_l are the different bulk temperatures and

$$h^*_{h,l} = 0.0535 \cdot \left(\frac{g\,\beta_{h,l}}{\nu^2_{h,l}}\right)^{1/3} Pr^{0.417}_{h,l}\; k_{h,l} \tag{2.3.4-3}$$

is a special quantity related to the heat transfer coefficient by

$$h_{hl} = h^*_{hl}\,(T_{h,l} - T_i)^{1/3} \quad . \tag{2.3.4-4}$$

The interface temperature is determined by

$$T_i = T_l + \frac{\left(h_h^*\right)^{-3/4}}{\left(h_h^*\right)^{-3/4} + \left(h_l^*\right)^{-3/4}} (T_h - T_l) . \qquad (2.3.4\text{-}5)$$

Werle evaluated his model experiments using silicone oil/water and silicone oil/wood metal systems by determination of the factor

$$\gamma = \frac{(Q/A)_i}{(Q/A)_{i,0}} \qquad (2.3.4\text{-}6)$$

describing the enhancement of heat transfer by gas percolation in comparison with pure thermal convection. A reasonable fit of his data is

$$\gamma = 1 + 608 \left(\frac{v_g}{u_b}\right) Ar^{-0.43} \qquad (2.3.4\text{-}7)$$

with the Archimedes number

$$Ar = \left|\frac{\rho_l - \rho_h}{\rho_l}\right| \cdot \qquad (2.3.4\text{-}8)$$

In Figure 15, a comparison of the experimental data with Eq. (2.3.4-7) is given.

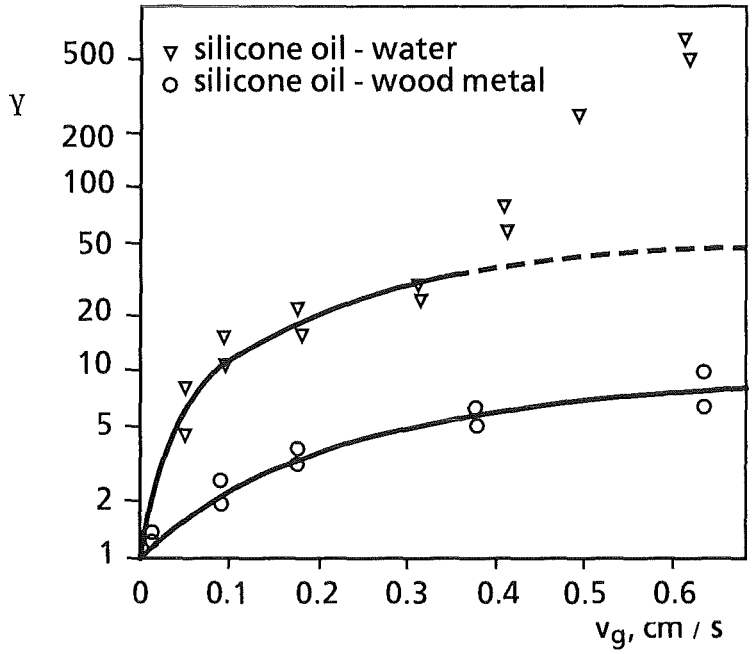

Figure 15: Enhancement of heat transfer between liquid layers percolated by gas bubbles.

The equation above holds as long as a distinct interface exists between the liquid layer and emulsifying effects are not decisive. The formation of emulsions was observed when the densities of the liquid layers were nearly equal or the viscosity of the oxide liquid was very high and the gas velocity was high. In Figure 11, the onset of emulsion formation is marked by a further increase in heat transfer in the oil/water system. In the oil/wood metal system, such a behavior could not be observed up to the maximum superficial gas velocity. In a core meltdown accident emulsification may occur at an intermediate stage, as was discussed above. On the other hand, the heat exchange between the molten layers is rather intense, even if the emulsifying effects are left out of consideration so that the temperature differences between the layers are generally small. A further improvement of heat transfer modeling would produce only a minor effect.

In the late phase of low-power BETA experiments, the metal bulk has a higher temperature than the oxide bulk. In that case, $T_m > T_o$, a metal crust may occur at the interface between metal and oxide. On the other hand, in the course of a core melt accident, the oxide bulk may have a higher temperature than the metal bulk. Thus, when $T_m < T_o$, an oxide crust may develop at the interface between metal and oxide. The metal is then either liquid at the interface, or the metal bulk is completely frozen so that a hot solid block of metal acts on the concrete structure.

This means, that a crust can only be formed at the metal/oxide interface in the high temperature phase. The heat conduction inside the crust is modeled in agreement with Section 2.2.6 either as a steady-state process (Figure 12b) for thin crusts or a transient process if the crust thickness exceeds the predefined mesh width (Figure 12c). The heat transfer coefficient at the interface between the melt layers and at the solidified interface is determined according to Eq. (2.3.4-1). For the first case, the driving temperature difference is $T_i - T_l$, whereas for the latter case, $T_h - T_{freez,h}$ is valid.

If the metal layer has completely solidified, the discrete bubble type heat transfer equation given in Eq. (2.2.7-8, 9) is used again.

2.3.5 Heat Transfer from the Top of the Melt

The gas bubbles rise through the oxide layer and break through the surface. By this mechanism, heated liquid is "pumped" to the free surface and a thermal boundary layer is formed.

From the top of the melt, the heat is carried away mainly by thermal radiation or - if the melt is flooded by water as may occur in core melt accidents with sump water ingression - by boiling heat transfer.

The heat transfer through the boundary layer under the melt surface is then represented by an expression similar to microconvective heat transport induced by a discrete bubble detaching from a gas emitting wall [27], again in agreement with Eq. (2.2.7-7, 8)

$$Nu_{o,s} = 0.040\, Re_b^{1/2}\, Pr_o^{0.42} \tag{2.3.5-1}$$

with

$$Nu_{o,s} = \frac{h_{o,s}\, r_{eq}}{k_o} \tag{2.3.5-2}$$

and the Reynolds-number of the bubble as defined in Eq. (2.3.1-2).

If the heat is carried away from the melt surface by thermal radiation, the resulting heat flux density

$$(Q/A)_{o,s} = h_{o,s}\,(T_o - T_{o,s}) \tag{2.3.5-3}$$

is balanced with the heat radiation from the surface to the surroundings

$$(Q/A)_{rad,s} = \varepsilon_{s\infty}\, c_0\, (T_{o,s}^4 - T_\infty^4) \tag{2.3.5-4}$$

with

$$\varepsilon_{s\infty} = \frac{1}{\frac{1}{\varepsilon_{o,s}} + \frac{1}{\varepsilon_\infty} - 1}\,. \tag{2.3.5-5}$$

The resulting equation is solved for the surface temperature.

If a crust is formed at the top of the melt, the additional heat resistance due to heat conduction in the crust has to be taken into account; the heat conduction is considered again to be stationary for a thin crust or transient for a thick crust, as described in Section 2.2.6. When a crust is present, the surface temperature $T_{o,s}$ must be replaced by T_{freez} in Eq. (2.3.5-3).

In the BETA tests, strong splashout of oxide melt was observed in high power tests with high superficial gas velocities. To take into consideration this effect in WECHSL, an empirical model was established. It is assumed that splashout acts on an annular region adjacent to the side wall of the concrete structure of width λ, where λ is the wavelength defined by Eq. (2.2.3-5). Thus, the effective surface area for splashout is

$$A_{eff} = (d_o - \lambda)\lambda\pi \,. \tag{2.3.5-6}$$

If the superficial gas velocity

$$v_g > 0.04\ m/s\,, \tag{2.3.5-7}$$

the mass flux of oxides splashed out onto the side wall is given by the equation

$$\frac{m_o}{C_o A_{eff}} = \left(\frac{v_g}{0.04} - 1 \right)^{1.8} \tag{2.3.5-8}$$

where

$$C_o = 600\ \frac{kg}{m^2 s}\,. \tag{2.3.5-9}$$

The material is splashed out at oxide bulk temperature and returns into the pool at the mean temperature

$$T = (T_o + T_{freez})/2\,. \tag{2.3.5-10}$$

By this empirical model, the strong cooling effect caused by splashout due to the violent gas evolution in the high-power BETA tests could be reproduced adequately in the WECHSL code. In a core melt accident, the surface area ratio A_{eff}/A_{tot} is very small and, consequently, the cooling effect due to splashout is only of minor importance.

If the liquid oxide pool is flooded by water at high temperature, oxide droplets may be entrained into the water bulk. This may cause steam explosions, as reported in [39]. Of course, agitation of the gas bubbles breaking through the pool surface enhances the entrainment of oxide and the possibility of steam explosions as well. In a core melt accident in a large German standard PWR, it is very likely that sump water ingression occurs only in the late phase of core melt/concrete interaction, several hours after the start of interaction. In that situation either solid crusts have been formed at the pool surface or the melt is highly viscous with a bulk temperature near the solidification temperature. This excludes serious

steam explosions resulting from late sumpwater ingression, but also prevents substantial fragmentation of the oxide surface so that a coolable particle bed has not to be expected [40, 41].

For the evaluation of heat transfer from the melt pool surface to the bulk of water it was considered sufficient to take into account in WECHSL boiling phenomena at a rigid horizontal surface. The correlations given below are taken from the "Handbook of Heat Transfer" [42].

Initially, when the water floods the melt surface, the surface temperature is around 1000 K. Hence, film boiling occurs. The heat transfer through the vapor film is given by

$$Nu_{fb} = 0.425 \left[Gr_v \, Pr_v \frac{h_{wv} + 0.4 c_{pv} \Delta T}{c_{pv} \Delta T} \right]^{1/4} \qquad (2.3.5\text{-}11)$$

with the driving temperature difference

$$\Delta T = T_{o,s} - T_w \, . \qquad (2.3.5\text{-}12)$$

Here and in the following equations, the index v characterizes vapor properties, whereas the index w indicates sump water properties in the state of saturation. $T_{o,s}$ is again the melt pool surface temperature.

The dimensionless groups in Eq. (2.3.5-11) are

$$Nu_{fb} = \frac{\alpha_{fb} \cdot a}{k_v},$$

$$Gr_v = \frac{\rho_v \, g(\rho_l - \rho_v) a^3}{\mu v^2}, \qquad (2.3.5\text{-}13)$$

$$Pr_v = \frac{\mu_v c_{pv}}{k_v} \, .$$

The characteristic length is the Laplace constant

$$a = \left[\frac{\sigma}{g(\rho_w - \rho_v} \right]^{1/2} \qquad (2.3.5\text{-}14)$$

The heat transfer coefficient is given by

$$\alpha_{fb} = 0.425 \left[\frac{k_v^3 \rho_v (\rho_w - \rho_v) g (h_{hw} + 0.4 c_{pv} \Delta T)}{\mu_v a \Delta T} \right]^{1/4} . \qquad (2.3.5\text{-}15)$$

The heat transmission by thermal radiation through the vapor film is given by

$$\alpha_{rad} = \varepsilon_{sw} c_o \left(\frac{T_{o,s}^4 - T_w^4}{T_{o,s} - T_w} \right) \qquad (2.3.5\text{-}16)$$

with

$$\varepsilon_{sw} = \frac{1}{\frac{1}{\varepsilon_s} + \frac{1}{\varepsilon_w} - 1} . \qquad (2.3.5\text{-}17)$$

The total heat flux density is evaluated by the approximation equation

$$(Q/A)_{fb} = (\alpha_{fb} + \frac{3}{4} \alpha_{rad}) (T_{0,s} - T_w) . \qquad (2.3.5\text{-}18)$$

The minimum heat flux density for destabilization of the gas film is again

$$(Q/A)_{min} = 0.09 \rho_v h_{wv} \left[\frac{\sigma g (\rho_w - \rho_v)}{(\rho_w + \rho_v)^2} \right]^{1/4} . \qquad (2.3.5\text{-}19)$$

The region of instable boiling is situated between the minimum heat flux density for film boiling and the maximum heat flux for nucleate boiling given by

$$(Q/A)_{max} = 0.18 \rho_v h_{wv} \left[\frac{\sigma g (\rho_w - \rho_v)}{\rho_v^2} \right]^{1/4} \left(\frac{\rho_w}{\rho_w + \rho_v} \right)^{1/2} . \qquad (2.3.5\text{-}20)$$

If the surface temperature $T_{0,s}$ is further reduced, the region of nucleate boiling is entered. The heat transfer is described e.g. by Rohsenow [42] by

$$Ste = \overline{C} Re_{bubble}^{1/3} Pr_w^s \qquad (2.3.5\text{-}21)$$

with

$$Ste = \frac{h_{wv}}{c_{pw}\Delta T}\,,$$

$$Re_{bb} = \frac{(Q/A)a}{\mu_w h_{wv}}\,. \qquad (2.3.5\text{-}22)$$

For water, s = 1 and $\bar{C} = 0.006$ are recommended. Thus, the heat flux density due to bubble boiling yields

$$(Q/A)_{bb} = \left[166.7\, \frac{k_w \Delta T}{a} \left(\frac{a}{\mu_w h_{wv}} \right)^{2/3} \right]^{1/3}. \qquad (2.3.5\text{-}23)$$

For the sake of completeness, natural convection at very small temperature differences is also considered. The heat transfer is characterized by

$$Nu_{conv.} = 0.14\,(Gr_w Pr_w)^{1/3} \qquad (2.3.5\text{-}24)$$

leading to

$$(Q/A)_{conv} = 0.14\,\Delta T \left[\frac{k_w \rho_w^2 g \beta_w \Delta T c_{pw}}{\mu_w} \right]^{1/3}. \qquad (2.3.5\text{-}25)$$

The boundary between natural convection and bubble boiling is fixed by

$$(Q/A) = Max\{(Q/A)_{bb}, (Q/A)_{conv}\}\,. \qquad (2.3.5\text{-}26)$$

With this set of equations, the complete boiling curves can be evaluated with the aid of a system of equations of state for equilibirium properties [43] and transport properties including the surface tension [44].

Figure 16 is a plot of the results obtained in the relevant pressure region between 1 and 10 bar. The computations have been carried out with a separate computer program BOIL.

The results as a function of equidistant logarithmic steps of the temperature difference ΔT are compiled in a set of data which is implemented into the subroutine SIEDE of the WECHSL code. Thus, the actual values for boiling heat transfer on the melt pool surface are determined by interpolation.

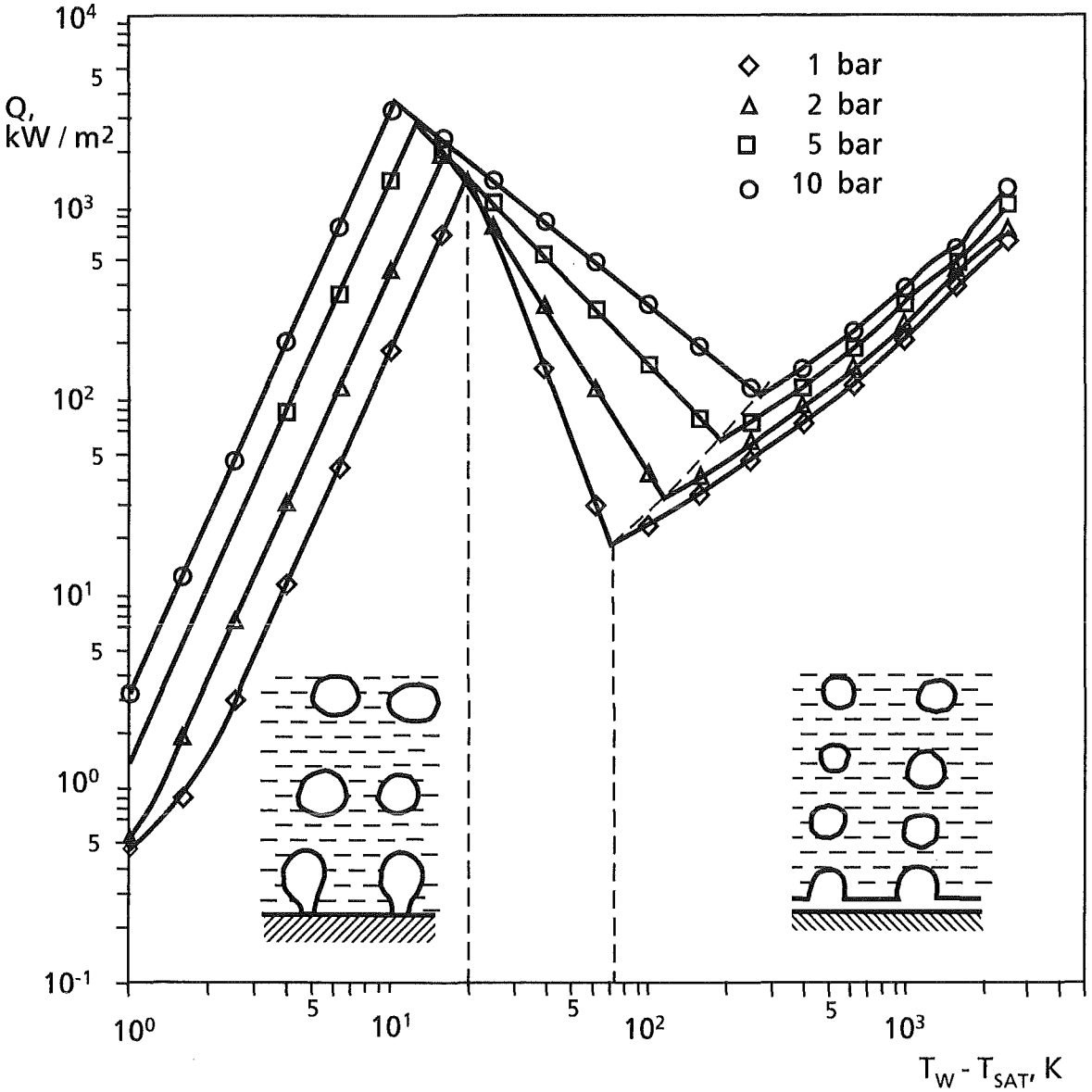

Figure 16: Boiling curves for water as a function of the system pressure.

2.3.6 Oxidation Reactions

Recently it was discovered that the reduction of the SiO_2 by the metallic zirkonium plays an important role. In the temperature range below about 2200 K the SiO_2 is reduced mainly to the metallic Si in an exothermic reaction. In addition the steam and the carbon dioxide bubbling through the metallic melt is reduced according to the reactions given below:

$$Zr + SiO_2 \rightarrow ZrO_2 + Si + r_{Zr,\,SiO_2} \,, \tag{2.3.6-1}$$

$$r_{Zr,SiO_2} = 2.1 \cdot 10^3 \quad in\ J/g\ Zr \,, \tag{2.3.6-2}$$

$$Zr+2H_2O \rightarrow ZrO_2+2H_2+r_{Zr,H_2O} ,$$

$$r_{Zr,H_2O}=7760+1.15(T_m-2000) \quad in\ J/g\ Zr ,$$

$$Zr+2CO_2 \rightarrow ZrO_2+2CO+r_{Zr,CO_2} ,$$

$$r_{Zr,CO_2}=5926 \quad in\ J/g\ Zr , \qquad (2.3.6\text{-}3)$$

$$Si+2H_2O \rightarrow SiO_2+2H_2+r_{Si,H_2O} ,$$

$$r_{Si,H_2O}=17.9\cdot 10^3 \quad in\ J/g Si , \qquad (2.3.6\text{-}4)$$

$$Si+2CO_2 \rightarrow SiO_2+2CO+r_{Si,CO_2} ,$$

$$r_{Si,CO_2}=12.3\cdot 10^3 \quad in\ J/g\ Si , \qquad (2.3.6\text{-}5)$$

$$2Cr+3H_2O \rightarrow Cr_2O_3+3H_2+r_{Cr,H_2O} ,$$

$$r_{Cr,H_2O}=3504+2.79\,(T_m-2000) \quad in\ J/g\ Cr , \qquad (2.3.6\text{-}6)$$

$$2\,Cr+3CO_2 \rightarrow Cr_2O_3+3CO+r_{Cr,CO_2} ,$$

$$r_{Cr,CO_2}=2780 \quad in\ J/g\ Cr , \qquad (2.3.6\text{-}7)$$

$$Fe+H_2O \rightarrow FeO+H_2+r_{Fe,H_2O} ,$$

$$r_{Fe,H_2O}=56.7-2.24\cdot 10^{-5}\,(T_m-2000) \quad in\ J/g\ Fe , \qquad (2.3.6\text{-}8)$$

$$Fe+CO_2 \rightarrow FeO+CO+r_{Fe,CO_2} ,$$

$$r_{Fe,CO_2}=-377+0.0271(T_m-2000) \quad in\ J/g\ Fe . \qquad (2.3.6\text{-}9)$$

Other reactions are also possible theoretically, but it can be found in the literature that the equilibrium constants for reactions yielding Fe_2O_3, Fe_3O_4 and NiO are such that only a very small fraction of the gases can be reduced in these reactions.

Calculations based on a diffusion model [45] show that the above reactions proceed rapidly towards equilibrium. The equilibrium constants for the reactions (2.3.6-1) through (2.3.6-7) lie very near to complete reduction of H_2O and CO_2. For the reactions (2.3.6-8, 9), equilibrium constants are given in the relevant literature, they do not suggest that the reaction of the gases is complete. However, the composition of the gas recorded in the BETA tests could be reproduced much better under the assumption of complete reduction of steam and carbon dioxide to hydrogen and carbon monoxide by oxidation of iron.

The reactions are assumed to proceed in the order Zr:Si:Cr:Fe so that Fe is oxidized only when all available Zr, Si and Cr has been burnt out.

The reaction enthalpies per g metal are also given in Eqs. (2.3.6-1, 2, 3, 4, 5, 6, 7, 8, 9). Reactions (2.3.6-1) through (2.3.6-7) are strongly exothermic. Reaction (2.3.6-8) is slightly exothermic and reaction (2.3.6-9) is slightly endothermic.
It is assumed that each bubble contains a single gas constituent; therefore, the water-gas reactions do not compete with the gas-metal reactions within the melt. The rationale for this assumption is that each bubble is probably generated from a relatively small area of concrete. Some bubbles are expected to contain mostly CO_2, from decomposition of a lump of limestone; other bubbles will contain mostly H_2O, from decomposition of the cement matrix. However, above the melt the gases will be well mixed, and the water-gas reaction can be expected to be homogeneous:

$$H_2O + CO \rightleftharpoons H_2 + CO_2 \,. \tag{2.3.6-10}$$

The equilibrium constant depending on the reaction temperature T_{reac} is given by

$$log_{10} K_p = -1.7778 + \frac{2010}{T_{reac}} \tag{2.3.6-11}$$

where

$$K_p = \frac{p_{H_2}\, p_{CO_2}}{P_{H_2O}\, P_{CO}} \,. \tag{2.3.6-12}$$

An additional reaction considered in the WECHSL code is the thermite reaction

$$Zr + 2FeO \rightarrow ZrO_2 + 2Fe + r_{Zr\,FeO} \,, \tag{2.3.6-13}$$

$$r_{Zr\,FeO} = 5124 \quad in\ J/g\ Fe \,.$$

This reaction is strongly exothermic and extremely rapid. In combination with the reactions (2.3.6-1, 2, 3) any metallic zirconium present would be depleted within a short period of time.

2.3.7 Material Properties

Powers and Frazier have described in [46] the VISRHO subroutine, i.e. a method of accurate computation of densities and viscosities of magmatic melts containing silicates. This method is applied in WECHSL to the constituents of a core melt in a core melt accident and a thermite melt in a simulation test, respectively. The formation of $CaAl_2O_4$ is taken into account if CaO and Al_2O_3 are constituents of the melt.

The density of each phase is computed from the mole fraction X_i, the molecular weight M_i, the partial molar volume V_{Mi}, the thermal coefficient of volumetric expansion β_i, and the bulk temperature T by

$$\rho = \frac{\sum_{i=1}^{n} X_i M_i}{\sum_{i=1}^{n} X_i V_{Mi}\left(1+\beta_i (T-1673)\right)} . \qquad (2.3.7\text{-}1)$$

The values of the molar mass M_i; best estimate values of the molar volume V_{Mi} and the thermal coefficient of volumetric expansion β_i at a reference temperature of 1400 °C are compiled in Table 3.

In VISRHO the dynamic viscosity of a magmatic melt in Poise is obtained from

$$\mu = exp\left\{\sum_{i=1}^{n} X_i D_i\right\} \qquad (2.3.7\text{-}2)$$

where the coefficients D_i are tabulated in [46] for different ranges of silica contents between 35 mole% and 85 mole% and for temperatures ranging between 1200 °C and 1800 °C. From these tables, Arrhenius coefficients A_i, B_i are evaluated and used in WECHSL. They describe the temperature dependence of the coefficients D_i by

$$D_i = A_i + \frac{B_i}{T} . \qquad (2.3.7\text{-}3)$$

Component	M_i g/mole	V_i cm^3/mole	β_i (K^{-1})
UO_2	270	26.76	1.2x10^{-5}
ZrO_2	123.2	23.32	5.88x10^{-5}
FeO	71.85	12.8	16x10^{-5}
CaO	56.08	16.5	18x10^{-5}
SiO_2	60.09	26.8	0.9x10^{-5}
Al_2O_3	101.96	37.96	2.6x10^{-5}
Cr_2O_3	152	30.11	2.6x10^{-5}
$CaAl_2O_4$	142.04	54.5	20.6x10^{-5}
Fe	55.85	7.7	3.1x10^{-5}
Zr	91.22	15.7	1.65x10^{-5}
Cr	52.0	8.67	1.8x10^{-5}
Ni	58.71	7.55	3.9x10^{-5}

Table 3: Masses and densities of oxidic and metallic constituents, reference temperature 1400 °C.

No data are available in [46] for the constituents UO_2 and ZrO_2 . For these substances, the coefficients for TiO_2 are used. The Arrhenius coefficients are extrapolated for low silica fractions to give reasonable results for pure corium and pure Al_2O_3, respectively, and for high silica fractions to reproduce the viscosity data of pure silicate.

In the method originally described in [46] coefficients were used which were considered to be constant within a range of silica contents. However, it has been found that the jumps in viscosity in passing from one silica range to the next may cause severe numerical disturbances under some circumstances. Therefore, linear interpolation is used to give smooth transitions.

Skoutajan et al. [47] investigated experimentally the viscosity of corium/silicate melts at temperatures between 1300 °C and 1600 °C. They found that the VISRHO calculations give values far below the experimental data. A much better representation of their experimental data can be found by presuming the precipitation of solid particles of the high melting oxides (i.e. UO_2, ZrO_2, CaO) between the liquidus and the solidus temperatures of the melt. The empirical Kunitz-formula [48] for liquid/solid mixtures

$$\frac{\mu_{LS}}{\mu} = \frac{1+0.5\,\Gamma}{(1-\Gamma)^4} \qquad (2.3.7\text{-}4)$$

with

$$\Gamma = \frac{T_L - T_{LS}}{T_L - T_S} \sum_{i=1}^{n_h} \Psi_i \qquad (2.3.7\text{-}5)$$

is used, where μ_{LS} is the viscosity of the liquid/solid mixture at a temperature T_{LS} between the liquidus temperature T_L and the solidus temperature T_S, and $\Sigma\psi_i$ is the sum of weight fractions of the high melting constituents (i.e. UO_2, ZrO_2, CaO).

In Figure 17, the results of the modified VISRHO calculations are compared with the experimental data. As can be seen, most of the measurements are made between case A (reactor concrete as given in [47] with 73.1 wt.-% SiO_2) and case B (87.2 wt.-% SiO_2). For 0%/100 % and 10 %/90 % corium/concrete mixtures, the measurements carried out beyond the liquidus temperature, for the 30 %/70 % and 50 %/50 % corium/concrete mixtures the measurements have been carried out between the solidus and the liquidus temperature where Eq. (2.3.7-4) is applicable.

In the simulation experiments performed in the BETA test facility, the oxidic corium melt is replaced by the oxidic part of a thermite melt which is usually Al_2O_3. Consequently, the knowledge of the viscosity of mixtures containing Al_2O_3 and SiO_2 is also important in the evaluation of the simulation tets. In [46], measurements of the dynamic viscosity of Al_2O_3/SiO_2 mixtures are compiled from the literature. They were performed at temperatures between 1900 °C and 2350 °C which is always beyond the relevant liquidus temperature. Figure 18 gives the comparison of the modified VISRHO calculation with the experimental data.

For the metallic phase, the viscosity is assumed to be that of pure iron, the major metallic constituent. According to the data of [49], the metal viscosity is equated by

$$log_{10}\left(\frac{\mu}{\mu_o}\right) = \frac{2385.2}{T} - 0.5958\ . \qquad (2.3.7\text{-}6)$$

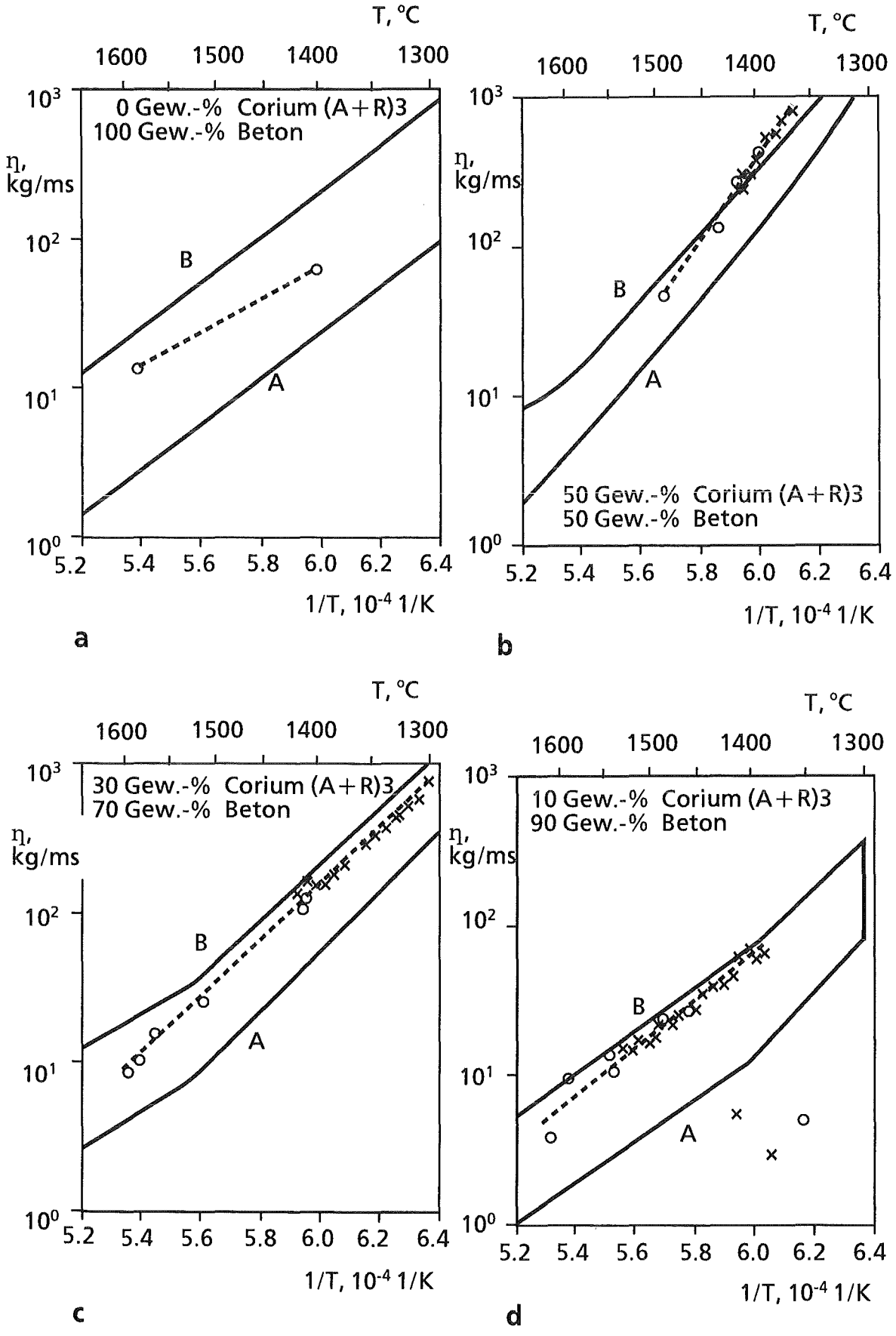

Figure 17: Comparison of viscosity measurements with calculated results of corium mixed with siliceous concrete.

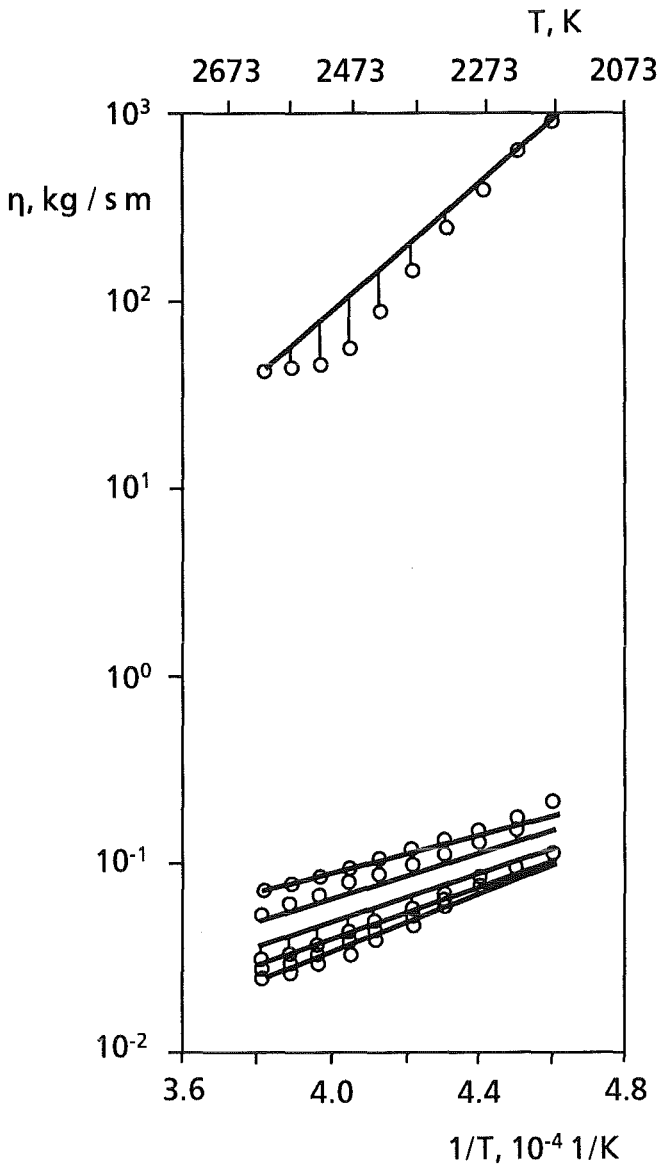

Figure 18: Comparison of viscosity measurements with computed results for molten Al_2O_3/SiO_2 mixtures.

Specific heat, latent heat of freezing and surface tension are computed with the simple mixture theory. In general the thermal conductivity of two phase materials will not obey the rule of mixtures, i.e. the resulting conductivity of a mixture of two phases will not only depend on the conductivitiy of the pure phases and their concentration. Assuming a spherical shape of the dispersed metallic phase the conductivity λ_{Mix} of the oxide/metal mixture is calculated in accordance with [55] from the following equation:

$$[(1-c_m)(\lambda_m-\lambda_o)]^3 = (\lambda_m-\lambda_{Mix})^3 \frac{\lambda_o}{\lambda_{Mix}} \qquad (2.3.7\text{-}6a)$$

where

c_m is the volume fraction of the dispersed metal in the oxidic phase.

The conductivity of the metallic phase is given by

$$\lambda_m = \frac{1}{2}\left[\sum_{i\in\{M\}} f^i_m \lambda^i_m + \left(\sum_{i\in\{M\}} \frac{f^i_m}{\lambda^i_m}\right)^{-1}\right] \qquad (2.3.7\text{-}6b)$$

and that of the oxidic phase by

$$\lambda_o = \left(\sum_{i\in\{O\}} \frac{f^i_o}{\lambda^i_o}\right)^{-1} . \qquad (2.3.7\text{-}6c)$$

f^i_m and f^i_O are the mass fractions of the i-th metallic component and i-th oxidic component, respectively.

Enthalpies are determined as shown in Figure 19. The enthalpy is approximated by

$$h = c\,(T - T_o)\ ,\ T_o = 298\,K \qquad (2.3.7\text{-}7)$$

in the solid region,

$$h = c(T - T_o) + h_{LS}\frac{T - T_S}{T_L - T_S} \qquad (2.3.7\text{-}8)$$

in the region between liquidus and solidus temperatures and

$$h = c\,(T - T_o) + h_{LS} \qquad (2.3.7\text{-}9)$$

in the liquid region of each molten layer. Note that the specific heat capacity is assumed to be constant over the temprature range of interest. This approximation is reasonably good for liquid metal, but it is not very accurate for some of the oxide constituents.

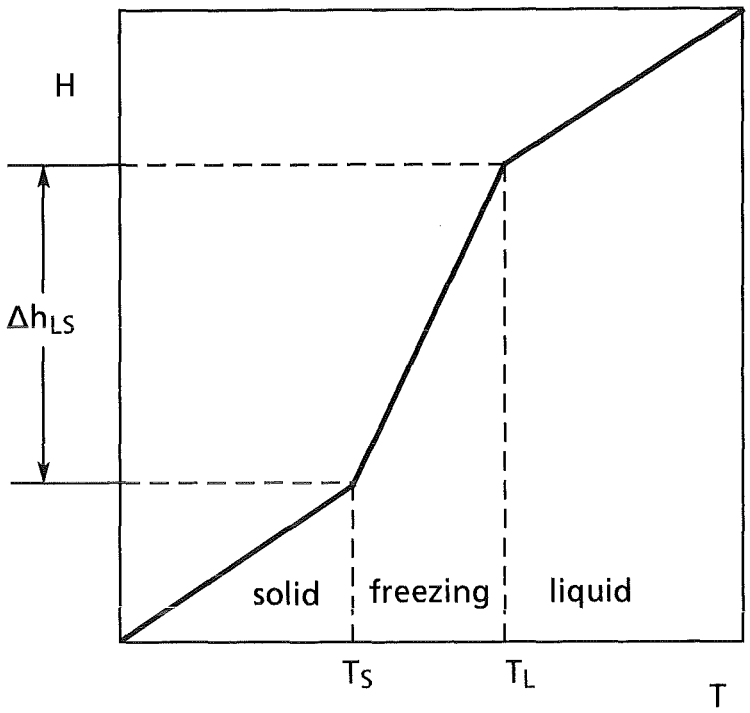

Figure 19: Enthalpy determination for each layer of the melt.

For the description of the gas behavior (i.e. in the gas film or discrete bubble model), properties of the steam/carbon dioxide mixture released from the concrete must be provided. The properties of the individual species, namely specific volume v_1 at reference pressure

$$p_1 = 1\ bar \tag{2.3.7-10}$$

specific heat capacity c_p, dynamic viscosity μ, and thermal conductivity k, are evaluated in WECHSL from tables given in [50] within the temperature range

$$373\ K < T < 3600\ K \tag{2.3.7-11}$$

For determining the density of the gas mixture, the gas species are considered as perfect gases.

Then, for a given temperature, the actual gas constant for each species i is:

$$R_i = \frac{p_1 v_{1i}}{T} \tag{2.3.7-12}$$

and the actual molecular weight is

$$M_i = \frac{\mathbb{R}}{R_i}\ . \tag{2.3.7-13}$$

For a given mass fraction γ_i, the molar fraction X_i is

$$X_i = \frac{\gamma_i / M_i}{\sum_i \gamma_i / M_i} . \tag{2.3.7-14}$$

Then, the gas constant of the mixture is

$$R_{mix} = \frac{\mathbb{R}}{\sum_i \gamma_i M_i} \tag{2.3.7-15}$$

and the density of the mixture yields

$$\rho_{mix} = \frac{p}{R_{mix} T} . \tag{2.3.7-16}$$

The specific heat capacity is

$$c_p = \sum_i \gamma_i c_{pi} . \tag{2.3.7-17}$$

The transport properties of the gas mixture are derived by a method described in reference [51]. The dynamic viscosity of the mixture is

$$\mu_{mix} = \sum_{i=1}^{n} \frac{X_i \mu_i}{\sum_{j=1}^{n} X_j \Phi_{ij}} \tag{2.3.7-18}$$

and the thermal conductivity

$$k_{mix} = \sum_{i=1}^{n} \frac{X_i k_i}{\sum_{j=1}^{n} X_j \Phi_{ij}} \tag{2.3.7-19}$$

where

$$\Phi_{ij} = \frac{1}{2\sqrt{2}} \left(1 + \frac{M_i}{M_j} \right)^{-1/2} \left\{ 1 + \left[\frac{\mu_i}{\mu_j} \left(\frac{M_j}{M_i} \right)^{1/2} \right]^{1/2} \right\}^2 . \tag{2.3.7-20}$$

2.3.8 Freezing Behavior

The solidus and liquidus temperatures of the oxide phase are computed by a method suggested by Ondracek [52]. In this procedure, the multiphase melt is reduced to a binary system with a high melting point component (the molten corium oxides UO_2, ZrO_2 and CaO, Cr_2O_3 with melting temperatures between 2700 K and 3000 K, index 1) and a low melting point component (SiO_2, FeO, $CaSiO_3$ with melting temperatures around 1800 K, index 2).

If ideal mixing of the liquid components and formation of ideal mixture crystals are assumed, the van Laar Equations (see i.e. [53]) are valid:

$$X_L = \frac{exp(N_L) - 1}{exp(N_L) - exp(M_L)} \tag{2.3.8-1}$$

and

$$X_S = \frac{exp(N_S) - 1}{exp(N_S + M_S) - 1} \tag{2.3.8-2}$$

with

$$N_{L,S} = \frac{\Delta H_{LS,2}}{\mathbb{R}} \left(\frac{1}{T} - \frac{1}{T_{(L,S),2}} \right) \tag{2.3.8-3}$$

and

$$M_{L,S} = \frac{\Delta H_{LS,1}}{\mathbb{R}} \left(\frac{1}{T_{(L,S),1}} - \frac{1}{T} \right) \tag{2.3.8-4}$$

where

X	- molar concentration,
ΔH_{LS}	- molar latent heat of freezing,
$T_{L,S}$	- liquidus and solidus temperatures, resp.,
T	- melt bulk temperature,
$\mathbb{R}$	- universal ideal gas constant.

The data for the molar latent heat of freezing ΔH_{LS} given in the literature ranges for the constituents of the oxide melt between 7680 J/mol for SiO_2 and 138 000 J/mol for FeO.

By selecting values for ΔH_{LS} and $T_{L,S}$ of the low and high melting point components and by solving the above equations, the composition dependent liquidus and solidus temperatures of the fictitious two-phase melt with ideal mixing behavior are found.
Skokan et al. [9] measured the composition dependent solidification temperature for mixtures of corium at different oxidation levels with different types of concrete.

As shown in Figure 20, their experimental data for siliceous concrete can be

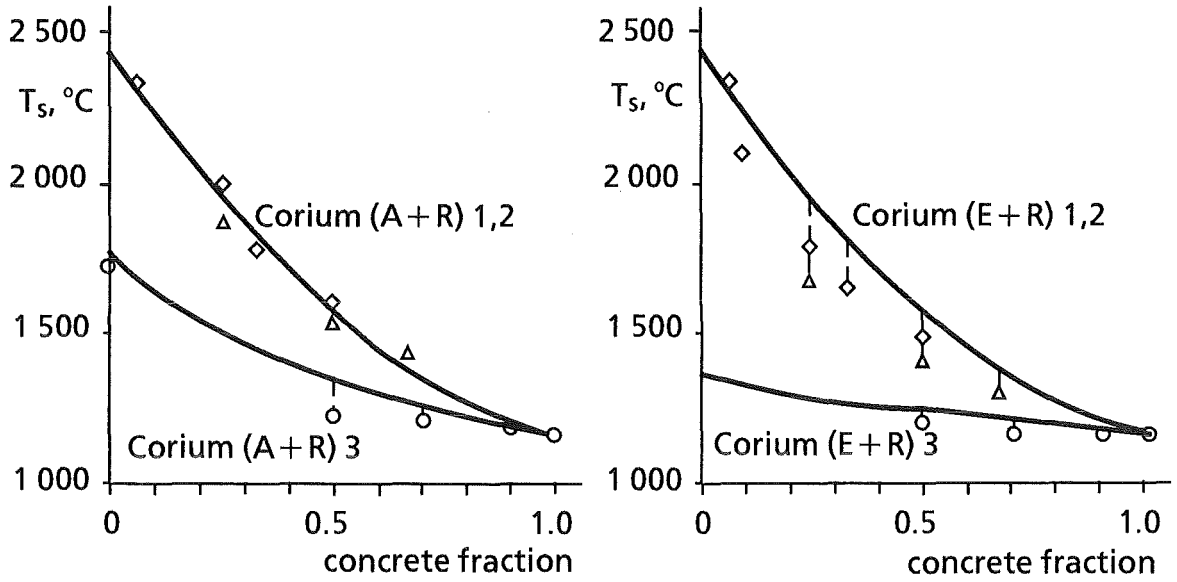

Figure 20: Solidification temperature of corium/concrete mixtures: comparison of measured and calculated values.

reproduced with sufficient accuracy when selecting for completely oxidized corium (A+R, E+R) 3 is selected:

$$T_{S,1} = 2323\ K,\ \Delta H_{LS,1} = 80\,000\ J/mol,$$
$$T_{S,2} = 1423\ K,\ \Delta H_{LS,2} = 24\,840\ J/mol. \qquad (2.3.8\text{-}5)$$

For partly or not oxidized corium (A+R, E+R) 1,2 the following equations hold:

$$T_{S,1} = 2723\ K,\ \Delta H_{LS,1} = 110\,000\ J/mol,$$
$$T_{S,2} = 1423\ K,\ \Delta H_{LS,2} = 14\,000\ J/mol. \qquad (2.3.8\text{-}6)$$

It should be noted that the liquidus and solidus points in the oxide phase are being constantly lowered as the siliceous concrete constituents dilute the oxide material. At the same time, the melt temperature drops because of cooling. The apparent specific heat of the melt is higher between the solidus and liquidus temperatures because of partial solidification of the melt; this, evidently, decreases the cooling rate.

The concept of ideal mixing is not applicable to calcareous concrete without any silicates. The measurements [9] show a minimum for the solidification

temperature at 50 wt.-% corium/50 % wt.-% calcareous concrete indicating strong deviations from the ideal mixing behavior.

It is assumed that the solidus and liquidus temperatures of a dispersed melt equal the ones of pure oxidic melt.

The principal constituents of the metal melt are Cr, Fe, and Ni. The metal melt may freeze during an accident. Consequently, the phase diagram of this ternary system must be considered for the solidification process. A single fit to the ternary Cr-Fe-Ni phase diagram was constructed by Bartel et al. [54]. The liquidus and solidus temperatures, expressed in Kelvin, are approximated by

$$\begin{aligned} T_L = max\,(&2130 - 510\,\Psi_{Fe} - 1140\,\Psi_{Ni}\,,\\ &1809 - 90\,\Psi_{Cr} - 440\,\Psi_{Ni}\,,\\ &1728 - 200\,\Psi_{Cr} - 40\,\Psi_{Fe}\,,\\ &1793 - 230\,\Psi_{Cr} - 130\,\Psi_{Ni})\,, \end{aligned} \tag{2.3.8-7}$$

$$\begin{aligned} T_S = max\,(&2130 - 730\,\Psi_{Fe} - 3310\,\Psi_{Ni}\,,\\ &1809 - 90\,\Psi_{Cr} - 560\,\Psi_{Ni}\,,\\ &1728 - 250\,\Psi_{Cr} - 100\,\Psi_{Fe}\,,\\ &1783 - 310\,\Psi_{Cr} - 140\,\Psi_{Ni}, 1613) \end{aligned}$$

where are the weight fractions of the metal melt. The current coding ignores the presence of other elements in the metallic phase, and renormalizes so that

$$\Psi_{Cr} + \Psi_{Fe} + \Psi_{Ni} = 1\,. \tag{2.3.8-8}$$

It is known that Si which is formed during the condensed phase Zr/SiO_2 chemistry Eq. (2.3.6-1) will lower the solidus temperature of the metallic melt. This effect is not yet modeled in WECHSL. As it was shown in the BETA V.5 test series [56], the B_4C has only a minor influence on the solidus temperature of the metallic phase.

In general, the surface temperatures of the molten pool are below the bulk temperatures. Consequently, these temperatures will drop at first below the freezing temperature of the melt and crust formation will occur. The process of

onset of crust formation and crust growth with transient heat conduction inside the crust is described in Section 2.2.6.
For the oxide phase, the criterion of crust formation is that the temperature in the boundary layer drops below the solidus temperature of the oxide.

For the metal phase, the criterion of crust formation is that the boundary layer temperature drops below a freezing temperature situated between the solidus and liquidus temperatures of the mutal phase as defined below:

$$
\begin{aligned}
&If \quad T<T_{sol} \quad : T_{freez} = T_{sol} \; ; \\
&If \quad T_{sol}<T<T_{liq} \quad : T_{freez} = \frac{2T_0 + T_{sol}}{3} \; ; \\
&If \quad T>T_{liq} \quad : T_{freez} = \frac{2T_{liq} + T_{sol}}{3} \; .
\end{aligned}
\tag{2.3.8-9}
$$

With this criterion of freezing, a reasonable behavior was obtained of the WECHSL computations compared with the low power BETA test results.

2.4 Supplementary Features of the WECHSL Code

2.4.1 Cavity Shape

The cavity is constrained to be axially symmetric; except for this constraint, any shape may be selected. Because of the variation in erosion rate around the periphery and the constantly changing level of the melt, the cavity shape undergoes permanent alteration.

The pool is divided into segments which are chosen such that the peripherial lengths Δ_s are equal with the exception that the phase boundary and the upper surface always occur at the segment boundaries. Each segment has the form of a (conical) frustum between two nodes (Figure 21).

The heat fluxes and the resulting erosion velocity are computed at the nodes; it is assumed that the velocity vector at each node in the outward direction normal to the rotational symmetric segment is limited by a circle passing through that node and the two adjoining nodes. New node positions are computed, and the periphery is rezoned so that all nodes are again equidistant from each other (except for the nodes at the phase boundary and at the free surface). This rezoning introduces a rough form of filtering so that bizarre cavity shapes caused by numerical problems are inhibited.

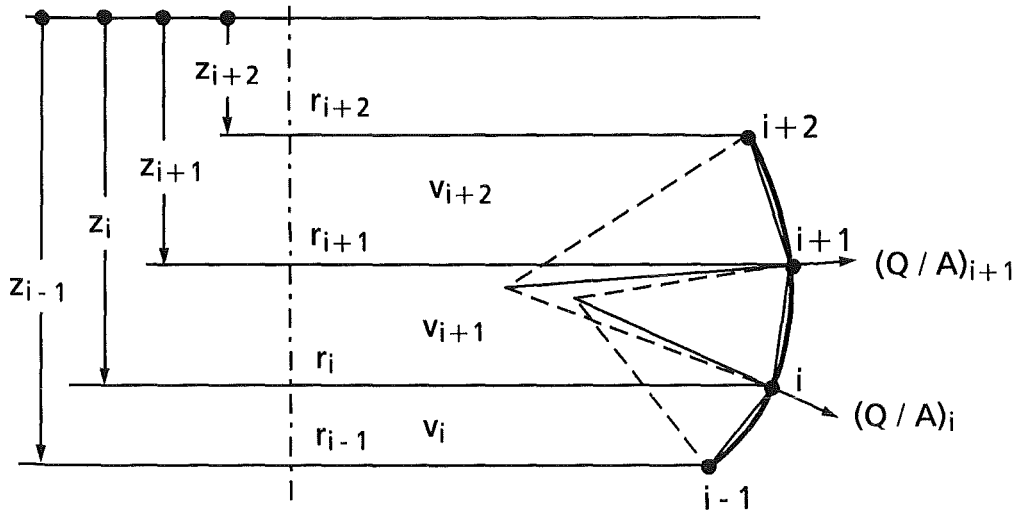

Figure 21: Cavity geometry.

It should be pointed out that the velocity vector is based on a rotational symmetric segment limited by a circle passing through three adjacent nodes, whereas the surface integral of heat flux and the new volumes are computed as if the cavity were composed of conical frusta. The new positions of the nodes are based on the assumptions first made. This could lead to discrepancies between the mass and volume. The mass discrepancy has been checked for a number of typical runs and found to amount to less than 1 % after several thousand time steps if cavity zoning is sufficiently fine.

During a core melt accident, crust formation and freezing is calculated to start at the metal layer, whereas the freezing temperature of the oxide layer is continuously being reduced. Thus, the situation occurs where the rate of melt front propagation of the oxide layer is higher than that of the metal slug. Consequently, the oxide pool starts to bypass the metal slug, as shown in Figure 22. Geometrical modeling in the WECHSL code was extended to cover also that situation.

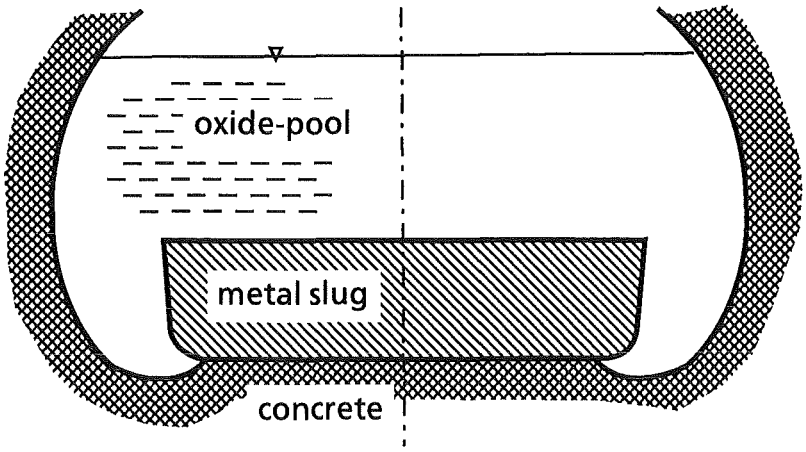

Figure 22: Cavity formation for a heavily encrusted or solidified metal layer.

2.4.2 Simplified Calculation Scheme for the Gas Film Model

2.4.2.1 Laminar Flow Regime

Calculations with the WECHSL code proved that numerical integration of the differential equations (2.2.3-27) for the laminar gas film and (2.2.4-27,43) for the turbulent gas film by means of a RUNGE-KUTTA-method required too much computation time compared with other parts of the code. Therefore, Reinecke [24] developed a simplified calculation scheme both for the laminar and turbulent gas films which shall be summarized here.

Equation (2.2.3-27) (valid for the laminar gas film) can be rearranged to give

$$\frac{\delta^3}{1+Nu_{rad}\delta}d\delta=\frac{4}{3\phi-2}\frac{\Psi_g}{Gr\,Pr\,Ste\,\sin\alpha}d\zeta. \qquad (2.4.2\text{-}1)$$

As Nu_{rad} depends only on the temperatures at the melt surface and at the concrete surface which are constant for each melt layer, Nu_{rad} is constant in Eq. (2.4.2-1). The other dimensionless groups, namely Gr, Pr, and Ste, depend only on material properties and are again constant between the melt layer and the concrete. However, the angle of inclination α of the melt front with respect to the horizontal can change very strongly according to the shape of the cavity. Therefore, Eq. (2.4.2-1) cannot be integrated in a closed form but only stepwise with constant angle of inclination α. In WECHSL, the interval is given as the distance $\Delta\zeta$ between two nodes i, i+1. This integration yields

$$6(Nu_{rad}\delta)_{i+1} - 3(Nu_{rad}\delta)^2_{i+1} + 2(Nu_{rad}\delta)^3_{i+1} - 6ln(1+Nu_{rad}\delta)_{i+1} = \tag{2.4.2-2}$$

$$\frac{4}{3\phi - 2\,Gr\,Pr\,Ste\,sin\alpha}\frac{\Psi_g}{}6Nu^4_{rad}\Delta\zeta + 6(Nu_{rad}\delta)_i - 3(Nu_{rad}\delta)^2_i + 2(Nu_{rad}\delta)^3_i - 6ln(1-Nu_{rad}\delta)_i$$

or, abbreviated

$$A_{i+1} = \frac{4}{3\phi - 2\,Gr\,Pr\,Ste\,sin\alpha}\frac{\Psi_g}{}6Nu^4_{rad}\Delta\zeta + A_i \tag{2.4.2-3}$$

where A is a function of the parameter $Nu_{rad}\,\delta$. The inverse function is

$$Nu_{rad}\delta = f(A) \tag{2.4.2-4}$$

and it is attempted now to find an analytical approximation function in the possible range of values of the quantity A. After some trials, the function

$$Nu_{rad}\delta = 10^b A^n \tag{2.4.2-5}$$

was found to be most convenient. The parameters b and n can be derived from Table 4 by interpolation

A	b	n
$4.21532\cdot10^{-4}$	$-1.38655\cdot10^{-2}$	0.255701
$4.59945\cdot10^{-3}$	$-4.57386\cdot10^{-5}$	0.260525
$1.01591\cdot10^{-2}$	$4.40342\cdot10^{-3}$	0.262577
$5.00419\cdot10^{-2}$	$1.26954\cdot10^{-2}$	0.267651
0.101325	$1.58377\cdot10^{-2}$	0.270342
0.502209	$2.05461\cdot10^{-2}$	0.277689
1.00494	$2.10744\cdot10^{-2}$	0.281254
4.97413	$1.79809\cdot10^{-2}$	0.290184
200.0766	$8.05687\cdot10^{-3}$	0.299708

Table 4: Parameters for laminar gas film.

To compute the melt front propagation, the mean value of the film thickness in the considered interval $\Delta\zeta$ must be evaluated. For that purpose, the exponents b and n are determined from Table 4 for the mean value of A_i and A_{i+1}. Then, the integrated mean value of the gas film thickness yields by integrating Eq. (2.4.2-5)

$$\delta_{i+\frac{1}{2}} = \frac{10^b \quad A_{i+1}^{n+1} - A_i^{n+1}}{Nu_{rad}(n+1)(A_{i+1} - A_i^{)}} \tag{2.4.2-6}$$

Equation (2.2.3-20) applies again for calculating the total heat transfer, with the mean film thickness δ as given by Eq. (2.4.2-6).

2.4.2.2 Turbulent Flow Regime

In the turbulent regime, the increase in the laminar sublayer characterizing the heat transfer is described by the system of coupled differential equations (2.2.3-27,43). An analytical solution in an interval as derived for the laminar flow regime is not possible in the turbulent region. Some substantial simplifications must be introduced in order to obtain an approximative solution.

The basic idea in solving the problem comprises again a stepwise integration of the differential equation over an interval. At first, the ratio of the total film thickness to the thickness of the laminar sublayer,

$$\Theta_{i+1} = \left(\frac{\delta_c}{\delta} \right)_{i+1} \tag{2.4.2-7}$$

is calculated with the value δ_i kept constant over the interval $i \rightarrow i+1$ to give, in principle

$$\Theta_{i+1} = \Theta_i + A_1 \frac{1 + Nu_r \delta_i}{\delta_i} \Delta\zeta \, . \tag{2.4.2-8}$$

Equation (2.2.3-43) may be written in a simplified form as

$$\frac{d\delta}{d\zeta} = \frac{A_1(1 + Nu_r \delta) + A_2 + A_3 \Theta \delta^3}{\Theta - A_4} \, . \tag{2.4.2-9}$$

This non-linear differential equation cannot be solved analytically. In order to establish an approximative solution, the variable thickness of the laminar sublayer is written as

$$\delta_{i+1} = \delta_i + \Delta\delta) \tag{2.4.2-10}$$

or

$$\delta_{i+1} = \delta_i (1 + \varepsilon) \, .$$

Consequently, Eq. (2.4.2-9) yields

$$\frac{d}{d\zeta}(\Delta\delta)=\frac{A_1(1+Nu_r\delta_i)+A_2-A_3\Theta\delta_i^3}{\Theta-A_4} + \frac{A_1 Nu_r - A_3\Theta\delta_i^2(3+3\varepsilon+\varepsilon^2)}{\Theta-A_4}\Delta\delta \,. \tag{2.4.2-11}$$

If the factor ε is kept constant inside the interval, Eq. (2.4.2-11) is transferred into a linear differential equation with the solution

$$\Delta\delta=\frac{B_2}{B_1}[1-exp(-B_1\Delta\zeta)]\,. \tag{2.4.2-12}$$

The constants in the equation above are defined as

$$A_1=\frac{\rho_g}{\rho_c}\frac{g}{y^{+2}PrSte}\,,$$

$$A_2=\frac{f_{TP}}{2}+\frac{\rho_g}{\rho_c}\frac{1}{y^{+2}}\,, \tag{2.4.2-13}$$

$$A_3=\frac{\rho_g}{\rho_c}\frac{Gr\sin\alpha}{y^{+4}}\,,$$

$$A_4=1-\frac{1}{3}\frac{\rho_g}{\rho_c}\,,$$

$$B_1=\frac{3A_1\Theta\delta_i^2(1+\varepsilon+\frac{\varepsilon^2}{3})-A_1Nu_r}{\Theta-A_4}\,, \tag{2.4.2-14}$$

$$B_2=B_1\frac{A_1(1+Nu_r\delta_i)+A_2-A_3\Theta\delta_i^3}{3A_3\Theta\delta_i^2(1+\varepsilon+\frac{\varepsilon^2}{3})-A_1Nu_r}\,.$$

Extensive numerical investigations revealed that the accuracy of the result is dependent on a convenient estimation of the parameter ε, especially in the regime of transition from laminar to turbulent flow. Finally, the following attempt proved to be successful:

By division of Eq. (2.4.2-12) by δ_i and using the definition of the constants (2.4.2-13, 14)

is obtained. Under the assumption

$$\varepsilon_{i+1} = \frac{A_1(1+Nu_r\delta_i)A_2 - A_3\Theta\delta_i^3}{3A_3\Theta\delta_i^3(1+\varepsilon_i+\frac{\varepsilon_i^2}{3}) - A_1 Nu_r \delta_i} \cdot \left[\, 1-exp(-B_1\Delta\zeta) \,\right] \tag{2.4.2-15}$$

$$\varepsilon_{i+1} = \varepsilon_i = \varepsilon, \tag{2.4.2-16}$$

Eq. (2.4.2-15) yields

$$\varepsilon\left[a_2(1+\varepsilon+\frac{\varepsilon^2}{3}) - a_3 \right] = -a_1 \left\{ 1-exp\left[[a_4(1+\varepsilon+\frac{\varepsilon^2}{3}) - a_5]\Delta\zeta \right] \right\} \tag{2.4.2-17}$$

with the constants being defined by

$$a_1 = A_3\Theta\delta_i^2 - \frac{A_1(1+Nu_r\delta_i)+A_2}{\delta_i},$$

$$a_2 = 3A_3\Theta\delta_i^2,$$

$$a_3 = A_1 Nu_r, \tag{2.4.2-18}$$

$$a_4 = \frac{a_2}{\Delta - A_4},$$

$$a_5 = \frac{a_3}{\Delta - A_4}.$$

Equation (2.4.2-17) must be solved by an iteration scheme based on regula falsi. Test calculations involving variation of all parameters revealed a systematic underestimation on the order of 6.5 % of the heat transfer rate by the approximative solution when compared with the values obtained by direct integration of the differential equation using a RUNGE-KUTTA-method. Consequently, a correction factor f was introduced

$$f = \frac{1}{1-(1-c)f_T} \tag{2.4.2-19}$$

where

$$f_T = 1 \quad for\ T - T_{freez} \geq 200$$

and (2.4.2-20)

$$f_T = \frac{T-T_{freez}}{200} \quad for\ T - T_{freez} \leq 200.$$

The constant c is defined by

$$c = 1 - 0.0642 \cdot \left[\, 1-exp(-3.89 \cdot \Delta\zeta) \,\right]. \tag{2.4.2-21}$$

To evaluate the melt front propagation, a mean thickness of the laminar sublayer characteristic of heat transfer in the turbulent flow regime is needed. The relevant equations are

$$\overline{\Delta\delta}_{i\to i+1} = \frac{B_2}{B_1} - \frac{\Delta\delta_{i+1}}{B_1 \Delta\zeta} ,$$
$$\overline{\delta}_{i\to i+1} = \delta_i + \overline{\Delta\delta}_{i\to i+1} . \qquad (2.4.2\text{-}22)$$

With the approximative calculation scheme for gas film heat transfer as described above for the laminar and turbulent flow regimes, the melt front propagation as calculated by direct integration of the differential equations by means of a RUNGE-KUTTA-method has been reproduced with sufficient accuracy. As an example, Figure 23 shows a comparison of both methods of cavity formation during a core melt accident in the cylindrical cavity of a German standard PWR.

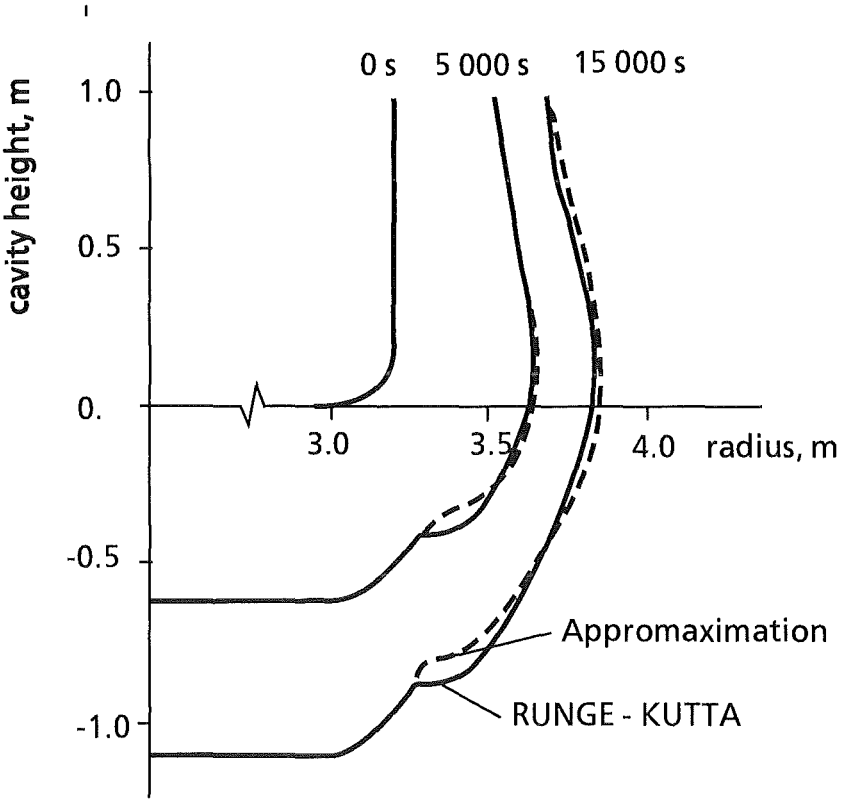

Figure 23: Comparison of cavity formation during a core melt accident:
a) by approximative gas film calculation scheme;
b) by integration of the differential equations by means of a RUNGE-KUTTA-method.

2.4.3 Energy Balance

The internal heat sources from the decay heat can be prescribed in WECHSL as a function of time for each layer of the melt. The energy flux balance considers the energy gain by these internal sources from chemical reactions, and by the enthalpy fluxes into each phase; the energy gain or loss by exchange of energy between the phases and by exothermal or endothermal chemical reactions, and the energy losses from each phase by heat transfer to the concrete, enthalpy fluxes out of the phase, and heat radiation from the upper surface to the environment yields an energy flux balance for an isobaric system:

$$\frac{dH_b}{d\tau} = \sum_k \boldsymbol{m}_k h_k + \sum_\ell Q_l + \Omega_{chem} + \Omega_{decay} \qquad (2.4.3\text{-}1)$$

where H_b is the bulk enthalpy of the melt layer under consideration, Ω_{decay} is the heat source due to nuclear decay, Ω_{chem} is the heat gain or loss due to exothermal or endothermal chemical reactions inside this layer, $\mathbf{m}_k$ are the mass fluxes of material entering or leaving the layer and carrying the specific enthalpy h_k, and Q_l are the convective heat fluxes passing the boundaries of the layer.

At each time step, properties are computed with the bulk temperatures and the melt composition from the previous time step; heat transfer rates are computed on the basis of these properties.
The new bulk enthalpy for the time $\tau_{j+1} = \tau_j + \delta\tau$ is then computed by

$$H_{bj+1} = H_{bj} + \left[\sum_k \boldsymbol{m}_k h_k + \sum_\ell Q_l + \Omega_{chem} + \Omega_{decay} \right] \delta\tau \qquad (2.4.3\text{-}2)$$

and the new mass of the melt layer is

$$m_{bj+1} = m_{bj} + \sum_k \boldsymbol{m}_k \delta\tau \qquad (2.4.3\text{-}3)$$

New temperatures are then computed by

$$T_{bj+1} = \left(\frac{H_{bj+1}}{m_{bj+1}} + \Delta + c_p T_o \right) / c, \qquad T_o = 298\,K \qquad (2.4.3\text{-}4)$$

where

$$for \quad T_{bj} \le T_{sol}: \ \Delta = 0, c = c_p$$

$$for \quad T_{liq} > T_{bj} > T_{sol}: \Delta = \frac{h_{LS}}{T_{liq} - T_{sol}} T_{sol}; \quad c = c_p + \frac{h_{LS}}{T_{liq} - T_{sol}} \tag{2.4.3-5}$$

$$for \quad T_{bj} \geq T_{liq}: \Delta = -h_{LS}; \quad c = c_p$$

The new melt layer temperatures are determined by Eqs. (2.4.3-4,5) for homogeneous layers (completely liquid, slurry, or solid). At the surfaces of the metal layer facing the concrete and the oxide layer, crusts of substantial thickness may be formed. In that case, the metal bulk mass is split up into a liquid and a solid fraction.

As for the crust formation only a one-dimensional model is used, the actual fraction of the solid material is unknown. In order to get an appropriate first estimation of the fractions of solid and liquid materials, the surface areas of the metal layer covered by crusts, i.e., the area facing the concrete and the interface area between the metal and the oxide layer, are multiplied by the relevant increase in the crust thickness, as determined by the one-dimensional transient crust growth model, and the density, to give the solid mass change Δm_s. With the solid fraction ϕ_s evaluated by adding the mass increase to the solid mass and dividing by the total metal mass m_b, energy balances are established to give the new enthalpies for the liquid fraction

$$H_{lj+1} = H_{lj} + \left[\left(\sum_i m_i h_i + \Omega_{chem} + \Omega_{decay} \right) \left(1 - \phi_s \right) + Q_{int} - \gamma \cdot Q_{conc} \right] \delta\tau - \Delta m_s h_{LS} \tag{2.4.3-6}$$

and for the solid fraction

$$H_{sj+1} = H_{sj} + \left[\left(\sum_i m_i h_i + \Omega_{chem} + \Omega_{decay} \right) \phi_s - (1-\gamma) Q_{conc} \right] \delta\tau + \Delta m_s h_{LS} \tag{2.4.3-7}$$

where Q_{int} is the heat gain through the metal-oxide interface, Q_{conc} is the heat consumed by the highly endothermal concrete decomposition process, and γ is the ratio of heat fluxes entering the crust by thermal conduction at the metal melt/solid interface and leaving the crust to cause concrete decomposition. The total bulk enthalpy is the sum of the liquid and solid enthalpies as given in Eqs. (2.4.3-6,7).

The temperature of the solid fraction is evaluated as being the mean temperature of the crusts by using the temperature distribution inside the crusts as evaluated

with the transient heat conduction model. With these temperatures, $H_{l\,j+1}$ is recalculated by

$$H_{lj+1} = H_{bj+1} - c_p (T_{sw} \cdot m_{sw} + T_{si} \cdot m_{si}) \qquad (2.4.3\text{-}8)$$

where subscript "sw" assigns the metal crust facing the concrete and subscript "si" the metal crust at the metal/oxide interface. The temperature of the liquid fraction is then computed by means of Eqs. (2.4.3-4,5).

For complete freezing of the metal layer, two cases are considered:

- the solid mass fraction exceeds the total mass of the metal layer, or
- the temperature of the liquid bulk drops below the thermodynamic freezing temperature.

After complete freezing, one-dimensional, transient heat conduction is considered in vertical direction inside the metal slug and a correction is used for taking into account sidewall effects.

An integrated energy balance and an integrated mass balance are maintained and can be printed out periodically. Because of numerical roundoff and approximations, the enthalpy or mass at any time will not be equal to that computed from the inital enthalpy or mass and the integrated gains and losses. However, the errors are always less than 1 % and normally insignificantly small.

3. Description of the CALTHER Code

The CALTHER subroutine package can be activated as an option in WECHSL-MOD3.

It allows calculation of the radiative heat transfer from the corium to the walls and bottom of the dry reactor vessel cavity. The bottom can be considered to consist of steel (it could represent the non-molten part of the RPV) or concrete. Under radiative heat transfer, the walls heat up and are allowed to melt. The molten products are then added to the corium mass, and the resulting gases to the gases originating from the corium.

In the current version, the gas temperature has been assumed until now to be the mean temperature between the gas temperature as calculated in WECHSL before water-gas reaction and the temperature of the concrete cavity walls.

In the version, proposed here, only H_2O is considered to be an absorbing gas in radiative heat transfer.

As a consequence, the CALTHER subroutines package gives a correct answer for the effects on the MCCI thermohydraulic in the current version, but care must be taken regarding the results on gas production as separate components (H_2, H_2O, CO, CO_2).

3.1 General description and modelling

The part of the reactor vessel cavity not in contact with the corium must be defined as being composed of the following "components":

- the top surface (or the free surface) of the corium;
- the concrete walls of the reactor vessel cavity which can be modelled as annular surfaces, each assumed to be at a uniform axial temperature;
- the remaining reactor vessel (RPV) which can be modelled as steel slabs;
- the gas mixture with the absorbing gases H_2O, CO_2 and CO produced during decomposition of the concrete.

NOTA: The top surface of the corium is not allowed to move, i.e. the height of the annular surfaces stays constant all over the calculation.After the first minutes of MCCI, when the void fraction of the corium is less than 10 percent, this assumption is correct for a reactor basemat composed of a silicate - containing concrete, because of the low

gas content of this kind of concrete (less than 6 percent mass of water per kg of eroded concrete) when erosion takes place.
For a limestone-common sand type of concrete the free surface of the corium decreases with time, after the first swelling of the melt.

It means that, in all cases, the CALTHER option must be used with care, and common sense of the engineer is necessary.

The aerosol release during an MCCI would affect radiative heat transfer in the cavity, causing absorption and scattering effects. The lack of experimental data on these aerosols characteristics does not allow us to properly model these effects, which may be significant only during the initial high-temperature phase of the interaction.

Figure 24 shows a simple example of a cavity configuration used in CALTHER:

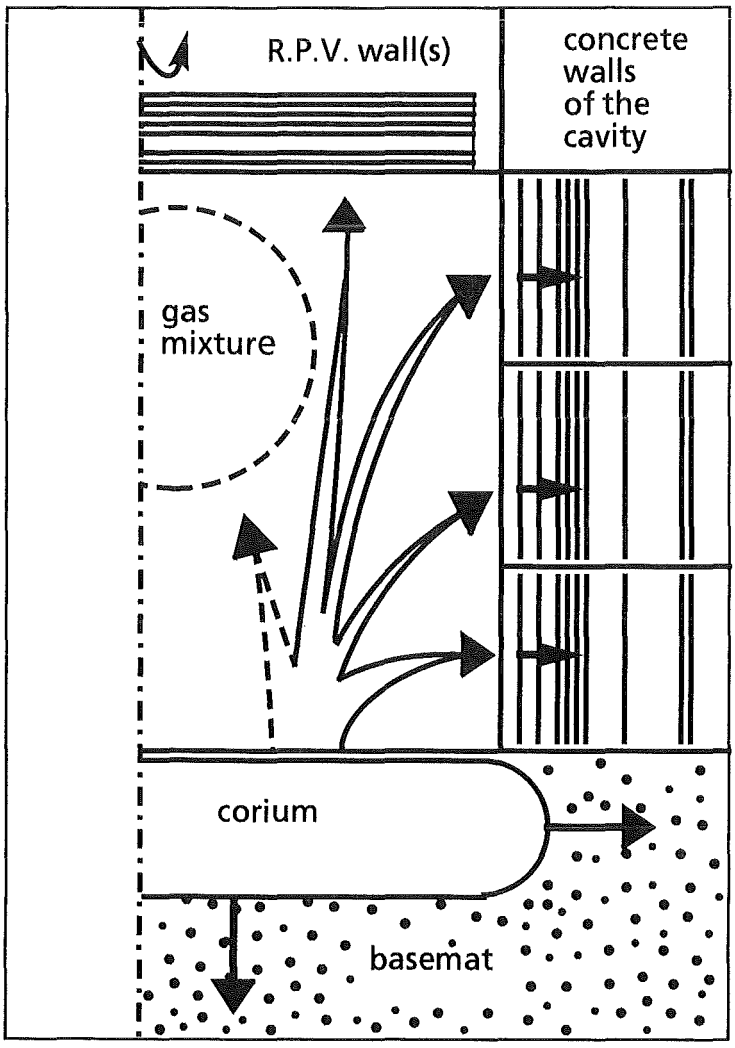

Fig. 24: Cavity configuration: corium, 3 concrete walls, gas mixture

At the beginning of a time step, all the surface temperatures are known (the surface temperature of the corium is given by WECHSL).

A gas absorption model calculates the mean transmittance of the gas mixture from the characteristics of each absorption band. Then a radiative heat transfer model determines the net heat flux to each surface as well as to the gas mixture, which is supposed to be at a temperature between the levels of the various wall components of the cavity. This assumption is valid when no significant cooling by natural convection occurs in the cavity due to an almost plugged venting shaft.

In that case preliminary computations have shown that the exchanges by internal natural convection are always negligible. The present version of the code does not consider convection effects.

The net surface fluxes previously computed by the radiative heat transfer model are used as internal boundary conditions by the thermal conduction model to calculate the thermal behavior and the ablation of each wall component. This model is linked to a mechanistic model of gas release for concrete walls.
In spite of the possible ablation of the walls, the view factors and the mean beam lengths are kept constant during the calculation.

3.2 The radiative heat transfer model of the cavity

This model provides:

- the net radiative heat flux on each component of the cavity enclosure as a function of wall and gas temperatures;
- the energy deposited in the gas mixture, which may absorb and emit radiation.

The geometrical configuration of the cavity (Fig. 25) is described by view factors and geometric mean beam lengths between the surfaces of the enclosure. All the surfaces are treated as gray diffuse emitters and reflectors. The gas mixture is assumed to be isothermal.

The general steady-state equations for determining radiative exchanges in a gray diffuse enclosure of N surfaces are based on the net-radiation enclosure model [61], using the total interchange area S_iS_j between the wall surfaces and the gas mixture [62]. The surface factors S_iS_j, which characterise the geometry and reflectivity of the cavity, represent the part of the surface A_i whose radiative emission is absorbed after reflections at all surfaces by the surface j:

$$Q_{i \to j} = S_i \; S_j \; C_o \; T_i^4$$

These S_iS_j quantities are the solution of the following relations which are solved by Gaussian elimination.

$$\sum_{m=1}^{N}\left[\frac{\delta_{mk}}{\varepsilon_m A_m}-\frac{(1-\varepsilon_m)}{\varepsilon_m A_m}F_{km}\,TR_{km}\right]S_j\,S_m=\varepsilon_j\,F_{kj}\,TR_{kj}\quad with\ k=1,...,N\ and\ j=1,...,N$$

ε_m: emissivity of surface m
F_{km}: view factor between the two surfaces k and m
TR_{km}: mean gas transmittance between surfaces k and m
A_m: area
δ_{mk}: Kronecker delta

The SiSj surfaces are calculated with a much lower frequency than the thermal behaviour of the walls because these parameters are weak functions of the temperatures of the enclosure.

The total interchange are S_iS_g between a surface and the gas mixture results from the equation of conservation of the energy emitted by this surface:

$$A_i\,\varepsilon_i=\sum_{j=1}^{N}S_i\,S_j+S_i\,S_g$$

The net radiative flux on a surface S_i and on the gas mixture is:

$$Q_i==\sum_{j=1}^{N}(S_i\,S_j\,E_i-S_jS_i\,E_j)+S_i\,S_g\,E_i-S_g\,S_i\,E_g$$

$$Q_g=-\sum_{j=1}^{N}Q_j\quad (energy\ balance\ in\ the\ cavity\ enclosure)$$

3.3 The gas-absorption model

This model provides for each absorbing gas:

- the characteristics of each absorption band;
- the transmittance TR_{ij} (B) between the surfaces i and j for each band B.

A mean transmittance TR_{ij} is calculated by summing up the contributions of the (2B+1) spectral intervals delimited by the B bands of the gas mixture (B=5 for H_2O alone). This sum is weighted by the Planck black-body radiation distribution.

Outside an absorption band, TR_{ij} (B) is equal to 1. The transmittance TR_{ij} (B) can be evaluated at the temperature T_i of the radiation emitting surface through the gas or at the mean temperature (choice in the input data).

The transmittance of each band is obtained from the statistical Goody-Mayer model assuming a random distribution of spectral lines within a band. Under the conditions of a MCCI, the line profile obeys the Lorentz profile (collision broadening lines), and TR_{ij} (B) is a simple expression of the characteristics of the absorption bands (bandwidth, line width-to-spacing ratio, band intensity). These band properties which depend on the gas nature, partial and total pressure and gas temperature, are given by the Thomson correlations.

The only gas component calculated in the current version is H_2O. The non-condensable gases CO_2 and CO, which have also a few important absorption bands, are not yet introduced. A user option enables calculations to be made without an absorbing gas mixture.

3.4 Thermal conduction model

The one-dimensional heat conduction equation is solved implicitly for each wall by a finite difference approximation of the following equation:

$$C_v\, r^a\, \frac{dT}{dt} = -\frac{d\phi}{dr} + qvol\, r^a \qquad \phi = -r^a\, k\frac{dT}{dr}$$

qvol: volumetric heat source J/m3
α: geometrical factor (plane: α=0; cylindric: α=1)
C_v: volumetric heat capacity J/m3

The 1D-approximation is sufficient because the changes in T in the radial direction are much greater than the changes in the axial direction.

3.5 Boundary conditions

The flux ϕ_s calculated by the heat exchange model is imposed at the inner surface, and a temperature for the outer surface is contained in the input data. The inner surface may move with time due to ablation. In this case, the velocity of the melt front is given by:

$$\frac{dX}{dt} = \frac{1}{h_d}\left\{\phi_s + r^a\, k(T)\frac{dT}{dr}\right\}$$

h_d: specific latent heat of melting, in J/m^3
ϕ_s: heat flux at the inner surface, in W/m^2
and the temperature of the face mesh is limited to the melting temperature. This mesh is eliminated when it is completely molten. Inside a partially melted mesh the melt front can also move back in case of freezing. Typical mesh sizes in the concrete and steel walls at the melt front location are 0.01 m and 0.10 m, respectively. The multi-layer wall slabs use a node-size distribution defined in the data.

3.6 Gas-release model

Only the most important aspects are computed: the energy sinks due to concrete decompositions, the location of the three decomposition fronts, and the mass flow rates of free water, bound water and CO_2. This model is strongly linked to the thermal conduction model. Continuity equations describe the composition distributions. Momentum equations are not considered; thus, the pressure distribution and the gas flows inside the walls are not calculated.

When a concrete wall is heated, the conditions for various types of release are:

- Free water at the local saturation temperature inside the wall. This value is contained in the data (approximately 400 K for MCCI conditions).
- Bound water between 530 K and 770 K due to decomposition of hydroxides.
- CO_2 between 900 K and 1300 K due to decomposition of calcium carbonates.

The free-water release mechanism is similar to the mechanism of ablation. Bound water and CO_2 are released according to Arrhennius kinetic laws which, using the concrete decomposition heats, permit to calculate the corresponding energy sink.

3.7 Validation of the thermal and gas-release models

A series of realistic-scale experiments have been conducted at the CEA to study the thermal response and gas release of concrete cylindrical specimens (1 m length and 1.13 m diameter). The slabs were heated on one side and quite well instrumented to measure the temperature on different axes and at different levels. The CO_2 kinetic correlation developed with these results has been incorporated into the code. Figures 25 and 26 illustrate a comparison between data and the calculation of a test performed with a limestone-common sand type of concrete sample.
The comparisons show that this simple model is sufficient to calculate the thermal behaviour of the cavity under MCCI conditions.

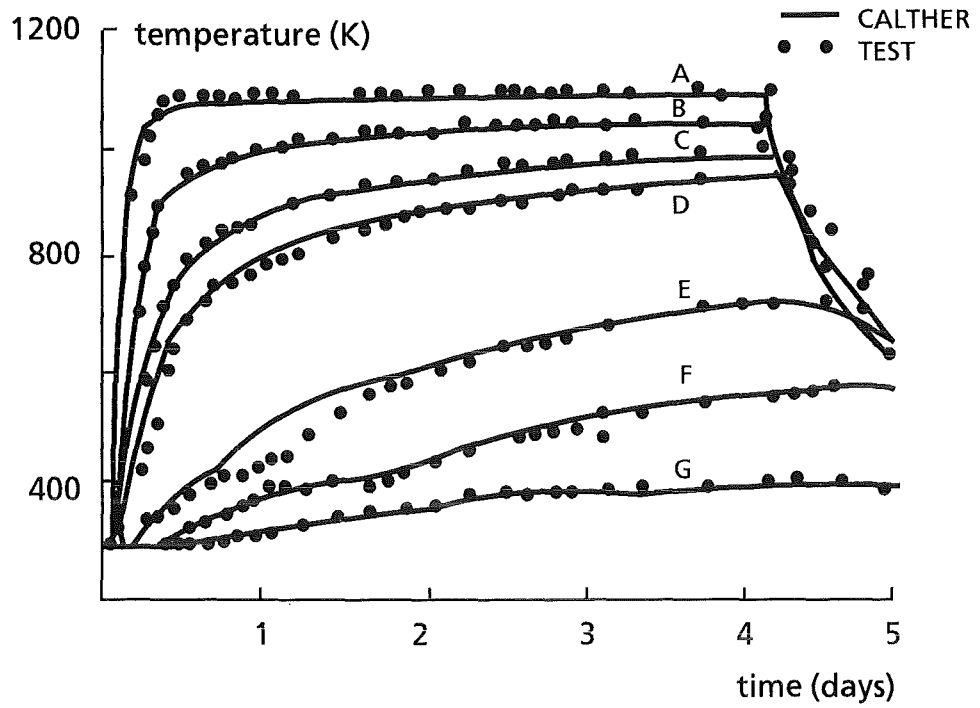

Fig. 25: Temperature evolution at different elevations

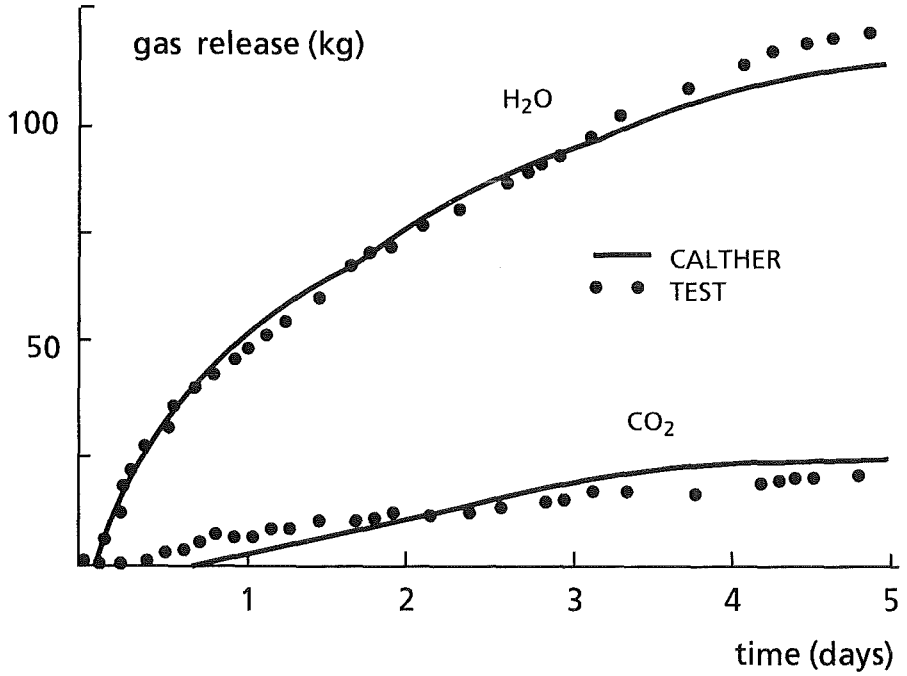

Fig. 26: Total mass of released H_2O and CO_2

4. Instructions for the Use of the WECHSL Code

4.1 WECHSL Code Characteristics

The code is written in FORTRAN 77, input and output data are in SI units. The amount of printout and of plot output data is user controlled.

The WECHSL code is capable of restart. The following input and output files are provided:

Content	Dataset reference number
- control parameters	1
- initial input data	3
- cleaned data (auxiliary)	4
- restart input (unformatted)	2
- print of detailed results	6
- print of selected results as time dependent tables	30 to 35
- plot data for diagrams	8
- plot data for cavity shape	9
- output for next restart (unformatted)	22

The principal structure of the MAIN program operating the WECHSL subroutine is shown in Figure 27. The program starts by reading the variable ISTEU from the control parameter file.

For an initial WECHSL run, ISTEU = 0.
Then the initial input data are read and handled with the help of an auxiliary dataset, which may be temporary.

For a restart run, i.e. continuing the execution of the same problem, ISTEU has to be greater than 0. In that case, the new end time is read from the control parameter file and the actual values as well as the input tables are restored from the restart file. The initial input file itself is no longer used. As the print and plot options chosen for the initial run remain unchanged, they must be carefully selected for the initial data set.
Subsequently, the time loop is executed until the prespecified time limit is exceeded. It will be aborted before the end time is reached, if one of the following events occurs:

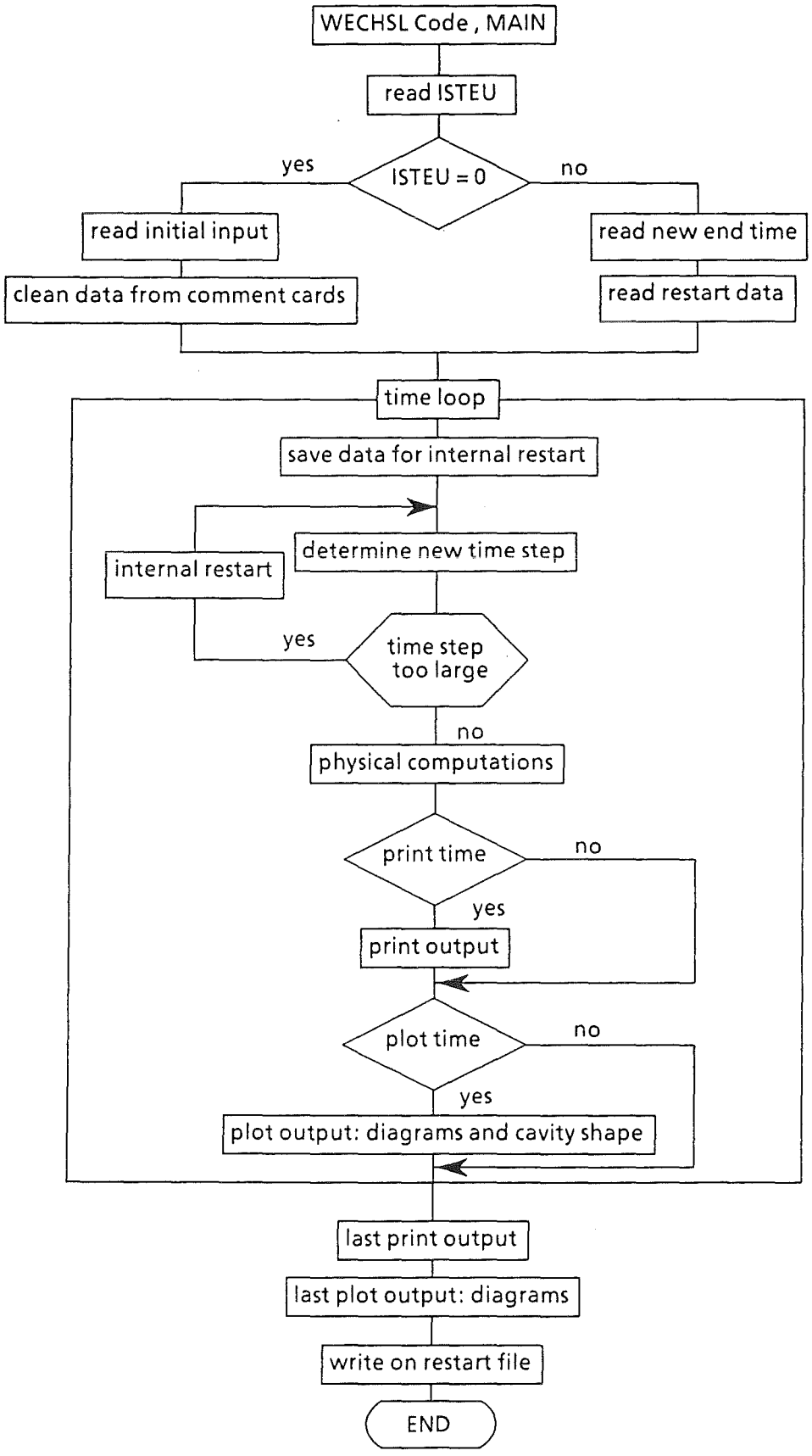

Figure 27: Simplified layout of data handling in the WECHSL code.

- The boundary temperature drops below the concrete ablation temperature.
- The single oxide layer is frozen.
- The basemat is penetrated by the melt.

The size of the time step is governed by the heat from oxide to concrete within the limits given by the user.

In the time loop, the output for print (detailed at particular times and summarized in tables) and the output of plot data (separately for diagrams and cavity shape) are made at intervals specified by the user. In order to reduce the amount of data, the list does not contain all the cavity coordinates but only those that were changed during the last time step.

After termination of the time loop, a final printout with a complete set of cavity points and plot output for diagrams is created. The cavity plot output is omitted if it does not match the prescribed time inteval. Finally, all the variables and arrays used for the calculation of this problem are stored in the restart output dataset. The problem can be restarted as many times as desired.

In the next sections, the input data are described in detail. Furthermore, the WECHSL output on the print and plot files are presented.

4.2 Input Description

4.2.1 Control Parameters

The first card has to be present in any case.

Card 1: (integer value)

ISTEU	=0 means initial run
	>0 means restart run

If ISTEU = 0, the next card may be omitted and the code proceeds by reading the initial input data. Additionally, the cleaned data file has to be allocated.

If ISTEU > 0, the next card gives the new end time and a restart input file must be available.

Card 2: (real value) - not used if ISTEU = 0.

TF	final problem time for the restart run in seconds

4.2.2 Initial Input Data

In contrast to Mod2, the present version requires input in free format. These data are necessary for the first run of a problem only. The number of input data cards varies depending on the type of the problem. Those cards which must always be present, are marked with the symbol '!'. To copy some of the input data, the "cleaned data file" must be allocated (see Section 3.3).

Comment Cards

It is convenient to insert comment cards in order to achieve a better readability. The symbol '*' in the first column identifies a card as a comment. It may be used at any place.

Data Cards

Problem identification:

! Card 1: 72 characters for text of problem identification

Thermite Addition:

! Card 2: (2 real values)
WTHEM - rate of thermite addition, kg/s
THERM - final time for thermite additions, s

Thermite is assumed to be added at a constant rate of WTHEM kg/s over THERM seconds. This card is used for some simulation tests in which a certain quantity of thermite is poured into the crucible at the beginning of the test. For calculation of melt down accidents, the variables can be entered as zeroes.

Metal and Oxide Addition

! Card 3: NADD - number of material (melt) additions to the crucible (integer value in the range of 0 to 10)

If NADD is not equal to zero, the set of the following 3 cards has to be available NADD times.

Card 4: addition characteristics (3 real values)
TADDB - initial time for addition, s
TADDE - final time for addition, s
TEMADD - temperature of added materials, K

Card 5: added oxides (7 real values)

KGADD (1) - added mass of UO_2 during this time, kg
KGADD (2) - added mass of ZrO_2 during this time, kg
KGADD (3) - added mass of FeO during this time, kg
KGADD (4) - added mass of CaO during this time, kg
KGADD (5) - added mass of SiO_2 during this time, kg
KGADD (6) - added mass of Al_2O_3 during this time, kg
KGADD (7) - added mass of Cr_2O_3 during this time, kg

Card 6: added metals (4 real values)

KGADD (11) - added mass of Fe during this time, kg
KGADD (12) - added mass of Zr during this time, kg
KGADD (13) - added mass of Cr during this time, kg
KGADD (14) - added mass of Ni during this time, kg

The input of the material is at a constant rate during each addition. The materials may be solid or liquid.
Note: TADDB (I+1) must be greater than or equal to TADDE (I), for all values of I.

Concrete Characteristics

! Card 7: (4 real values)

FC1 - weight fraction of $CaCO_3$ in concrete
FC2 - weight fraction of $Ca(OH)_2$ in concrete
FC3 - weight fraction of SiO_2 in concrete
FC4 - weight fraction of free water in concrete

Note: The weight fraction of Al_2O_3 is assumed to be FC5=1.-FC1-FC2-FC3-FC4.
The fractions are related to concrete without steel reinforcement.

! Card 8: (4 real values)

RBR - fraction of reinforcing steel: kg steel per kg concrete without reinforcement
TSB - melting temperature of concrete without steel, K
HC - decomposition enthalpy of concrete without steel, J /kg
RHC - density of concrete without steel, kg/m^3

Liquidus - Solidus Curves

Cards 9 to 13 define the liquidus and solidus curves for the oxide phase. A group of high melting points and a group of low melting points are considered.

Note: To simulate a core meltdown accident, the high temperature group would normally be UO_2 and ZrO_2. Note, however, that very small amounts of iron oxide drastically reduce the melting point and the reduced melting point should be used here. The low temperature group would normally be the concrete constituents, i.e. CaO and SiO_2. The latent heat is due to phase change only, and is not equivalent to the decomposition enthalpy of concrete.

The curves can either be given as an input table or calculated by the code with the help of the Schröder-van Laar equation (Eq. 2.3.8-1) with two components. The latter case requires the input of the effective latent heat, the solidus and the liquidus temperatures.

! Card 9: index variable for liquidus-solidus curves for the oxide phase (integer)

IMAT =1 means calculation with Schröder van Laar equation

>1 means table input with IMAT points (IMAT≤11)

! Card 10: low temperature material group (integer values)

NCOM1 - number of components in this group (1≤NCOM1≤6)

ICOM1(1) - index of the first component

ICOM1(2) - index of the second component

Repeat up to ICOM1(NCOM1), as required.

The indices for the components are as follows:

1 = UO_2 4 = CaO

2 = ZrO_2 5 = SiO_2

3 = FeO 6 = Al_2O_3

The calculation with the Schröder-van Laar equation (IMAT=1) requires the following card:

(!) Card 11a: properties of the low temperature group (3 real values)

DHS1	- effective latent heat of melting, J/mol
TS1	- solidus temperature for 'pure' low temperature group, K
TL1	- liquidus temperature for 'pure' low temperature group, K

Table input for the low temperature group ($1 < IMAT \leq 11$):

(!) Card 11b: input table with IMAT points (real values)

CCL (1)	- molar concentration for liquidus
TLL (1)	- liquidus temperature, K
CCL (2)	- as above
TLL (2)	- as above

Repeat until IMAT pairs are reached using additional cards if necessary.

! Card 12: high temperature material group (integer values)

NCOM2	- number of components ($1 \leq NCOM2 \leq 6$)
ICOM2(1)	- index of the first component
ICOM2(2)	- index of the second component

Repeat up to ICOM2(NCOM2), as required.

Indices for the components are the same as for the low temperature group.

The calculation using the Schröder-van Laar equation ($IMAT = 1$) requires following card:

(!) Card 13a: properties of the high temperature group (3 real values)

DHS2	- effective latent heat of melting, J/mol
TS2	- solidus temperature for 'pure' high temperature group, K
TL2	- liquidus temperature for 'pure' high temperature group, K

The table input for the high temperature group is analogous to that of the low temperature group:

(!) Card 13b: input table with IMAT points (max. 11) (real values)

CCS(1) - molar concentration of solidus

TSS(1) - solidus temperature, K

etc.

Repeat until IMAT pairs are reached using additional cards if necessary.

Description of the Oxide Phase of the Melt

! Card 14: initial oxide masses, kg (7 real values)

WT(1) mass of UO_2

WT(2) mass of ZrO_2

WT(3) mass of FeO

WT(4) mass of CaO

WT(5) mass of SiO_2

WT(6) mass of Al_2O_3

WT(7) mass of Cr_2O_3

Note: The problem must start with a finite mass of oxides.

! Card 15:

TO - initial temperature of oxides, K (real)

IVISC - option for calculation with an increased oxide viscosity during freezing (should be used only for tests with limestone concrete) (1 = yes, integer value)

Cards 16 through 18 give the internal heat sources in the oxide as a function of time.

! Card 16:

NIO number of pairs in the internal power table for oxide (integer value in the range of 0 to 80)

Note: If NIO = 0, the internal power of oxide is assumed to be zero.

Card 17: has to be omitted if NIO = 0 (2 real values)

TSH - shift time for internal heat generation, s

QIFAC - multiplication factor for internal heat source (oxide and metal)

The code shifts the time scale given in the table below for TSH seconds. The time difference between the time origin of the internal heat source and the contact time of the melt and concrete is taken into account by this shift.

Card 18: table of internal power of oxide - to be omitted for NIO = 0 (real values)

TIO(1)	- time for first point, s
QIO(1)	- power for first point, W
TIO(2)	- time for second point, s
QIO(2)	- power for second point, W
etc.	

Repeat up to NIO points, using additional cards if required.
Note: TIO(I + 1) must be greater than TIO (I), for all values of I.

Description of the Metal Phase of the Melt

! Card 19: initial metal masses, kg (4 real values)

WT(11)	- mass of Fe
WT(12)	- mass of Zr
WT(13)	- mass of Cr
WT(14)	- mass of Ni

Note: The initial mass of metal may be zero.

! Card 20: (1 real, 3 integer values)

TFM	- initial temperature of metals, K
IMEND	- option: remainder of metal will be neglected after complete oxidation of Zr (was used for a special test)
IZRCH	- option: reactions between Zr and SiO_2 will take place
IMIX	- option: metal phase is considered to be dispersed in the oxide phase and not to be a separate layer

Note: An option is operative when the corresponding index variable is set to 1 = yes

Card 21 and 22 give the internal energy sources in the metal as a function of time.

! Card 21:

NIM - number of pairs in the internal power table for metal (integer value in the range of 0 to 80)

Note: If NIM = 0, the internal power of the metal is assumed to be zero.

Card 22: table of the internal power of metal - to be omitted for NIM = 0
(real values)
TIM(1) - time for first point, s
QIM(1) - power for first point, W, etc.
Repeat up to NIM points using additional cards, if required.

Note: TIM (I+1) must be greater than TIM (I), for all values of I.

Time Characteristics for Execution of the Calculation

! Card 23: (4 real values)
DT - initial time step, s
TF - final time for calculation, s
DTMIN - minimum time step allowed, s.
DTMAX - maximum time step allowed, s.

Note: The initial time step should be chosen so that the temperature change is small, say ≤ 5 K. It is suggested that an initial trial be made with a roughly estimated time step. The code optimizes the time step in the range given by DTMIN and DTMAX.

Printout Times

! Card 24:

NTPR - number of different printout intervals (integer value in the range of 1 to 80)

! Card 25: table of printout intervals (real values)

TPR(1) - start time for the first printout interval, s

DPR(1) - time step for printout in first interval, s

etc.

Repeat as often as necessary up to TPR (NTPR), DPR (NTPR). Use additional cards, if required.

Note: TPR(I+1) must be greater than TPR(I), for all values of I.

Ambient Athmospheric Pressure

! Card 26:

NPP - number of couples in time-pressure table (integer value in the range of 1 to 80)

! Card 27: pressure table (real values)

TP(1) - time for first point, s

PP(1) - pressure for first point, bar

etc.

Repeat up to TP(NPP), PP(NPP). Use additional cards, if required.

Note: TP(I+1) must be greater than TP(I), for all values of I.

Ambient Temperature for Radiation from the Top of the Corium

! Card 28:

NTT - number of pairs in time-temperature table (integer value in the range of 1 to 80))

! Card 29: temperature table (real values)

TIT(1) - time for first point, s

TAM(1) - temperature for first point, K

etc.

Repeat up to TIT (NTT), TAM (NTT). Use additional cards if required.

Note: The time points must be written in ascending order.

Cavity Shape

There are different ways of defining the initial cavity shape. The type of card 31 and the use of card 32 depend on the option selected on card 30.

Note: The cavity must be deep enough to accommodate the entire melt including the increase of the volume of the melt caused by an increase of the void fraction during the concrete erosion process. The program stops, if the melt will spill over. The maximum allowable cavity discretization points are set to be 300. However, the initial number of cavity nodes should be less than 300 in order to account for the increase of the volume of the melt due to an increase of the void fraction. For a axisymmetric cavity, the right part of the cavity has to be defined in cylindrical coordinates. The initial bottom line of the cavity is located at y = 0.

! Card 30:	(2 integer values)		
	NB	- indicates the desired option and, in addition, the initial number of points for option I	
If NB < 1000 :		arbitrary shape with NB points	- Option I
If 1000≤NB<1500 :		cylinder with rounded corners	- Option II
If 1500≤NB<2000 :		cylinder with rounded corners and a conical upper part	- Option IIa
If NB≥2000		cylinder with hemispherical bottom	- Option III
	I1DIM	- option: one dimensional calculation, i.e. erosion only in downward direction (1 = yes)	

The next card has to be coded according to the selected option.

Option I - Arbitrary shape:

(!) Card 31/I	cavity points (real values)	
	RCAV(1)	- radius of the first point, m
	YCAV(1)	- height of the first point, m
	etc.	

Continue up to RCAV(NB), YCAV(NB). Use as many continuation cards as necessary.

Note: NB should not exceed 150 (see above)

000Option II - Cylinder with rounded corners:

(!) Card 31/II cavity description (2 integer, 4 real values)

NR - initial number of points in the horizontal part of the floor
NC - initial number of points in the rounded corner
RO - initial radius of the cylinder, m
RKL - initial radius of the corner, m
DELZ - initial interval between the points in cylindr. section, m
ZMX - initial height of the cavity, m

Option IIa - Additional input for conical section on the top of the cylinder, if option IIa is selected:

Card 32: (2 real values)

ZMXE - total height of the cavity, m
WIN - angle of inclination, deg.

Note: WIN is the angle between the conical part and the vertical center line of the crucible.

Option III - Cylinder with hemispherical bottom

(!) Card 31/III: cavity description (4 real values)

DPHI - initial central angle between points in the hemisphere, degrees
DELZ - initial interval between points in cylinder, m
RO - initial radius of hemisphere, m
ZMX - initial total height of cavity, m

(End of Option III)

! Card 33:

SMX - interval between cavity points during the execution of the program, m (real)

All points are automatically set to be equidistant.

Note: If SMX is too small, an excessive number of cavity points will be used. If SMX is too large, much of the cavity detail will be lost.

! Card 34: (3 real values)
RSUMP - radius for sump water ingression, m
ZMIN - erosion depth for basemat penetration, m
TSUMP - time for sump water ingression, s

Sump water floods the melt, if the radial erosion exceeds RSUMP or if the current time exceeds TSUMP. Flooding is avoided by choosing large values for RSUMP and TSUMP, respectively.

Print Options

! Card 35: index variables for printout (4 integer values)
KTEM - temperatures
KPROP - properties
KINT - interface
KMAS - masses

! Card 36: index variables for printout (cont.) (5 integer values)
KBAL - heat balance
KGAS - gas release
KCAV - cavity shape
KDIAG - diagnostics
K1DT - time dependent tables no. 4 to 6

If any of the quantities is different from zero, the corresponding print option will be executed. A zero value bypasses this print option.

Note: The time dependent tables number 1 to 3 are always printed.

Options for Output on Plot File

Note: The user has to provide his own plot programs.
For KfK-configuration standard programs are available.

! Card 37: index variable for plot output (2 integer values)
JCUR - plot of diagrams
JCAV - plot of cavity shape

Any value different from zero specifies that plot data are written on the plot files.

! Card 38: diagram plot (2 real, 1 integer value)
TPL - start time to write plot file, s
DPL - time step for writing data, s
IPLINT - option: change time step to 3600 s after 3600 s (in order to limit the amount of data) (1=yes)

! Card 39: cavity shape plot (2 real values)
TPLC - start time to write plot file, s
DPLC - time step for writing data, s

Note: Cards 38 and 39 must be present even if no plot output is desired.

! Card 40: JPDC - option: calculation with the CALTHER code linked to WECHSL (see CALTHER description for additional input) (1=yes, integer value)

4.3 Cleaned Data File

This file must be allocated during the initial run of a problem. The program copies data to this file which serves as a temporary storage for the input data, from which the comments have been removed.
The records are written in FORMAT (72A1).

4.4 Restart Files

As these files are not supposed to be read by the user, they contain unformatted data.

At the end of a regular run, i.e. if it is not aborted, the data required for program continuation are always stored on the restart output file.

If restart is desired, this former output file has to be used as input.

4.5 Output Description

4.5.1 Detailed Printout

At the beginning of an initial run, the input data are printed for control.

At the beginning of a restart run, the restart time is given.

Then, the actual values are printed at intervals defined by the user. The following data are given at each print time: time, next time step for computation, and cavity dimensions. Additional data output depends on the options selected on input cards 35 and 36.

If metal and oxide are situated in distinct layers, the following data are printed for metal and oxide separately. For metal dispersed in oxide only one value is available. The accompaning text will give the appropriate explanation.

KTEM $\neq 0$:

- pool (bulk) temperatures of the melt
- temperatures at the interface of the melt with concrete
- temperatures of the metal/oxide interface (if layered) and the surface of the melt
- actual liquidus and solidus temperatures of the melt
- temperatures of the gases leaving the melt
- temperature of the water-gas reaction
  This temperature is a constant predefined value in WECHSL.

KPROP $\neq 0$:

Bulk properties: density, thermal conductivity, specific heat, surface tension, and viscosity of the melt.

KINT≠0:
- erosion velocities for the pool/concrete interface
- energy fluxes at the pool bottom, sidewalls and surface
- information about the gas film model used

KMAS≠0:
- integrated mass balance in the melt
- masses, volumes, void fractions
- height of the melt
- weight fraction and percentage of each constituent in each phase
- crust thickness, if crust is formed at the boundaries of the melt

KBAL≠0:
- internal energy source, incoming and outcoming enthalpy fluxes, heats of chemical reactions, heat released to concrete, heat interchanged between the phases, heat radiated or evaporated from surface, heat loss due to splashout, and net heat gain or loss (denoted 'sensible heat')
- energy balance integrated from t=0 s, initial enthalpy, internal energy, incoming and outcoming enthalpy fluxes, reaction energy, energy transfered to concrete, energy radiated from the top of the melt, energy of splashout, sums of positive and negative energy, and the error in energy resulting from numerical balance

KGAS≠0:
- temperature of released gases
- heat flux, mass and molar rates, weight and molar fractions, total mass and moles released since t=0 s for each species of gas
- if sump water has flooded the corium: temperature, mass flow, enthalpy and total mass of the evaporated water. The reference point for the vapor enthalpy is 298 K, liquid water.

KCAV≠0:
- number of cavity coordinates relevant to the calculation
- coordinates in terms of radius and height

Note:
- The output at the start of a problem and at the end of each run contains the whole amount of cavity points.

- It can seen from the decrease of radius and hight in the same table that the oxides pass the metallic phase.

KDIAG≠0:
- diagnostics indicating numerical problems.

The occasional appearance of these diagnostics does not necessarily indicate a severe problem.

K1DT≠0:
- output for time dependent tables 4 to 6 will be generated

4.5.2 Table Printout

There are six time dependent tables printed during the program execution to give a general overview of the process. The time intervals are the same as for the detailed output.

Table 1:

- time, s
- heat flux radiated or evaporated at the top of the melt, W
- release of CO_2, kg/s
- release of CO, kg/s
- release of H_2O, including evaporated sump water, kg/s
- release of H_2, kg/s
- release of sump water, kg/s
- integrated mass of released CO_2, kg
- integrated mass of released CO, kg
- integrated mass of released H_2O, without sump water, kg
- integrated mass of released H_2, kg
- integrated mass of released sump water, kg

Table 2:

- time, s
- temperature of liquid metal, K
- temperature of solid metal, K
- temperature of oxide, K
- temperature of oxide surface, K
- temperature of released gases, K
- enthalpy stream of CO_2 gas, W
- enthalpy stream of CO gas, W
- enthalpy stream of H_2O gas, W
- enthalpy stream of H_2 gas, W
- enthalpy stream of all gases, W

The reference point for the gas enthalpies 298 K. To determine the energy fluxes into the containment, it is recommended to use instead of enthalpy fluxes the gas mass fluxes and associated gas temperatures as input for the containment code in order to avoid inconsistencies of enthalpy tables in different codes.

Table 3:

- time, s
- cavity radius at the top of the melt, m
- temperature of the oxide phase, K
- integrated mass of released CO, kg
- integrated mass of released CO_2, kg
- integrated mass of released H_2, kg
- integrated mass of released H_2O, without sump water, kg
- content of SiO_2 in the melt, kg

Table 4:

- time, s
- temperature of liquid metal, K
  (zero if not existent)
- temperature of solid metal, K
  (zero if not existent)
- temperature of released gases, K

- vertical erosion, mm
- release of H_2O, mole/s
- release of H_2, mole/s
- release of CO_2, mole/s
- release of CO, mole/s
- sum of released gases, mole/s

Table 5:

- time, s
- heat flux to the concrete at the bottom of the melt, kW
- heat flux to the concrete at the side of the melt, kW
- heat flux at the top of the melt due to gases and radiation, kW
- heat flux to the side in percent of the total heat flux given to the concrete, %
- vertical erosion, cm/h
- content of Zr in the melt, kg
- content of Cr in the melt, kg
- content of Ni in the melt, kg
- content of Fe in the melt, kg
- content of Si in the melt, kg
- content of C in the melt, kg

Table 6:

Originally created for special output of a evaluation of a particular experiment . In the present form not useful for other applications and therefore actually not printed.

4.5.3 Diagram Plot File

If an output for diagram plots is desired (option on input card 37), selected data are collected and written on this file so that the user can use them as input for his own plot program.

The time intervals are controlled by the content of card 38.

At the beginning of an initial run, the following records are written:

Section 1:

Record 1: Format (A72) - see input card 1
72 characters for problem identification

Record 2: Format (6E12.4) - see input card 11b
CCL(1), ... CCL(6) - molar concentration for liquidus curve

Record 3: Format (5E12.4) - as record 2
CCL(7),... CCL(11)

Record 4: Format (6E12.4) - see input card 11b
TLL(1), ... TLL(6) - liquidus temperature corresponding to CCL, K

Record 5: Format (5E12.4) - as record 4
TLL(7),... TLL(11)

Record 6: Format (6E12.4) - see input card 13b
CCS(1),... CCS(6) - molar concentration for solidus curve

Record 7: Format (6E12.4) - as record 6
CCS(7), ... CCS(11)

Record 8: Format (6E12.4) - see input card 13b
TSS(1), ... TSS(6) - solidus temperature corresponding to CCS, K

Record 9: Format (6E12.4) - as record 8
TSS(7), ... TSS(11)

Section 2:

At the end of each time interval records 10 to 25 are written on the plot file.
Note: The user should take care that for a restart run these data are appended to the previous data.

Record 10: Format (2I5)
NPARM - indicates the number of data to follow (starting from record 11)
NPARM is set to 139 by the code.

IFLOP - ≠3: oxide and metal are situated in distinct layers
- 3: oxide only or metal dispersed in the oxide phase

Record 11 to 24: Format (6E12.4)

Record 11:
time, s
integrated number of released moles of H_2
integrated number of released moles of H_2O
integrated number of released moles of CO
integrated number of released moles of CO_2
integrated number of released moles of all gases

Record 12:
power of released H_2, W
power of released H_2O, W
power of released CO, W
power of released CO_2, W
mass flow of H_2, g/s
mass flow of H_2O, g/s

Record 13:
mass flow of CO, g/s
mass flow of CO_2, g/s
surface temperature, K
power upward, W/m^2
internal energy, kW
power due to oxidation, kW

Record 14:
power released from the top of the melt, kW
power due to concrete decomposition, kW
power due to gas and oxides, kW
lost power in % of total power loss: upward
lost power in % of total power loss: concrete decomposition
lost power in % of total power loss: gas release

Record 15:
temperature of liquid metal, K

temperature of oxide, K
heat transfer between metal and oxide, MW
concrete erosion rate metal - bottom, cm/h
concrete erosion rate metal - wall, cm/h
energy flux oxide - wall, kW/m^2

Record 16:
energy flux metal - wall, kW/m^2
energy flux at the bottom, kW/m^2
temperature of liquid metal, K
solidus temperature of metal, K
power from metal to concrete, MW
axial concrete erosion, cm

Record 17:
radial concrete erosion (maximum), cm
mass of Zr in % of actual metal mass
mass of Cr in % of actual metal mass
mass of Fe in % of actual metal mass
mass of Ni in % of actual metal mass
temperature of oxide phase, K

Record 18:
solidus temperature of oxide, K
power transfered from oxide to concrete, MW
thickness of oxide crust: surface, cm
thickness of oxide crust: oxide/metal, cm
thickness of oxide crust: oxide/concrete, cm
mass of U_2O in % of actual oxide mass

Record 19:
mass of ZrO_2 in % of actual oxide mass
mass of SiO_2 in % of actual oxide mass
mass of CaO in % of actual oxide mass
temperature of liquid metal, K
temperature of oxide, K
temperature at the surface of the melt, K

Record 20:

pool height from initial bottom, cm
height of metal phase, cm
maximum vertical erosion, cm
actual mass of metal, t
actual mass of oxide, t
mass of eroded concrete, t

Record 21:

crust thickness in metal phase: metal / oxide, cm
crust thickness in metal phase: metal /concrete, cm
void fraction in oxide phase
void fraction in metal phase
molar ratio H_2/H_2O (without sump water)
molar ratio CO/CO_2

Record 22:

molar ratio H/C
internal power in melt, kW
molar flow of released H_2, mol/s
molar flow of released H_2O, mol/s
molar flow of released CO, mol/s
molar flow of released CO_2, mol/s

Record 23:

mass of released H_2, kg
mass of released H_2O (without sump), kg
used by CALTHER
used by CALTHER
used by CALTHER
used by CALTHER

Record 24:

mass of FeO in % of actual oxide mass
mass of Al_2O_3 in % of actual oxide mass
mass of Cr_2O_3 in % of actual oxide mass
erosion rate oxide/wall, cm/h
temperature of solid metal, K

internal power in metal phase, kW

Record 25:
internal power in oxide phase, kW
total mass of released CO, kg
total mass of released CO_2, kg
total mass of released H_2O from sump water, kg
mass of Si in % of actual metal mass
radial concrete erosion (at zero level), cm

Record 26 to 34:
data produced by CALTHER

4.5.4 Cavity Plot File

The coordinates of the cavity shape can be stored on this file for further processing by a user provided plot program (option on input card 37). The time interval of the output is set by the user on input card 39.

This output is divided into two sections corresponding to the diagram plot output: the first section is written once at the beginning of an initial run and the second is repeated at each time interval.

Section 1:

Record 1: Format (A72) - see input card 1
72 characters of problem identification

Record 2: empty

Record 3: Format (E12.4)
DPLC - time interval between outputs, s

Record 4: Format (7I5)
0, 0, 0, 0, 0, 0, 1 - required for KfK - plot program

Section 2:

Record 4: Format (I5, E12.4)

NB	number of cavity points to follow
TIME	time of output, s

Record 5: Format (6E12.4)

RCAV(1)	radius for point 1, cm
YCAV(1)	height for point 1, cm
	etc.

Record 5 is repeated until all NB points are written

Note: As for the print output, the whole cavity shape is given only at the start of a problem. For the next intervals, only those points are written, which are used during the calculation, i. e., which change their positions.

4.6 Compilation of the Subroutines and Functions Used in the WECHSL Code

This section is a brief description of the coding in WECHSL and its subroutines.

MMAIN

MMAIN calls:

HYPDAT, INIMAIN, CLEAN, READAT, CAVRID, HEAD1, INOUT, OPTION, HEAD2, STEP, PROUT, CURVES, SHAPE, SIGMET, SIGOXI.

SUBROUTINE BOULAY is called by CAVITY;
calls: GRENZ, GASMIX, KRUSTE, HYPDAT;
uses: CRKON

Computes the characteristics of the boundary layer at the interface of the melt facing the concrete and the interface temperature, the onset of crust formation and the characteristics when thin crust exists.

SUBROUTINE BUBBLE is called by WECHSL

Computes the bubble rise velocity inside a melt layer and the coalesence or breakup of gas bubbles.

SUBROUTINE CAVITY is called by WECHSL;
calls: BOULAY, SOLID, GASMIX, KONTUR, INICAV, HYPDAT, HTFILM, HEATTC, DECPRO

Computes the new cavity profile.

SUBROUTINE CAV1 is called by HEATTC;

This subroutine supports the calculations in HEATTC.

SUBROUTINE CLEAN is called by MMAIN

This subroutine removes comments starting with '*' from initial input data set and generates dataset without comments.

SUBROUTINE CPADD is called by READAT

CPADD provides the heat capacities of metal and oxide melt added to the melt bulk.

FUNCTION CRKON used in: BOULAY, GRENZ

Gives a linear transition from gas film driven boundary layer heat transfer to gas bubble driven heat transfer after a crust with defined thickness has formed.

SUBROUTINE CURVES is called by MMAIN

This subroutine writes data on tape JPL to plot curves.

SUBROUTINE CURCEA is called by MMAIN

This subroutine writes data on tape JPL to plot curves.

SUBROUTINE DECPRO is called by CAVITY,

This subroutine evaluates the masses of concrete decomposition products.

SUBROUTINE DENX is called by PROPS

DENX computes densities for the metal and the oxide.

SUBROUTINE DIAGPP is called by WECHSL

Diagnostics printout concerning physical phenomena.

SUBROUTINE ENTH is called by WECHSL, GASENT, ENTLEA, EQUIVT

Computes enthalpies of gases and oxides entering or leaving a melt layer.

SUBROUTINE ENTLEA is called by WECHSL;
calls: ENTH, HYPDAT, ENTM

Computes the temperature of the gas and the enthalpies of metals, oxides, and gas entering or leaving the melt.

SUBROUTINE ENTM is called by ENTLEA

Computes the enthalpies of metals entering or leaving the melt layer.

FUNCTION ERRST is used in: INICAV, INIWEC, WECHSL

Computes the freezing temperature between liquidus and solidus.

SUBROUTINE EQUIVT is called by: WECHSL;
calls: ENTH

Computes the equivalent temperature of the gas mixture composed of ($H_2O + H_2 + CO_2 + CO$) before water-gas reaction.

FUNCTION FANKT is used in: ITER

Provides the function for the iteration.

SUBROUTINE FIND is called by: WECHSL

Rearranges the cavity points to equal distances and computes the level and the volume of each melt layer.

SUBROUTINE GASENT is called by WECHSL;
calls: ENTH

Computes the enthalpies of each gas after the water-gas reaction.

SUBROUTINE GASMIX is called by: WECHSL, CAVITY, BOULAY, GRENZ;
calls: STH2O, STCO2

Computes the equilibrium and transport properties of a gas mixture containing the species H_2O and CO_2 and depending on pressure and temperature.

SUBROUTINE GRENZ is called by BOULAY;
calls: GASMIX, HYPDAT;
uses: CRKON

Computes the temperature at melt/gas film interface and onset of crust formation.

SUBROUTINE HEAD1 is called by MMAIN

This subroutine writes the heading of the files:

- JPL=8: plot data for diagrams;
- JPLC=9: plot data for cavity.

SUBROUTINE HEAD2 is called by MMAIN

Writes the heading of the files:

- IWT1=30: print out table 1;
- IWT2=31: print out table 2;
- IWT3=32: print out table 3;
- IWT4=33: print out table 4;
- IWT5=34: print out table 5;
- IWT6=35 print out table 6 (not active).

SUBROUTINE HEATTC is called by CAVITY
calls: CAV1

Computes the heat transfer to the concrete.

FUNCTION HMELT is called by READAT, WECHSL

Computes specific enthalpies for metal and oxide.

SUBROUTINE HTFILM is called by CAVITY;

Gas film model is computed.

SUBROUTINE HTBUB is called by KONTUR

Discrete BUBBLE model is computed.

SUBROUTINE HTMIX is called by KONTUR

Mixed (or transition) model between gas film and discrete BUBBLE model is computed.

SUBROUTINE HYPDAT is called by BOULAY, CAVITY, ENTLEA, GRENZ, INICAV, INIWEC, KONTUR, MMAIN, PROUT, QRAD, QTOP, SOLID, SPLASH, WECHSL

This subroutine gives the values of hypothetical data.

SUBROUTINE INICAV is called by CAVITY;
calls: HYPDAT;
uses: ERRST

This subroutine gives the actual properties and pressure on the bottom of the melt.

SUBROUTINE INIMAI is called by MMAIN

This subroutine initialises variables at the beginning of calculation.

SUBROUTINE INIWEC is called by WECHSL;
calls: HYPDAT, ERRST

This subroutine assigns values to property variables of the phase at the bottom.

SUBROUTINE INIVAR is called by WECHSL

This subroutine initialises data at the beginning of WECHSL.

SUBROUTINE INOUT is called by MMAIN, STEP

Restart subroutine:

- ISTEU = 1: reads from restart-file IDATI;
- ISTEU = 2: writes to restart-file IDATO;
- ISTEU = 3: reads from array for internal restart;
- ISTEU = 4: writes to array for internal restart.

SUBROUTINE INTERP is called by LAMIN, LATH, SOLLIQ, STCO2, STH2O, WECHSL, SIEDE, FSOUR, IMPR, TDGAZ

This subroutine provides linear interpolation.

SUBROUTINE ITER is called by VOID;
uses: FANKT

ITER executes iteration of the function FANKT.

SUBROUTINE KONTUR is called by CAVITY;
calls: LAMIN, TURBN, HYPDAT, HTBUB, HTMIX

KONTUR contains the heat transfer and geometry models for computing a new cavity point.

SUBROUTINE KRUSTE is called by BOULAY, QTOP, QINFAC, SOLID;
calls: PREP

KRUSTE calculates the transient, one-dimensional heat conduction inside a crust and the change of crust thickness.

SUBROUTINE LAMIN is called by KONTUR
Computes the gas film thickness for the laminar flow regime.

SUBROUTINE LATH is called by WECHSL;
calls: INTERP
LATH computes the latent heat of evaporation of water and the specific enthalpy of saturated steam.

SUBROUTINE LINIT is called by SIEDE
LINIT provides linear interpolation between two points.

SUBROUTINE LSCM is called by PROPS
Computes the liquidus and solidus curves for the metal phase.

SUBROUTINE LSCO is called by: READAT
Computes the liquidus and solidus curves for the oxide phase (Schroeder-van Laar Equation).

SUBROUTINE OPTION is called by MMAIN
This subroutine writes the specified options.

SUBROUTINE PREP is called by KRUSTE
PREP calculates the change of the crust thickness.

SUBROUTINE PROPS is called by READAT, WECHSL;
calls: LSCM, SOLLIQ, DENX
PROPS computes densities, specific heat capacities, thermal conductivities, liquidus and solidus temperatures, latent heat of phase change, and weight and molar fractions of each melt layer.

SUBROUTINE PROUT is called by MAIN;
calls: HYPDAT

Writes results on the following files:

- IWT. print out results;
- IWT1: print out table 1;
- IWT2: print out table 2;
- IWT3: print out table 3;
- IDT3: write table 3 on tape;
- IWT4: print out table 4;
- IWT5: print out table 5;
- IWT6: print out table 6 (not active).

SUBROUTINE QINFAC is called by WECHSL;
calls: KRUSTE

Computes the heat exchange between the metal and the oxide layer including onset and growth of crust at the relevant interface.

SUBROUTINE QRAD is called by QTOP;
calls: SIEDE, HYPDAT

QRAD computes the heat flux density and the surface temperature of the oxide melt pool by thermal radiation or by sump water evaporation including the onset of crust formation.

SUBROUTINE QTOP is called by WECHSL;
calls: HYPDAT, QRAD, SIEDE, KRUSTE

Computes the heat released through the top of the melt by thermal radiation or by sump water evaporation including the onset and growth of a crust.

SUBROUTINE REACT is called by WECHSL

Computes the exothermic and endothermic reaction enthalpies and the flow of materials changed by oxidation reaction inside the metal layer.

SUBROUTINE READAT is called by MMAIN;
calls: CPADD, LSCO, PROPS, HMELT

This subroutine reads the cleaned input data file and realises some calcultions.

SUBROUTINE SHAPE is called by MMAIN

This subroutine writes data on tape JPLC to draw the cavity shape.

SUBROUTINE SIEDE — is called by QTOP, QRAD;
calls: LINIT, INTERP

Computes the heat flux density for boiling heat transfer using pressure dependent boiling curves of water.

FUNCTION SIGMET — used in MMAIN, WECHSL

Calculation of the surface tension of metal phase.

FUNCTION SIGOXI — used in MMAIN, WECHSL

Calculation of the surface tension of oxide phase.

SUBROUTINE SOLID — is called by CAVITY;
calls: KRUSTE, HYPDAT

Computes the transient one-dimensional heat conduction inside the solidified metal with a correction term for the influence of radial heat conduction.

SUBROUTINE SOLLIQ — is called by PROPS;
calls: INTERP

Liquidus and solidus temperatures of oxide phase for a given concentration are computed.

SUBROUTINE SOLWET — is called by WECHSL

Computes the heat transfer between solid metal and oxide.

SUBROUTINE SPLASH — is called by WECHSL;
calls: HYPDAT

This subroutine takes into account the splashout of melt.

SUBROUTINE STCO2 — is called by GASMIX;
calls: INTERP

STCO2 evaluates the equilibrium and transport properties of carbon dioxide at 1 bar.

SUBROUTINE STEP is called by MMAIN;
calls: INOUT, WECHSL

Computes the new time step.

SUBROUTINE STH2O is called by GASMIX;
calls: INTERP

STH2O evaluates the equilibrium and transport properties of steam at 1 bar.

SUBROUTINE TMELT is called by WECHSL

Computes the temperature of the melt layer from melt mass and enthalpy;

- IPH = 1 means the phase is completely solid;
- IPH = 2 means the phase is a slurry (but homogeneous);
- IPH = 3 means the phase is completely liquid.

SUBROUTINE TURBN is called by KONTUR

Computes the thickness of the laminar sublayer of the turbulent gas film characteristic for the heat transfer.

SUBROUTINE VISME is called by WECHSL

This subroutine calculates the dynamic viscosity of the metal phase.

SUBROUTINE VISOX is called by WECHSL

This subroutine calculates the dynamic viscosity of the oxide.

SUBROUTINE VOID is called by WECHSL;
calls: ITER

Computes the void fraction inside the melt layer.

SUBROUTINE WASG is called by WECHSL

Computes the homogeneous water-gas reaction of the gases leaving the melt pool and estimates the new chemical equilibrium.

SUBROUTINE WECHSL

is called by STEP;
calls: HYPDAT, INIVAR, CPADD, INTERP, PROPS, VISOX, VISME, INIWEC, FIND, CAVITY, GASMIX, BUBBLE, VOID, SPLASH, QINFAC, SOLWET, STAR, PLOTVA, DATTAC, RELAXA, TDGAZ, RAYO1, XPHI, CALT, IMPR, QTOP, REACT, ENTLEA, EQUIVT, WASG, GASENT, LATH, ENTH, TMELT, DIAGPP, ERRST, HMELT, SIGMET, SIGOXI.

4.7 Installation of the WECHSL-Mod3 Code on IBM Compatible Personal Computer

To install and run WECHSL-Mod3 code on IBM compatible computer the following is needed:

Computer: IBM AT or compatible
Main Processor: Intel 80286 or higher
Math Co-processor: optional
Hard Disk: optional
Operating System: MS-DOS 3.00 or UNIX

Conventional Memory: 640 K
Extended Memory: > 2048 K

"Open file" statements have to be included in the WECHSL source code . It can be done in the MAIN program before the first READ statement. How to open files depends on the compiler type used. See FORTRAN Compiler Reference Manual for more details. Example of the part of the MAIN program with "open file" statements is given below. The changes are shown in lowercase letters. Different file names can be used

==========MAIN==========

```
C     RESTART FILE INPUT:                    FILE 2          ( IRESTI )
      open(02,file='file.02' ,form='unformatted' , status='unknown' )
C     RESTART FILE OUTPUT                    FILE 22         ( IRESTO )
      open(22,file='file.22' , form='unformatted' , status='unknown' )
C     READ FILE FOR WECHSL START:            FILE 3          ( IRC )
      open ( 3, file='input.dat',status='old')
C     READ FILE (CLEANED DATA):              FILE 4          ( IRD )
      open( 4,file='clean.dat' )
C     READ IN CONTROL PARAMETER:             FILE 1          ( IIN )
      open( 1,file='start.dat' )
C     PRINT OUT RESULTS:                     FILE 6          ( IWT )
      open ( 6,file='wexcmo.scr' , status='unknown' )
C     PRINT OUT TABLE 1:                     FILE 30         ( IWT1 )
      open( 30, file='file.30' , status='unknown' )
```

```
C     PRINT OUT TABLE 2:                    FILE 31          (IWT2)
      open(31,file='file.31', status='unknown')
C     PRINT OUT TABLE 3:                    FILE 32          (IWT3)
      open(32,file='file.32', status='unknown')
C     PRINT OUT TABLE 4:                    FILE 33          (IWT 4)
      open(33,file='file.33', status='unknown')
C     PRINT OUT TABLE 5:                    FILE 34          (IWT5)
      open(34,file='file.34', status='unknown')
C     PRINT OUT TABLE 6:                    FILE 35          (IWT6)
      open(35,file='file.35', status='unknown')
C     PLOT DATA FOR DIAGRAMS:               FILE 8           (JPL)
      open( 8,file='file.08', status='unknown')
C     PLOT DATA FOR CAVITY:                 FILE 9           (JPLC)
      open( 9,file='file.09", status='unknown')
C     TEST PRINTOUT
      open(10, file='con')
                    ==========MAIN==========
```

5. Instructions for Use of the CALTHER Code

5.1 Linking between WECHSL Mod3 and CALTHER

The CALTHER subroutine package is linked to the standard WECHSL code at three levels :

- The top surface heat flux from the corium is calculated with the CALTHER module from all the surrounding surface temperatures.
- The decomposition products from the cavity (molten concrete or molten steel) are added to the corium during MCCI calculation.
- The gases released from the cavity walls are added to the gas release calculated by WECHSL.

The CALTHER subroutine package is used as an optional user model.

5.2 Description of Input Data

The data described below are added after the input of the "standard" WECHSL code if the parameter JPDC is set equal to 1.
All formats, except alphanumeric formats, are free formats.
All alphanumeric formats are Format 9A8

Card 1 : Alphanumeric
TIT(I),I=1,9
Title card (72 characters at the maximum)

Card 2 :
ICALC
ICALC =0 (STATIONARY calculation)
ICALC =1 (TRANSIENT calculation)

Card 3 :
TDEB
Starting time of the CALTHER calculation (s)

Card 4 : Alphanumeric

GAZ, MODEL

GAZ is the kind of gas mixture in the reactor cavity :

GAZ = "TRANSPA" means a transparent gas mixture

GAZ = "GRAY" means a gray absorbing gas mixture

GAZ = "REAL" (not yet included in this version)

MODEL is the model of the band absorbtion characteristics :

MODEL = "LEBOURG" means that the Lebourgeois model (CEA model) is used

MODEL = "THOMSON" means that the Thomson model is used

Card 5 :

NBA

NBA is the number of absorption bands used in the gas absorption calculation.

Card 6 :

NTT

NTT is the number of points of the CALTHER computing table.

Card 7 : - NTT cards -

DTT(1), TPST(1)

DII(1) = first current time step (s) for the CALTHER calculation

TPST(1) = time for first point (s)

Repeat up to DTT(NTT) and TPST(NTT) (1 couple per card)

= = = > IF TIME .LE. 86400.(S) DTT = DT calculated by WECHSL.

Card 8 :

NTI

NTI is the number of points in the printout table.

Card 9 : - NTI cards -

DTI(1), TPSI(1)

DII(1) = first time step between 2 CALTHER calculation printouts

TPSI(1) = time for first point (s)

Repeat up to DII(NTI) and TPSI(NTI) (1 couple per card)

Card 10 :

NCOMP

NCOMP is the total number of components.

Example:
(top surface of corium + gas mixture + vessel + concrete slices).

Card 11 :

DIAM, HCUVE

DIAM is the inner diameter of the reactor cavity (m).

HCUVE is the height of the cavity space between the top surface of the corium and the lower R.P.V component (m).

Description and Meshing of the Cavity Wall Components:

Data are entered in two connected loops:

LOOP L1 for each "wall component" JC

A wall component is composed of several material slabs (maximum 10).

A slab is composed of various regions (max. 4), each with a constant space step.

The number of wall components is calculated by the code as NPAMU, with NPAMU = NCOMP-2 (the two components which are subtracted are the gas mixture and the upper surface of the corium).

Card 12 :

IALFC(1), NMIC(1)

IALFC(1) is the geometric index (= 0 for plane , = 1 for cylindric)

NMIC(1) is the number of material slabs in the first wall component

Warning: In this version, NMIC must always be unity.

LOOP L2 is for each material slab I of which the component may be composed. (For example, a wall component could be composed of a concrete "wall" and a "metal" wall.)

Card 13 :

NC(I,JC), RIC(I,JC), REC(I,JC)

NC(I, JC) is the total number of meshes in each material slab I inside each wall component JC.

RIC(I, JC) is the inner radius (m) of the material slab I which is a constituent of the wall component JC.

REC(I, JC) is the outer radius (m) of the material slab I which is a constituent of the wall component JC.

Repeat up to RIC (NMIC(JC),1) (1 couple per card).

Note: In this version, NMIC(I) is always set equal to 1.

Automatic calculation of the number of meshes in each slab:

IF NC(I,JC) > 0

Constant meshes in the material slab I of the wall component JC defined only by RIC(I,JC) and REC(I,JC)

IF NC(1,1) < 0

Variable meshes in the material slab I of the wall component JC defined by the following additional parameters:

Additional card :

IXM,NDX,DXC

IXM is the number of regions in slab I (maximum 4)

NDX(IX,I) is the number of space steps of size DXC (m) in the region IX of slab I.

DXC(IX,C) is the size (m) of the space step.

End **LOOP L2**

Return to card 12 for the next wall component.

End **LOOP L1**

Radiative Transfer Characteristics:

LOOP L3 on each boundary surface of each wall component

JC = 1 stands for the upper surface of the corium

JC = 2,3,.. for lateral wall components of the cylindrical cavity

JC = ..,NPAR for the top wall component of the cavity (e.g. reactor vessel)

Card 14 :

A(1), EMI(1)

A(1) = area (m^2) of first wall component inner surface (surface in contact with the gas mixture)

EMI(1) = emissivity of this surface

Card 15 :

FVU(1,J)

Shape factor between surface 1 and the other surfaces. The number of surfaces is (NCOMP - 1) (i.e. the total number of components minus the gas mixture).

Repeat up to (NCOMP - 1) for second index.

Repeat up to (NCOMP - 1) for first index.

Example:

READ first FVU(1,1) , FVU(1,2) , FVU(1,3) ,...,FVU(1,N)
READ then FVU(2,1) , FVU(2,2) , FVU(2,3) ,...,FVU(2,N)
READ finally FVU(N,1) , FVU(N,2) , FVU(N,3) ,...,FVU(N,N)

Return to card 14 (Repeat up to A(NCOMP-1) and EMI(NCOMP-1)).

End **LOOP L3**

Card 16 :

FCGA

FCGA is the correction coefficient for the mean beam length between two wall surfaces separated by an absorbing, emitting gas.
Warning: The gas is not assumed to be optically thin. In this version the recommended value is 0.9.

LOOP L4 on each boundary cavity component (index from 1 to JC)
JC = 1 stands for the upper surface of the corium
JC = 2,3,.. for lateral wall components of the cylindrical cavity
JC = ..,NPAR for the top wall component of the cavity (e.g. reactor vessel).

Card 17 :

CGA(1,J)

CGA(1,J) is the geometric mean beam length between surface 1 and the other surfaces J. The number of surfaces is (NCOMP - 1) (i.e. the total number of components minus the gas mixture).
Repeat up to (NCOMP - 1) for second index.
Repeat up to (NCOMP - 1) for first index.

Example:

READ first CGA(1,1) , CGA(1,2) , CGA(1,3) ,...,CGA(1,N)
READ then CGA(2,1) , CGA(2,2) , CGA(2,3) ,...,CGA(2,N)
READ finally CGA(N,1) , CGA(N,2) , CGA(N,3) ,...,CGA(N,N)

End **LOOP L4**

Thermal Exchange on Each Interface of a Wall Component:

Data are entered in two connected loops:

LOOP L5 on each wall component.
The number of wall components is calculated by the code NPAMU, with NPAMU = NCOMP-2 (the two components which are subtracted are the gas mixture and the upper surface of the corium).

An example is given below for wall component number 1:

LOOP L6 on each material slab interface of the component
(from 1 to IMF+1; IMF being the number of material slabs from which the wall component is composed, IMF+1 the number of interfaces)
The first interface is the inner surface of the component (e.g. inner surface of the cavity).
The second interface is the one between the two first materials of the wall, and so on.
The last interface is the outer surface of the component.

On the two external surfaces of the component (i.e the inner and outer surfaces of the component) and inside the component on each interface between two material slabs, three modes of heat exchange can be defined, separately or combined:
- heat transfer by thermal radiation,
- heat transfer by conduction,
- heat transfer by convection.

The choice is made with the following cards (1 card per interface between slabs; 6 parameters per card, I from 1 to IMF)

Card 18 : 6 parameters

First parameter: STEF(I,1): the Stefan constant, in $W/(m^2K^4)$
Set STEF(I,1) equal to 0 if there is no radiative heat transfer at this interface.
Warning: STEF(1,1) is not used for the inner surface because on the inner surface the heat flux is always given as a boundary condition. For this case, STEF(1,1) must always be equal to 0.
Idem for STEF (1,NPAMU)
Second parameter: ALAMB(I,1): thermal conductivity (W/(m.K))

Set ALAMB(I,1) equal to 0 if there is no heat transfer by conduction at this interface.
Warning: ALAMB(1,1) is not used for the inner surface because on the inner surface the heat flux is always given as boundary condition. For this case, ALAMB(1,1) must always be equal to 0.
Idem for ALAMB(1,NPAMU)
Note: ALAMB(I,1) =1.E10 for perfect contact.

Third parameter: COEH(I,1): convective heat transfer (W/(m^2.K))
Set COEH(I,1) equal to 0 if there is no heat transfer by convection at this interface.
Warning: COEH(1,1) is not used for the inner surface because on the inner surface the heat flux is always set as boundary condition. For this case, set always COEH(1,1) = 0.

Fourth parameter: EPSI1(I,1): emittance of the left surface (lower radius of the interface I = greater radius of slab I-1)

Fifth parameter: EPSI2(I,1): emittance of the right surface (greater radius of the interface I = smaller radius of slab I+1)

Sixth parameter: FG(I,1) : shape factor between left and right surfaces of interface I

End **LOOP L6**

End **LOOP L5**

Material Identification of Each Wall Component:
The data are entered in two connected loops:

LOOP L7 on each wall component
The number of wall components is calculated by the code as NPAMU, with NPAMU = NCOMP-2 (the two components which are subtracted are the gas mixture and the upper surface of the corium).

An example will be given below for wall component 1:

LOOP L8 for each material slab of the component.

Card 19 : 2 parameters
First parameter: IDC(I,1) : material identification
=1 for silicate concrete
=2 for limestone/common sand concrete
=3 INOX (not yet included in this version)
=4 stainless steel
Second parameter: SC(I,1) : volumetric heat source in the slab of the wall component (here number 1) in (W/m^3)

End **LOOP L8**

End **LOOP L7**

Thermal Boundary Conditions on Each Wall Component:
In CALTHER, a calculated radiated heat flux from the corium is always set as the thermal boundary condition for the inner external surface of each wall component, and the thermal boundary condition for the outer external surface of each wall component is always a temperature that the user must enter in this part as a function of time:

Data are entered in two connected loops:

LOOP L9 on each wall component
The number of wall components is calculated by the code as NPAMU, with NPAMU = NCOMP-2 (the two components which are subtracted are the gas mixture and the upper surface of the corium).

An example of wall component 1 will be given below:

Card 20 : 2 parameters
First parameter: N2
N2 is the number of points as a function of time for the external temperature
Second parameter: RC
RC is the radius where the external temperature is given.

LOOP L10 for each time point of the temperature.

Card 21 : 2 parameters
First parameter: TS2(I,1) = time (s)
Second parameter: CL2(I,1) = temperature , K

End **LOOP L10**

Card 22 :
NS
NS is the number of points as a function of time for the normalized power inside the wall component (component number 1 in this example)

LOOP L10 bis for each time point of the normalized power.

Card 23 : 2 parameters
First parameter: TS(I,1) = time (s)
Second parameter: FS(I,1) = normalized power

End **LOOP L10 bis**

End **LOOP L9**

Initial Temperature inside Each Wall Component:
The data are entered in two connected loops:

LOOP L11 on each wall component.
The number of wall components is calculated by the code as NPAMU, with NPAMU = NCOMP-2 (the two components which are subtracted are the gas mixture and the upper surface of the corium).

An example of wall component 1 will be given below:

Loop L12 for each material slab of the component.

Card 24 :
INIT
INIT =1 for a constant homogeneous initial temperature

Card 25 if INIT = 1 :

T0

T0 is the constant temperature in K

End **LOOP L12**

INIT = 2 for a linear temperature profile inside the wall component

If INIT = 2, two external surface temperatures for the component are needed which means that the following card is composed of 2 parameters:

Card 25 if INIT = 2 :

TI, TE

TI: inner temperature of the wall component, K

TE: outer temperature of the wall component, K

End **LOOP L12**

INIT = 3 for a defined radial temperature profile versus radius:

Card 25 if INIT = 3 :

TC(I,1) for I = K1 to K2

Temperatures TC(K,1), in Kelvin, for the different nodes, from node K1 to node K2.

Node K1 is the first node at the internal surface of the material slab.

Node K2 is the last node at the external surface of the material slab.

An example is given here of meshing for a wall component with one material and five constant space steps, six component nodes (0), and two external boundary condition nodes (*)

```
     /////  WALL COMPONENT  /////
   * 0-------0-----0-----0-----0-----0          *
   1 2(K1) 3     4     5     6     7(K2)    8 (NTC)
```

End **LOOP L12**

Gas Mixture:

The following input data are related to the characteristics of the gas mixture over the corium. This CALTHER version **does not compute** any gas equilibrium equivalent temperature or pressure, or water-gas reaction. As a consequence, the temperature of the gas mixture can be chosen as input table as a function of time, or calculated each time by CALTHER as the arithmetic mean of the wall external temperature and the corium exit gas temperature.

In the input data the mass fraction of H_2O in the gas mixture must also be given as a function of time, for absorption to be calculated.
The mass fraction of CO_2 and CO in the gas mixture must be entered as a function of time, but these input data are not yet used.
The next version of CALTHER will calculate all these data.

Gas mixture temperature input:

Card 26 :

NTG

Number of points of the temperature as a function of time.
If NTG < 0, the temperature is calculated in CALTHER
then go DIRECTLY TO CARD 27.

Extra card if NTG > 0 :

TTG(1), TG(1)

TTG(1) = first time point (s)
TG(1) = temperature, K
Repeat up to TTG(NTG) and TG(NTG) (1 couple per card)

Gas pressure input:

Card 27 :

NTP

Number of points of the gas pressure as a function of time.

Card 28 :

TTP(1), PGAS(1)

TTP(1) = first time point (s)
PGAS(1) = pressure, Pa
Repeat up to TTP(NTP) and PGAS(NTP) (1 couple per card)

H_2O mass fraction in the gas mixture input:

Card 29 :

NH2O

Number of points of the H_2O mass fraction in the gas mixture as a function of time.

Card 30 :

TH2O(1), YYH2O(1)

TH2O(1) = first time point (s)
YYH2O(1)= mass fraction
Repeat up to TH2O(NH2O) and YYH2O(NH2O) (1 couple per card)

CO_2 mass fraction in the gas mixture input:
Not taken into acccount in this CALTHER version, but must exist as input.

Card 31 :
NCO2
Number of points of the CO_2 mass fraction in the gas mixture as a function of time.

Card 32 :
TCO2(1), YYCO2(1)
TCO2(1) = first time point (s)
YYCO2(1)= mass fraction
Repeat up to TCO2(NCO2) and YYCO2(NCO2) (1 couple per card)

CO mass fraction in the gas mixture input:
Not taken into account in this CALTHER version, but must exist as input.

Card 33 :
NCO
Number of points of the CO mass fraction in the gas mixture as a function of time.

Card 34 :
TCO(1), YYCO(1)
TCO(1) = first time point (s)
YYCO(1)= mass fraction
Repeat up to TCO(NCO) and YYCO(NCO) (1 couple per card)

Characteristics of the concrete material:

Card 35 :
RHOB, RHOE, CPB, CPE
RHOB = total density of the concrete (Kg/m^3)
RHOE = density of the free water in the concrete (Kg/m^3)
CPB = RHOB*CP= volumetric heat capacity of the concrete ($J/(m^3*K)$)
CPE = RHOB*CP= volumetric heat capacity of the free water ($J/(m^3*K)$)

Card 36 :

TSAT, DTSAT, TFUS, HB, XSIO2, XCAO, XAL2O3

TSAT = saturation temperature of water inside the concrete walls, K

DTSAT, in "TSAT-DTSAT", for the beginning of free water release

= = > DTSAT = 2. is recommended

TFUS = melting temperature of the concrete (K)

HB = melting enthalpy of the remaining concrete (J/kg) after the total H_2O and CO_2 release

XSIO2 = SiO_2 mass fraction of the concrete

XCAO = CaO mass fraction of the concrete

XAL2O3 = Al_2O_3 mass fraction of the concrete

Card 37 :

CK1, CK2, CK3

Coefficients of concrete thermal conductivity calculation.

thermal conductivity = CK1*A1 for concrete with water, in W/(m*K)

thermal conductivity = (CK2+CK3*T)*A2 for dry concrete, in W/(m*K)

A1 = 1.16 and A2 = 1.16 for a silicate type of concrete.

A1 = 1. and A2 = 1. for a limestone/common-sand type of concrete.

Concrete gas release :

The following parameters are the input parameters indicated in the release laws used in CALTHER (vaporization at TSAT for free water and Arrhenius laws for bound water and CO_2 release)

Card 38 : 7 parameters , free water release law:

XW, HV, DUMMY, DUMMY, DUMMY, DUMMY, DUMMY

First parameter: mass fraction of free water in the concrete

Second parameter: vaporization enthalpy (J/kg) of the water at TSAT

Parameters 3 to 7: Put 0 as dummy values.

Card 39 : 7 parameters, bound water release law:

XW, HV, AK, EK, RK, TINF, TSUP

First parameter: mass fraction of bound water in the concrete

Second parameter: decomposition enthalpy (J/kg) of the $Ca(OH)_2$

Parameter number 3 : AK

Parameter number 4 : EK

Parameter number 5 : RK
are parameters of the Arrhenius kinetic law S=AK*Exp(EK/(RK*T))
Parameter 6 : TINF, at lower temperature of H_2O release, K
Parameter 7 : TSUP, at upper temperature of H_2O release, K

Card 40 : 7 parameters, CO_2 release law:
XW, HV, AK, EK, RK, TINF, TSUP
First parameter: mass fraction of CO_2 in the concrete
Second parameter: decomposition enthalpy (J/kg) of the $CaCO_3$
Parameter number 3 : AK
Parameter number 4 : EK
Parameter number 5 : RK
are parameters of the Arrhenius kinetic law S=AK*Exp(EK/(RK*T))
Parameter 6 : TINF, lower temperature of CO_2 release, K
Parameter 7 : TSUP, upper temperature of CO_2 release, K

Characteristics of the stainless steel material:
(INOX is missing, but in fact you can enter any properties you want: CALTHER will consider it as a pure element)

Card 41 :
RHOC, HBC, TFUSC
RHOC is the density of the stainless steel (kg/m3).
HBC is the melting enthalpy of the stainless steel (J/kg).
TFUSC is the melting temperature of the stainless steel (K).

5.3 List of the Subroutines and Input Data

All the subroutines of the CALTHER subroutine package are listed after the "standard WECHSL" subroutine at the end of the FORTRAN list of WECHSL Mod3.
Each subroutine describes its function and all parameters used are clearly identified.
The CALTHER option is chosen when the input data JPDC is set equal to 1.
An example of input data is given in Appendix B.

6. Literature

[1] Rassmussen, N.C.:
"Reactor Safety Study - An Assessment of Accident Risks in US Commercial Nuclear Power Plants," USNRC, WASH 1400 (NUREG-75/014), Oct. 1975.

[2] Der Bundesminister für Forschung und Technologie (editor):
"Deutsche Risikostudie Kernkraftwerke", Verlag TÜV Rheinland,Cologne, 1979.

[3] Alsmeyer, H., Peehs, M. and Perinic, D.:
"Untersuchung der Wechselwirkung einer Kernschmelze mit Beton in der BETA-Versuchsanlage", PNS Annual Colloquium 1982, KfK 3470.

[4] Alsmeyer, H.:
"BETA-experiments in verification of the WECHSL-Code: Experimental results on the melt-concrete interaction", Nucl. Engrg. Des. 103 (1987), pp. 115-125.

[5] Murfin, W.B.:
"A Preliminary Model for Core/Concrete Interactions", SAND77-0370, Sandia Laboratories, Albuquerque N.M., Aug. 1977.

[6a] Reimann, M., Murfin, W.B.:
"The WECHSL Code: A Computer Program for the Interaction of a Core Melt with Concrete." KfK 2890, Kernforschungszentrum Karlsruhe, Nov. 1981.

[6b] Reimann, M., Stiefel, S.:
The WECHSL-Mod2 Code: A Computer Program for the Interaction of a Core Melt with Concrete including the Long Term Behavior. Model Description and User's Manual. KfK 4477, Kernforschungszentrum Karlsruhe, Juni 1989.

[7] Powers, D.A., Dahlgren, D.A., Muir, J.F., and Murfin, W.B.:
"Exploratory Study of Molten Core Material/Concrete Interactions", SAND77-2042, Sandia Laboratories, Albuquerque N.M., Feb. 1978.

[8] Perinic, D., Kammerer, B., Knauß, H., Mack, A., and Stuka, B.:
"Betontiegelversuche mit Thermitschmelzen", KfK 2572, Kernforschungszentrum Karlsruhe, July 1979.

[9] Skokan, A., Hollek, H., and Peehs, M.:
"Chemical Reactions Between Light Water Reactor Core Melt and Concrete", Nucl. Techn. 46 (1979)2, p. 255.

[10] Alsmeyer, H., Dres, K. Reimann, M., Stiefel, S.:
"Modellentwicklung zur analytischen Beschreibung von Kernschmelzunfällen" in "Projekt Nukleare Sicherheit, Jahresbericht 1986", KfK 4100 (1986), pp. 4300-14/4300-32.

[11] Peehs, M., Skokan, A., and Reimann, M.:
"The Behavior of Concrete in Contact with Molten Corium in the Case of a Hypothetical Core Melt Accident", Nucl. Techn. 46 (1979)2, pp. 192-198.

[12] Powers, D.A.:
"Kinetics and Stochiometry of the Thermal Decomposition of Concrete", LWR Safety Program, Quaterly Report Jan.-March 1986, SAND76-9369, Sandia Laboratories, Albuquerque N.M., Sept. 1976.

[13] Alsmeyer, H., Reimann, M.:
"On the Heat and Mass Transport Processes of a Horizontal Melting or Decomposing Layer under a Molten Pool", Nucl. React. Safety Heat Transf., Winter Annual Meeting ASME, Atlanta Ga., Nov. 1977, pp. 47-53.

[14] Landau, H.G.:
"Heat Conduction in a Melting Solid", Quat. Appl. Math. 8 (1951), pp. 81-94.

[15] Höpfl, R., Peehs, M.:
"Kalorische Größen von Reaktorbeton unter dem Aspekt des hypothetischen Kernschmelzunfalls", Jahrestagung Kerntechnik, Mannheim 1982, pp. 319-322.

[16] Copus, E.R., Bradley, D.R.:
"Interaction of Hot Solid Debris With Concrete", NUREG/CR-4558, SAND-85-1739, Sandia National Laboratories, Albuquerque, W.M., June 1986.

[17] Berenson, P.J.:
"Film Boiling Heat Transfer from a Horizontal Surface", Journ. Heat Transf., 38C (1961), pp. 351-358.

[18] Bromley, L.A.:
"Heat Transfer in Stable Film Boiling", Chem. Engng. Progr. 46 (1950)5, pp. 221-227.

[19] Hsu, Y.Y., Westwater, J.W.:
"Approximate Theory for Film Boiling on Vertical Surfaces", Chem. Engng. Progr. Symp. Ser. 56 (1960) 30, pp. 15-24.

[20] Dhir, V.K., Castle, J.N., and Catton, I.:
"Role of Taylor Instability on Sublimation of a Horizontal Slab of Dry Ice", Journ. Heat Transf. 99 (1977) 3, pp. 411-418.

[21] Reimann, M., Murfin, W.B., and Alsmeyer, H.:
"On the Penetration of Hot Melts into Concrete Structures", The European Nuclear Conference, Trans.ANS 31 (1979), p. 371-373.

[22] Reimann, M., Murfin, W.B.:
"Calculations for the Decomposition of Concrete Structures by a Molten Pool", Europ. Appl. Res. Rept. 1 (1979) 6, p. 1554-1566.

[23] Schlichting, H.:
"Grenzschichttheorie", G. Braun, Karlsruhe 1975, p. 556 ff.

[24] Reineke, H.H., Hahn, K.:
"Ein vereinfachtes Rechenmodell für den Wärmeübergang von einer Schmelze an Beton bei Anwesenheit eines Dampffilms", IVA Ingenieurbüro für Berechnung und Entwicklung verfahrenstechnischer Anlagen, July 1984.

[25] Reimann, M., Alsmeyer, H.:
"Hydrodynamische und thermische Modelle zur Wechselwirkung einer Kernschmelze mit Beton" in: PNS-Halbjahresbericht 1978/2, KfK 2750, Kernforschungszentrum Karlsruhe, Oct. 1979.

[26] Lock, R.C.:
"The Velocity Distribution in the Laminar Boundary Layer Between Parallel Streams", Quart. Journ. Mech. Appl. Math. 4 (1951) 1, pp. 42-63.

[27] Reineke, H.H., Rinkleff, L., and Schramm, R.:
"Heat Transfer Between Molten Core Material and Concrete", Proc. 3rd Post Accident Heat Removal Int. Exch., ANL-78-10, Argonne Ill., Nov. 2-4, 1977.

[28] Schramm, R.:
"Untersuchungen zur Wechselwirkung von Kernschmelzen und Beton", BMFT-FB (RS166-79-05) Abschlußbericht Band Ib, TU Hannover, Sept. 1980.

[29] Schwarzott, W. et al.:
"Detaillierung von KAVERN und Programmentwicklung zur Gasabströmung aus der Schildgrube", BMFT 150379, Abschlußbericht 1983.

[30] Grigull, U., Sandner, H.:.
"Wärmeleitung", Springer, Berlin 1979.

[31] Levich, V.G.:
"Physicochemical Hydrodynamics", Prentice-Hall, New York 1962.

[32] Mendelson, H.D.:
A.I.Ch.E.J. 13 (1967), p. 250.

[33] Haberman, W.F., Morton, R.K.:
"An Experimental Investigation of the Drag and Shape of Air Bubbles Rising in Various Liquids", Rept. 802, David, W. Taylor Basin, Sept. 1953.

[34] Le Clair, B.P., Hamielec, A.E.:
"Strömung durch Teilchenansammlungen" in "Kinetik metallurgischer Vorgänge bei der Stahlherstellung", Verlag Stahleisen, Düsseldorf 1972.

[35] Nicklin, D.J.:
Chem.Engng. Sci. 17 (1962), p. 693.

[36] Nikolopoulos, P. Ondracek, G.:
unpublished report of the Kernforschungszentrum Karlsruhe, 1979

[37] Werle, H.:
"Einfluß eines Gasstroms auf den Wärmeübergang zwischen zwei Flüssigkeitsschichten" in: PNS-Halbjahresbericht 1978/2, KfK 2750, Kernforschungszentrum Karlsruhe, October 1979, p. 4300/79-182.

[38] Haberstroh, R.D., Reinders, R.D.:
"Conduction Sheet Model for Natural Convection through a Density Stratified Interface", Int. J. Heat Mass Transf. 17 (1974), pp. 307.

[39] Bermann, M.: "Light Water Reactor Safety Research Program Semiannual Report October 1983 - March 1984, NUREG/CR-4459, SAND85-2500, Sandia National Laboratories, Albuquerque, N.M., 1986.

[40] Alsmeyer, H., Dres, K.:
"Modellexperimente zur analytischen Beschreibung von Kernschmelzen-unfällen" in Sicherheitsorientierte LWR-Forschung, PRS-Jahresbericht 1987, KfK 4450 (1987), pp. 113-128.

[41] Blose, R.E. et al.:
"SWISS: Sustained Heated Metallic Melt/Concrete Interactions with Overlying Water Pools", NUREG/CR-4727 (1977).

[42] Rohsenow, W.M., Hartnett, J.P.:
"Handbook of Heat Transfer", McGraw Hill, New York 1973.

[43] Pollak, R.:
"Eine neue Fundamentalgleichung zur konsistenten Darstellung der thermodynamischen Eigenschaften von Wasser", BWK 24 (1975) 5, p. 210.

[44] Schmidt, E.:
"Zustandsgrößen von Wasser und Wasserdampf in SI-Einheiten", 3. Edition., Springer, Berlin, 1982.

[45] Alsmeyer, H., Barleon, L., Koster, J., Michael, I., Müller, U., and Reimann, M.:
"Ein Modell zur Beschreibung der Wechselwirkung einer Kernschmelze mit Beton", KfK 2395, Kernforschungszentrum Karlsruhe, Oct. 1977.

[46] Powers, D.A., Frazier, A.W.:
"VISRHO - A Computer Subroutine for Estimating the Viscosity and Density of Complex Silicate Melts", SAND76-0649, Sandia Laboratories, Albuquerque N.M., June 1977.

[47] Skoutajan, P., Baukal, W., König, R., Wagner, W., and Walter, G.:
"Durchführung von Viskositätsmessungen an oxidischen Corium - Beton - Schmelzen", BMFT-RS214A, Battelle-Institut Frankfurt/Main, May 1979.

[48] Kunitz, W.:
Journ. General Physiology 9(1926), p. 715.

[49] Gmelin-Durrer:
"Metallurgie des Eisens", Vol. 5, Berlin-Heidelberg-New York 1978, p. 23a ff.

[50] Wargaftik, N.B.:
"Tables of the Thermophysical Properties of Liquids and Gases" 2nd edition, Hemisphere, Washington, London, 1975.

[51] Bird, R.B., Stewart, W.E., Lightfoot, E.N.:
"Transport Phenomena", J. Wiley, New York, London, 1960.

[52] Misaelidis, P., Ondracek, G.:
unpublished report of the Kernforschungszentrum Karlsruhe, 1978.

[53] Prigogine, J., Defay, R.:
"Chemische Thermodynamik", VEB Verlag für Grundstoffindustrie, Leipzig 1962, p. 378 ff.

[54] Muir, J.F.:
Sandia Laboratories, Albuquerque N.M., (private communication).

[55] Schulz, B.:
"Thermal conductivity of composites", Proceedings of the International Conference on Composite Materials, Vol. 2 (1975).

[56] Alsmeyer, H., Adelhelm, C., Dillmann, H.-G., Heinle, M., Ratajczak, W., Schumacher, G., Schöck, W., Skokan, A., Tromm W.:
"BETA Experiments on Zirconium Oxidation and Aerosol Release during Melt-Concrete Interaction." Second OECD (NEA) CSNI Specialist Meeting on Molten Core Debris-Concrete Interactions. Karlsruhe, Germany, 1-3 April 1992.

[57] Thompson, D.H., Fink, J.K., Armstrong, D.R., Spencer, B.W. , Sehgal, B.R.:
"Thermal-Hydraulic Aspects of the Large-Scale Integral MCCI Tests in the ACE Program." Second OECD (NEA) CSNI Specialist Meeting on Molten Core Debris-Concrete Interactions. Karlsruhe, Germany, 1-3 April 1992.

[58] Copus, E.R., Blose, R.E., Brockmann, J.E., Simpson, R.B., Lucero, D.A.:
"Core Concrete Interactions using Molten UO_2 with Zirconium on a Basaltic Basemat: The SURC-2 Experiment." NUREG/CR-5563, SAND90-1022, R3, R4, R7.

[59] Renault, C., Foit, J.J.:
"Assessment Status of the WECHSL-Mod3 Code". Second OECD (NEA) CSNI Specialist Meeting on Molten Core Debris-Concrete Interactions. Karlsruhe, Germany, 1-3 April 1992.

[60] Foit, J.J.:
"Improved WECHSL Models Including Zirconium Oxidation and its Verification by New BETA Experiments". Second OECD (NEA) CSNI Specialist Meeting on Molten Core Debris-Concrete Interactions. Karlsruhe, Germany, 1-3 April 1992.

[61] Siegel, R., Howell, J.R.:
"Thermal Radiation Heat Transfer". 2nd edition, McGraw Hill, New York 1981.

[62] Hottel, M.C., Sarofim, A.F.:
"Radiative Transfer". McGraw Hill, New York 1967.

Appendix A: Sample Calculations with WECHSL

A.1 BETA Test

The main objectives of the BETA experiments were to investigate the melt concrete interaction in a two-dimensional concrete crucible. The BETA V5.1 test was carried out in order to investigate the Zr/SiO_2 condensed phase chemistry during the interaction of a metallic melt with a siliceous concrete. The melt consisted of 300 kg steel and 150 kg oxide. The temperature of the melt at the beginning of the interaction was about 2000 °C. In the subsequent chapters of the Appendix the cavity shape, the melt temperatures, the gas release rates as well as the fraction of Zr and Si in the melt are given among other quantities calculated by WECHSL.

A.1.1 Input Data

```
  BETA-TEST V 5.1   (ISP-30)
* MATERIAL ADDITION FROM 0. TO 14. S
*
*
*--------  THERMITE ADDITION:  RATE AND TIME OF POURING  ---------------
*  KG/S  |  SEC.   |
        0.        0.
*
*
*--------  ADDITION OF OTHER MATERIALS  -------------------------------
*  NUMBER OF ADDITIONS :
       2
* 1. ADDITION : START TIME, END TIME (SEC), TEMPERATURE (K)
*               AS MIXTURE TEMPERATURE OF HOT FE,CR,NI AND COLD ZR
                    0.          10.5          1964.5
*    ADDED MASS (KG) OF EACH SPECIES DURING THIS TIME :
*    UO2 |    ZRO2 |     FEO |     CAO |    SIO2 |   AL2O3 |   CR2O3 |
      0.       0.         0.       0.        0.         0.       0.
*    FE  |    ZR   |     CR  |     NI  |
    272.96    77.77      16.       15.38
*
* 2. ADDITION : START TIME, END TIME (SEC), TEMPERATURE (K)
                   10.5          14.           2170.
*    ADDED MASS (KG) OF EACH SPECIES DURING THIS TIME :
*    UO2 |    ZRO2 |     FEO |     CAO |    SIO2 |   AL2O3 |   CR2O3 |
      0.       0.         0.       7.425      9.99    32.175     0.
*    FE  |    ZR   |     CR  |     NI  |
      0.       0.         0.        0.
*
*--------  CHARACTERISTICS OF CONCRETE WITHOUT STEEL  ---------
*  WEIGHT FRACTION OF THE COMPONENTS : (AL2O3 IS THE COMPLEMENT)
*  CACO3 | CA(OH)2 |    SIO2 | FREE H2O|
     .0546     .1355    .703       .0411
* STEEL; MELT TEMP.; DECOMP. ENTH. ; DENSITY  - ALL WITHOUT STEEL
*G/KGCON.|  KELVIN |    J/KG |   KG/M3 |
       0.0     1573.   2.075E6    2.22E3
*
*
*------ CHARACTERISTICS OF THE LIQUIDUS/SOLIDUS CURVE OF THE OXIDE PHASE
*       SCHROEDER-VAN LAAR EQUATION: IMAT=1
*MAT|
    1
*    LOW TEMPERATURE GROUP :
*NUMBER OF SPECIES; SPECIES:1=UO2; 2=ZRO2; 3=FEO; 4=CAO; 5=SIO2; 6=AL2O3
*---|----|----|----|----|----|----|
    3    3    4    5
*EFFECTIVE LATENT HEAT , SOLIDUS AND LIQUIDUS TEMPERATURE OF THE PHASE :
* J/MOLE |  KELVIN |  KELVIN |
    24840.     1423.     1473.
*    HIGH TEMPERATURE GROUP :
*NUMBER OF SPECIES; SPECIES:1=UO2; 2=ZRO2; 3=FEO; 4=CAO; 5=SIO2; 6=AL2O3
*---|----|----|----|----|----|----|
    1    6
*EFFECTIVE LATENT HEAT , SOLIDUS AND LIQUIDUS TEMPERATURE OF THE PHASE :
* J/MOLE |  KELVIN |  KELVIN |
   110000.     2218.     2268.
*
```

```
*--------  CHARACTERISTICS OF THE OXIDE PHASE  ------------------------
* INITIAL MASS OF OXIDES IN KG :
*    UO2 |    ZRO2 |     FEO |     CAO |    SIO2 |   AL2O3 |   CR2O3 |
       0.        0.        0.    0.075      0.01     .325         0.
*INITIAL TEMP. OF OXIDE / VISCOSITY INCREASE DURING FREEZING (LIMESTONE)
* KELVIN |  1=YES  |
    2170.         0
* POWER IN THE OXIDE PHASE :
* NUMBER OF COUPLES : (TIME IN SEC. ; INTERNAL POWER IN WATT )
*---| IF THIS NUMBER IS 0,GOTO METAL PHASE(NO CARDS FOR SHIFT AND POWER)
   0
*
*
*--------  CHARACTERISTICS OF THE METAL PHASE  ------------------------
* INITIAL MASS OF METALS IN KG :
*     FE |      ZR |      CR |      NI |
     2.76      0.79      0.16      0.16
*INITIAL TEMPERATURE OF METAL / OMIT REST OF METAL AFTER ZR BURNED OUT
*REACTION ZR-SIO2             / METAL MIXED INTO OXIDE <=============
* KELVIN |  1=YES  |   1=YES |   1=YES |
    2170.         0         1         0
* POWER IN THE METAL PHASE :
*NUMBER OF COUPLES : (TIME IN SEC. ; INTERNAL POWER IN WATT )
*CORRECTED AFTER EXPERIMENT
*---| IF THIS NUMBER IS 0,GOTO THE CARD : TIME STEP AND FINAL TIME.
  28
*COUPLES (TIME IN SEC. ; INTERNAL POWER IN WATT ) ( 3 COUPLES/CARD )
*   TIME |   POWER |    TIME |   POWER |    TIME |   POWER |
       0.   100.0E3       1.5   100.0E3       7.0   540.0E3
      14.5   720.0E3      30.0   740.0E3      50.0   760.0E3
      55.0   825.0E3      72.0   760.0E3      86.0   820.0E3
     100.0   740.0E3     116.0  1030.0E3     156.0   720.0E3
     168.0   440.0E3     200.0   460.0E3     210.0   520.0E3
     235.0   430.0E3     800.0   320.0E3    1600.    180.0E3
    1610.    240.0E3    1650.    240.0E3    1700.    185.0E3
    1750.    215.0E3    1800.    185.0E3    1870.    200.0E3
    1939.    180.0E3    1940.   0.000E3     2000.   0.000E3
    5000.   0.000E3
*
*
*------------ TIME CHARACTERISTICS  ---------------------------------
*TIME STEP, FINAL TIME, MIN/MAX TIME STEP:
*  SEC.  |   SEC.  |   SEC.  |   SEC.  |
      0.05     2000.     0.003      0.25
*
* PRINTOUT :
* NUMBER OF PRINTOUT COUPLES :
   3
*COUPLES ( START PRINTOUT TIME,S ; PRINTOUT INTERVAL,S) ( 3 COUPLES/CARD
*   TIME |    STEP |    TIME |    STEP |    TIME |    STEP |
       0.       10.      100.       50.      200.      100.
*
*
*--------  AMBIENT ATMOSPHERIC PRESSURE  -----------------------------
* NUMBER OF COUPLES
*---|
   2
* COUPLES (TIME IN SEC. ; PRESSURE, BAR ) ( 3 COUPLES/CARD )
*   TIME | PRESSURE|    TIME | PRESSURE|---------|---------|
       0.        1.      1.E6        1.
```

```
*--------  AMBIENT TEMPERATURE FOR RADIATION ON THE TOP OF CORIUM ------
* NUMBER OF COUPLES
*---|
    8
*COUPLES (TIME IN SEC. ; TEMPERATURE, K ) ( 3 COUPLES/CARD )
*   TIME | TEMPERA.|    TIME | TEMPERA.|---------|---------|
*       0.      300.       30.     1573.     4000.     1573.
        0.      255.      135.    1837.5      300.    1250.0
     322.5     787.5      450.     562.5     697.5     500.0
    2000.0     500.0     6100.     500.0
*
*
*--------  INITIAL CAVITY SHAPE  ------------------------------------
*NUMBER OF CAVITY POINTS : 1500<=NB<2000: CYL.WITH ROUNDED CORNER+
*                          CONICAL SECTION
*  ONE-DIMENSIONAL CALCULATION DESIRED (1=YES)
*---|----|
 1601    0
*NUMBER OF POINTS ON FLOOR AND CORNER, RADIUS OF CYLINDER AND CORNER,
*INTERVAL BETWEEN POINTS ON CYLINDER, CYLINDER HEIGHT.
*LO.|COR.|RADIUS,M |CORNER,M |INTERV.,M| HEIGHT,M|
   11    5      0.19      0.05      0.02      0.65
         3.      12.5
*
*== INTERVAL BETWEEN CAVITY POINTS DURING PROGRAM RUN.
*  METER |
      .020
*
*== RADIUS FOR SUMP WATER / BASEMAT THICKNESS / TIME SUMP WATER
*  METER |   METER |    SEC. |
     1000.     1000.      1.E7
*
*
*--------  PRINTOUT OPTIONS: ( 0 = NO   ,  1 = YES ) (FORMAT I10 )
* TEMP.  / PROPERT./ INTERFA./ MASS BAL/
         1         1         1         1
*ENER.BAL/ GAS REL./  CAVITY /DIAGNOST./ 1D-TAB. /
         1         1         1         1         1
*
*
*--------  PLOT FILE OPTIONS: ( 0 = NO   ,  1 = YES ) (FORMAT I10 )
*DO YOU WANT DIAGRAMS ?   DO YOU WANT THE CAVITY SHAPE ?
* DIAGS  /  CAVITY /
         1         1
*START TIME AND INTERVAL TO WRITE PLOT FILE, SEC.(THIS CARD MUST STAY)
* WARNING ! FOR KFK PLOT PROGRAM, NO MORE THAN 500 TIMES CAN BE WRITTEN!
* SWITCH TO 3600 S AFTER 1 HOUR
* START  | INTERVAL|  1=YES  |
        0.        5.        0
*START TIME AND INTERVAL TO WRITE CAVITY PLOT, SEC (THIS CARD MUST STAY)
* START  | INTERVAL|
        0.      100.
* CALL CALTHER?  1=YES
   0

*-------  END OF WECHSL INPUT DATA  ---------------------------------
```

A.1.2 Results

A.1.2.1 Print Output Example

```
*************************
*                       *
*  TIME =   2000.15 SEC  *        NEXT TIME STEP= 0.2500 SEC
*                       *
*************************


CAVITY DIMENSIONS, M :

       VERTICAL EROSION  :  -0.377
       MAXIMAL RADIUS    :   0.282
       ZERO LEVEL RADIUS :   0.255

TEMPERATURES, K :

       POOL -      LIQ. METAL: 1787.1   OXIDE    :  1660.2
                   SOL. METAL: 1747.6
       SURFACES -  MET./CONC.: 1719.2   OX./CONC.:  1632.0
                   MET./OX.  : 1783.6   OX./SURF.:  1587.5
       LIQUIDUS -  METAL     : 1786.0   OXIDE    :  1820.5
       SOLIDUS  -  METAL     : 1776.0   OXIDE    :  1490.0
       GAS LEAVING THE MELT  : 1625.6
       WATER GAS REACTION    : 1200.0

PROPERTIES:
                                        METAL            OXIDE
       DENSITY, KG/M3                :    6171.            2754.
       HEAT CONDUCTIVITY, W/(M.K):  45.277              2.667
       HEAT CAPACITY , J/(KG.K)  :     752.             1224.
       SURFACE TENSION, KG/S2    :   1.782              6.389
       VISCOSITY , KG/(S.M)      : 0.5481E-02       0.7255E+02

POOL-CONCRETE INTERFACE :
                              BOTTOM     METAL/WALL  OXIDE/WALL  OXIDE/SURFACE
       EROSION SPEED, CM/S :  0.5128E-02  0.3425E-02  0.1001E-02
       EROSION SPEED, CM/H :    18.46       12.33        3.60
       ENERGY FLUX,   W/M2 :  0.2362E+06  0.1578E+06  0.4612E+05  0.1920E+06
       ENERGY FLUX,  KW/M2 :     236.       158.         46.         192.

       HEAT TRANSFER FOR BOTTOM/CONCRETE FILM MODE

INTEGRATED MASS BALANCE IN THE MELT, TONS :

       INITIAL MELT MASS:    0.436    ACTUAL MASS OF MELT  :    0.800
       ERODED (CONC.+FE):    0.379    MASS OF LEAVING GASES:    0.015

       SUM OF LEFT TERMS:    0.815    SUM OF RIGHT TERMS   :    0.815
       THE DIFFERENCE BETWEEN THE 2 SUMS IS  0.286E-05 TONS, I.E   0.351E-03 %

MASSES ,VOLUMES AND HEIGHTS :
                                                  METAL       OXIDE
       MASS ,TONS                                :    0.312       0.487
       VOLUME, (INCLUDING VOID FRACTION), M3 :    0.05        0.18
       VOLUME, (WITHOUT VOID FRACTION), M3   :    0.05        0.18
       VOID FRACTION , IN PERCENT            :    6.08        4.10
       DEPTH, M                              :    0.25        0.93
       POOL HEIGHT FROM INITIAL BOTTOM, M    :         0.80
       VOLUME OF ERODED CONCRETE, M3         :         0.17
       MASS OF ERODED CONCRETE, TONS         :         0.379
```

WEIGHT FRACTION AND WEIGHT OF SPECIES IN EACH PHASE :

METAL: (SUM: 312.33)	KG	%	OXIDE: (SUM: 487.49)	KG	%
ZR :	0.00	0.000	UO2 :	0.00	0.000
SI :	4.91	1.572	ZRO2 :	106.11	21.766
CR :	16.16	5.174	FEO :	0.00	0.000
FE :	275.72	88.279	CAO :	57.97	11.892
NI :	15.54	4.976	SIO2 :	265.97	54.559
			AL2O3 :	57.44	11.783
			CR2O3 :	0.00	0.000

CRUST THICKNESS IN EACH PHASE, CM :

IN THE METAL PHASE:		IN THE OXIDE PHASE:	
METAL/OXIDE:	0.00	OXIDE/METAL:	0.00
METAL/CONCRETE:	1.10	OXIDE/CONCRETE:	0.00
		OXIDE/SURFACE:	0.00

HEAT FLUX BALANCE IN EACH PHASE, WATT :

		METAL	OXIDE
POWER DUE TO DECAY HEAT	:	0.0000E+00	0.0000E+00
POWER ENTERING DUE TO GAS AND OXIDES	:	0.1114E+06	0.2070E+06
POWER LEAVING DUE TO GAS AND OXIDES	:	-0.1312E+06	-0.2603E+05
POWER DUE TO OXIDATION REACTIONS	:	0.6097E+05	0.0000E+00
POWER DUE TO CONCRETE DECOMPOSITION	:	-0.1122E+06	-0.7486E+05
CONDUCTION BETWEEN PHASES	:	-0.7988E+05	0.7988E+05
RADIATION OR EVAPORATED AT SURFACE	:	0.0000E+00	-0.4545E+05
SPLASHOUT	:	0.0000E+00	0.0000E+00
SENSIBLE HEAT	:	-0.1509E+06	0.1406E+06

INTEGRATED ENERGY BALANCE IN THE MELT, JOULE :

INITIAL ENTHALPIE	0.7033E+09	INTEGRATED ENTHALPIE	0.1356E+10
DECAY HEAT	0.6405E+09	CONCRETE DECOMPOSITION	0.7865E+09
ENTERING(GAS,OX.)	0.7856E+09	LEAVING (GASES)	0.9969E+08
OXIDAT. REACTIONS	0.4995E+09	RADIATION OR TO WATER	0.1130E+09
		SPLASHOUT	0.2738E+09
SUM OF LEFT TERMS	0.2629E+10	SUM OF RIGHT TERMS	0.2629E+10

THE DIFFERENCE BETWEEN THE 2 SUMS IS 0.4963E-03 J., I.E 0.1888E-10 %

GASES GOING IN THE CONTAINMENT, AT THE TEMPERATURE T= 1626. K.
AFTER THAT THE WATER-GAS REACTION OCCURED AT THE SURFACE :

	CO2	CO	H2O	H2
HEAT FLUX, WATT	0.1160E+04	0.1368E+04	0.1449E+05	0.8978E+04
MASS FLUX, KG/S	0.7584E-03	0.8947E-03	0.2715E-02	0.4432E-03
MOL. FLUX, MOL/S	0.1723E-01	0.3194E-01	0.1508E+00	0.2205E+00
WEIGHT FRACTION	0.1576E+00	0.1860E+00	0.5643E+00	0.9210E-01
MOLAR FRACTION	0.4099E-01	0.7598E-01	0.3586E+00	0.5244E+00
TOTAL MASS, KG	0.1720E+01	0.4697E+01	0.6360E+01	0.2428E+01
TOT.MOLS, MOL	0.3908E+02	0.1677E+03	0.3531E+03	0.1208E+04

THE CAVITY SHAPE HAS BEEN CALCULATED USING 73 POINTS, COORDINATES IN CM :
R=RADIUS ; Z=DEPTHNESS ; Z-REFERENCE: INITIAL BOTTOM OF THE CAVITY

R	Z	R	Z	R	Z	R	Z
0.0	-37.7	2.0	-37.7	4.0	-37.7	6.0	-37.7
8.0	-37.7	10.0	-37.7	12.0	-37.7	14.0	-37.6
16.0	-37.4	17.9	-36.9	19.8	-36.2	21.5	-35.1
23.0	-33.8	24.3	-32.3	25.3	-30.6	26.2	-28.8
26.9	-26.9	27.4	-25.0	27.7	-23.0	28.0	-21.0
28.1	-19.0	28.2	-17.0	28.2	-15.0	27.9	-12.5
27.7	-11.0	27.4	-9.1	27.1	-7.1	26.8	-5.1
26.5	-3.1	26.3	-1.1	26.0	0.8	25.8	2.8
25.6	4.8	25.5	6.8	25.3	8.8	25.1	10.8
25.0	12.8	24.9	14.8	24.8	16.8	24.7	18.8
24.6	20.8	24.5	22.8	24.4	24.8	24.3	26.8
24.3	28.8	24.2	30.8	24.2	32.8	24.1	34.8
24.1	36.8	24.1	38.8	24.0	40.8	24.0	42.8
24.0	44.8	24.0	46.8	24.0	48.8	24.0	50.8
24.1	52.8	24.1	54.8	24.3	56.8	24.4	58.8
24.6	60.8	24.8	62.7	25.0	64.7	25.3	66.7
25.6	68.7	25.9	70.7	26.3	72.6	26.7	74.6
27.0	76.6	27.4	78.5	27.5	80.0	27.6	82.5
27.7	84.5	27.9	86.5	28.0	88.5	28.2	90.9
28.6	94.1	28.8	96.1	29.1	98.1	29.4	100.8
30.1	104.8	30.9	109.2	31.3	111.3	31.6	113.6
32.1	116.1	32.4	118.1	32.8	120.1	33.1	122.1
33.5	124.0	33.9	126.0	34.2	127.9	34.6	129.9
35.1	132.4	35.6	134.9	36.0	137.3	36.6	140.2
37.3	144.4	38.0	148.2	38.5	151.0	39.1	153.5
39.8	157.0	40.7	160.8	41.1	162.8	41.5	164.7
42.0	166.7	42.4	168.6	42.8	170.6	43.3	172.5
43.7	174.5	44.1	176.4	44.6	178.4	45.0	180.3
45.4	182.3	45.9	184.2	46.3	186.2	46.7	188.1
47.2	190.1	47.6	192.0	48.0	194.0	48.5	196.0
48.9	197.9	49.3	199.9	49.8	201.8	50.2	203.8
50.6	205.7	51.1	207.7	51.5	209.6	51.9	211.6
52.4	213.5	52.8	215.5	53.2	217.4	53.7	219.4
54.1	221.3	54.5	223.3	55.0	225.2	55.4	227.2
55.8	229.1	56.3	231.1	56.7	233.0	57.1	235.0
57.6	237.0	58.0	238.9	58.4	240.9	58.9	242.8
59.3	244.8	59.7	246.7	60.2	248.7	60.6	250.6
61.0	252.6	61.5	254.5	61.9	256.5	62.3	258.4
62.8	260.4	63.2	262.3	63.6	264.3	64.1	266.2
64.5	268.2	64.9	270.1	65.4	272.1	65.8	274.1
66.2	276.0	66.7	278.0	67.1	279.9	67.5	281.9
68.0	283.8	68.4	285.8	68.8	287.7	69.3	289.7
69.7	291.6	70.1	293.6	70.6	295.5	71.0	297.5
71.4	299.4						

PREDEFINED STOP BECAUSE TIME= 0.2000E+04 SEC. REACHES THE TIME LIMIT
TF= 0.2000E+04 SEC. GIVEN IN THE INPUT DATA.

A.1.2.2 Cavity Shape

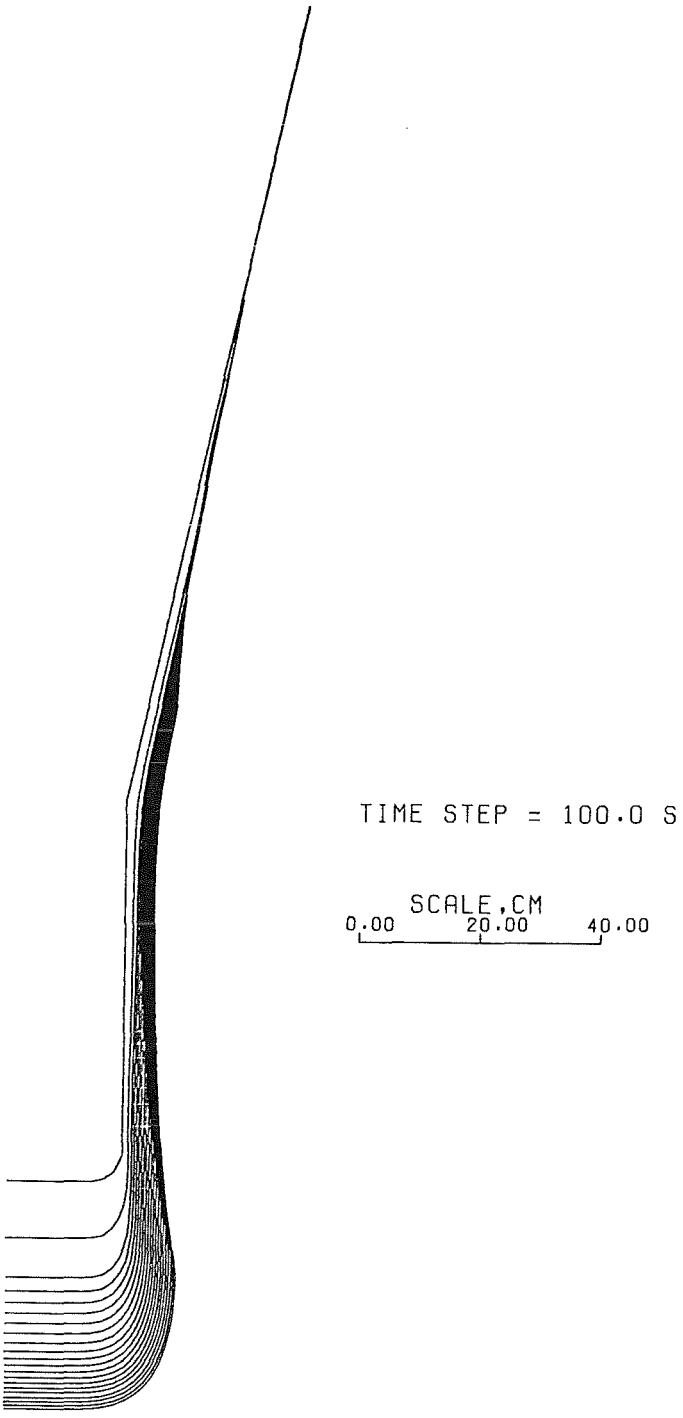

Fig. 28: Cavity shape (BETA Test)

A.1.2.3 Selected Diagrams

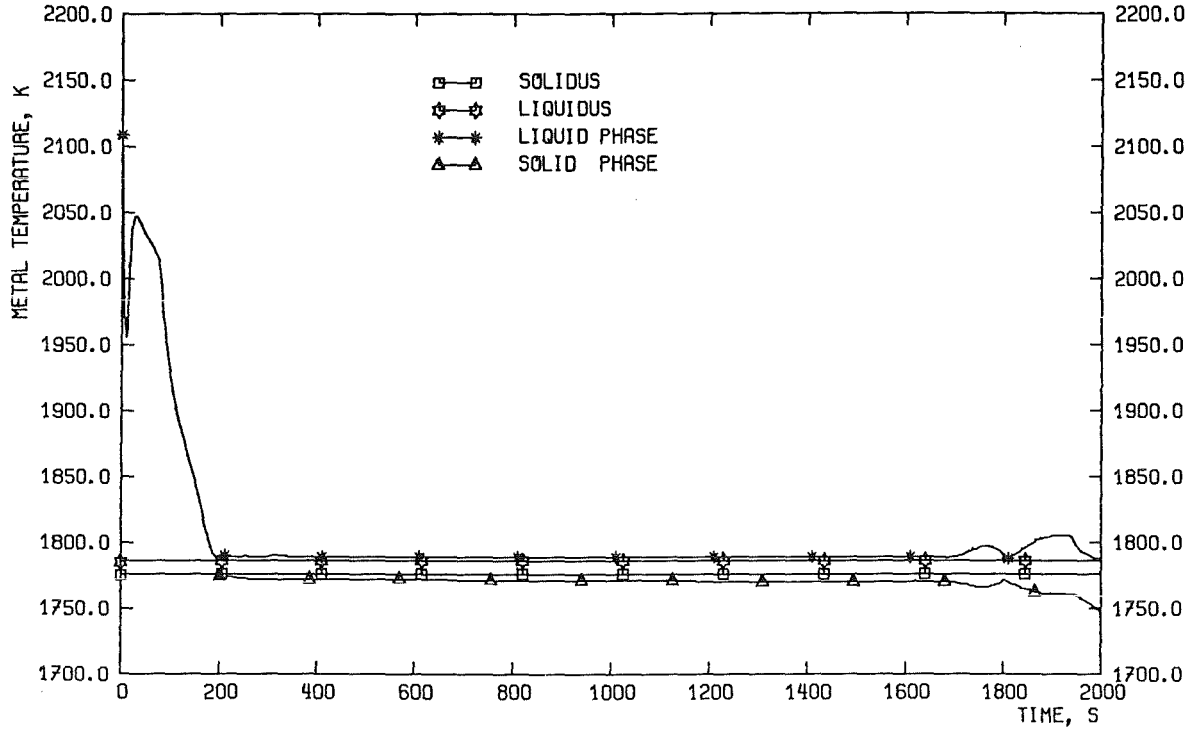

Fig. 29: Temperatures of metallic phase (BETA test)

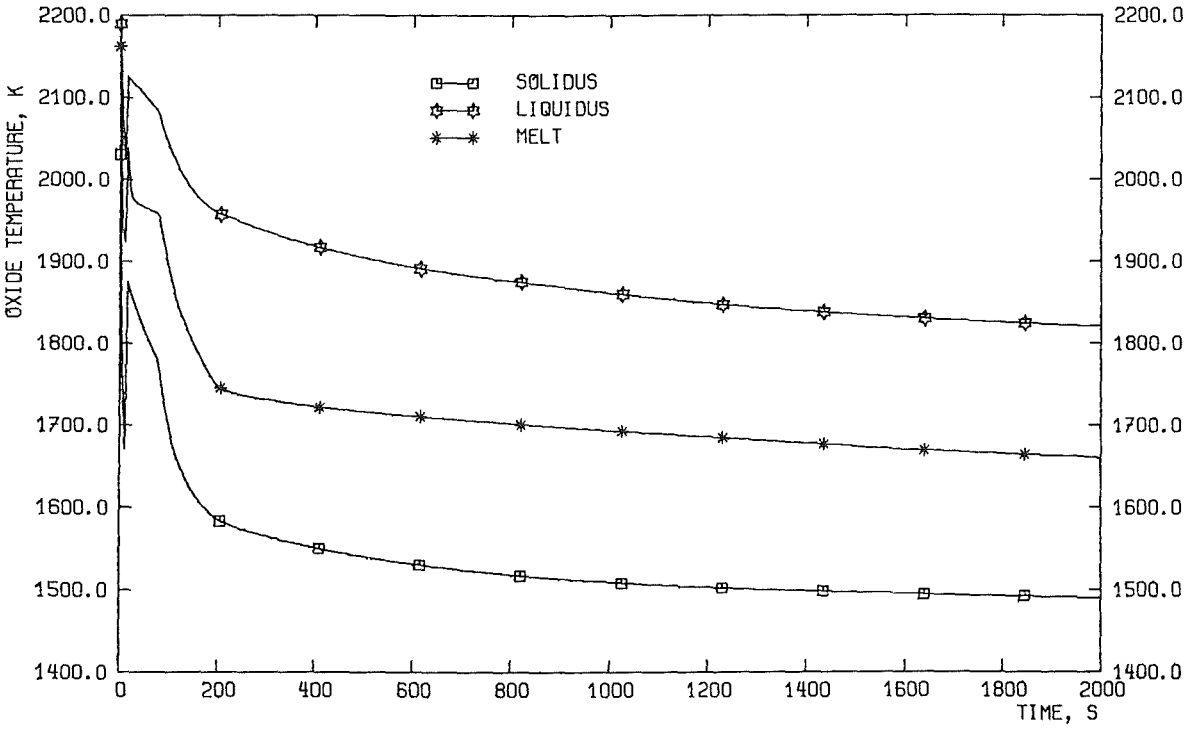

Fig. 30: Temperature of oxidic phase (BETA test)

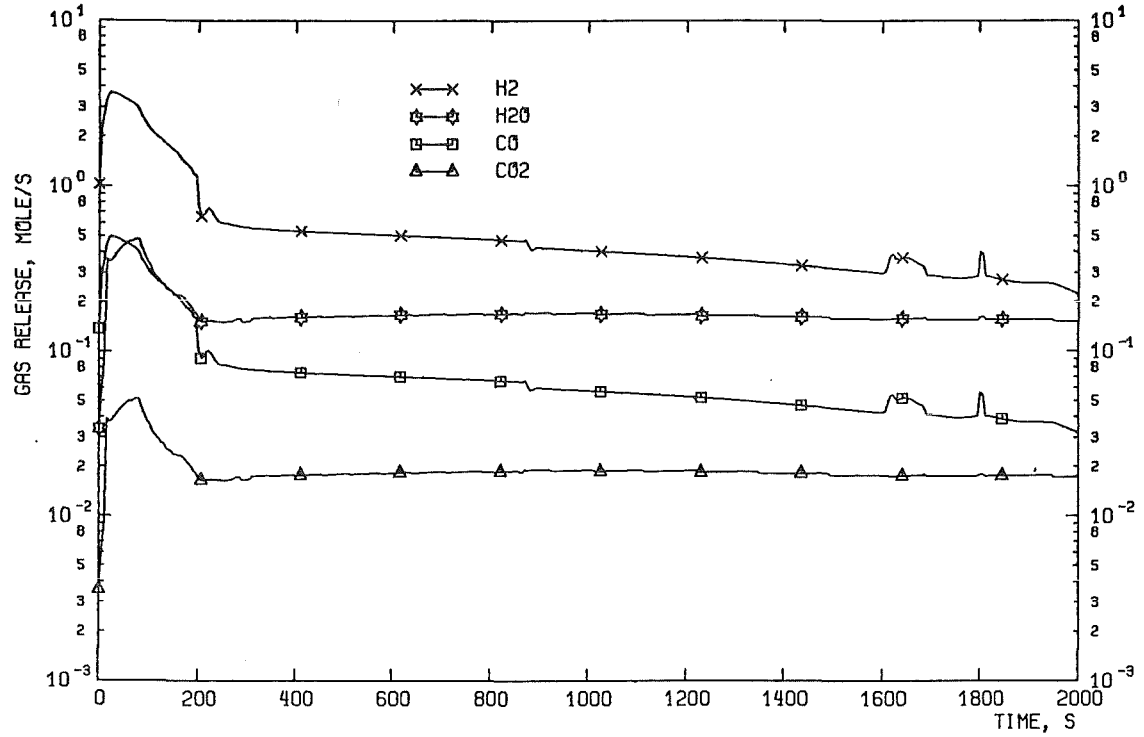

Fig. 31: Gas release rates (BETA test)

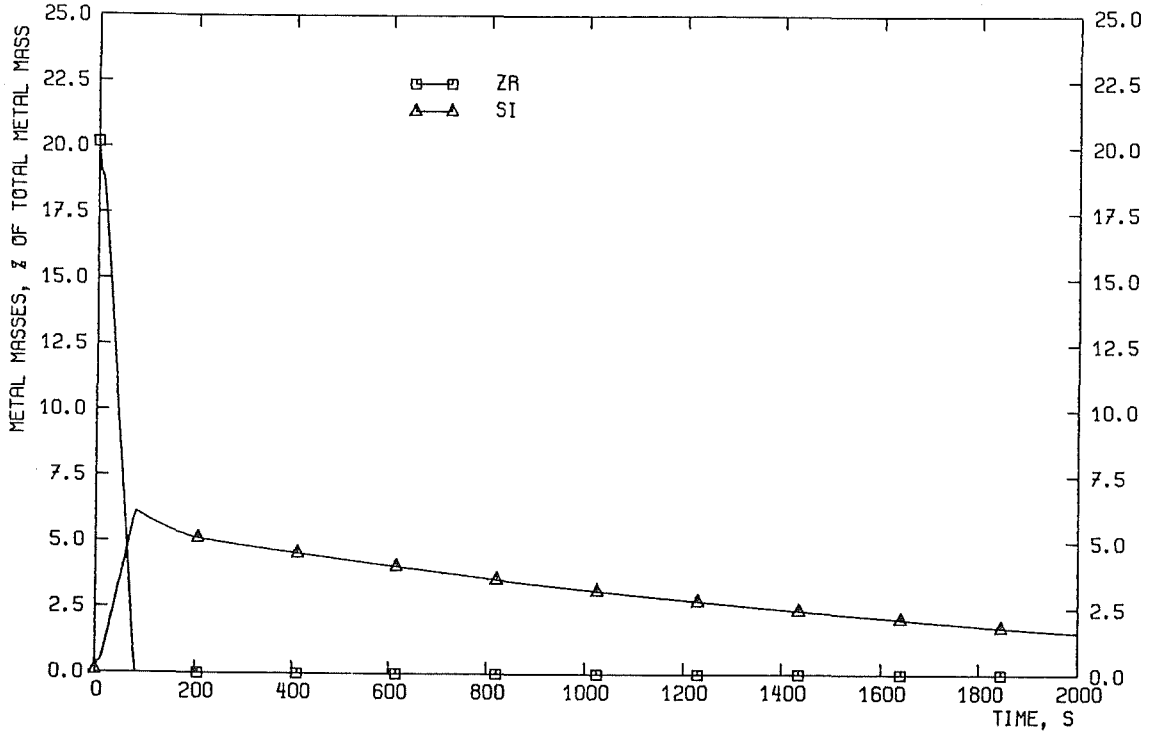

Fig. 32: Fraction of Zr and Si in the metal melt (BETA test)

A.2 SURC Test

In the SURC-2 experiment (performed at Sandia, USA) the corium was initially composed of oxides (UO_2, ZrO_2) and of approximately 8 % Zr. The melt temperature amounted to 2600 K at the beginning of concrete ablation of a one-dimensional basaltic crucible. The WECHSL calculation was performed using a one-dimensional cavity with an oxidic melt which contained a homgeneously dispersed metallic phase.

A.2.1 Input Data

```
  SURC-2, T=2600K
*      METAL DISPERSED INTO OXIDE, 1-DIMENSIONAL
*===========
*===========
*=======  THERMITE ADDITION:  RATE AND TIME OF REACTION
*  KG/S   |  SEC.    |
         0.         0.
*===========
*
*-------  ADDITION OF OTHER MATERIALS   --------------------------------
*  NUMBER OF ADDITIONS :
         0
*===========
*=======  CONCRETE CHARACTERISTICS :
*WEIGHT FRACTION OF THE COMPONENTS : (AL2O3 IS THE COMPLEMENT)
*  CACO3 | CA(OH)2 |    SIO2 | FREE H2O|
     .0568     .0742     .7000     .0239
*REINFORCED STEEL; MELT TEMP.; DECOMPOSITION ENTH. ; DENSITY :
*G/KGCON.|  KELVIN |    J/KG |   KG/M3 |
       0.0     1573.   2.075E6    2.25E3
*===========
*===========
*
*------ CHARACTERISTICS OF THE LIQUIDUS/SOLIDUS CURVE OF THE OXIDE PHASE
*       TABLE INPUT; NUMBER OF TABLE POINTS IMAT
*MAT|
   11
*
*    LOW TEMPERATURE GROUP :
*NUMBER OF SPECIES; SPECIES:1=UO2; 2=ZRO2; 3=FEO; 4=CAO; 5=SIO2; 6=AL2O3
*---|----|----|----|----|----|----|
    4    3    4    5    6
*LIQUIDUS: CCL,TLL (3 COUPLES PER CARD)
*     CCL|      TLL|      CCL|      TLL|      CCL|      TLL|
        .0     1573.        .1     1773.        .2     1893.
        .3     2073.        .4     2193.        .5     2293.
        .6     2373.        .7     2453.        .8     2523.
        .9     2583.        1.     2673.
*
*    HIGH TEMPERATURE GROUP :
*NUMBER OF SPECIES; SPECIES:1=UO2; 2=ZRO2; 3=FEO; 4=CAO; 5=SIO2; 6=AL2O3
*---|----|----|----|----|----|----|
    2    1    2
*SOLIDUS: CCL,TLL (3 COUPLES PER CARD)
*     CCS|      TSS|      CCS|      TSS|      CCS|      TSS|
        .0     1423.        .1     1483.        .2     1543.
        .3     1615.        .4     1715.        .5     1815.
        .6     1930.        .7     2073.        .8     2201.
        .9     2313.        1.     2423.
*
*
*
*       OXIDE PHASE :
*INITIAL MASS OF OXIDES IN KG :
*    UO2 |    ZRO2 |     FEO |     CAO |    SIO2 |   AL2O3 |   CR2O3 |
 140.8949  46.08140         0.      0.00       0.0      0.00        0.
```

```
*
*INITIAL TEMP. OF OXIDE / VISCOSITY INCREASE DURING FREEZING (LIMESTONE)
* KELVIN |  1=YES  |         |         |
     2600.         0         1         1
* POWER IN THE OXIDE PHASE :
* NUMBER OF COUPLES : (TIME IN SEC. ; INTERNAL POWER IN WATT )
*---| IF THIS NUMBER IS 0,GOTO METAL PHASE(NO CARDS FOR SHIFT AND POWER)
    9
*SHIFT TIME AND FACTOR FOR INTERNAL HEAT GENERATION (OXIDE AND METAL)
*  SEC.  |---------|
     7800.       1.0
*COUPLES (TIME IN SEC. ; INTERNAL POWER IN WATT ) ( 3 COUPLES/CARD )
*   TIME |   POWER |    TIME |   POWER |    TIME |   POWER |
     7800.   36.00E3     8400.   36.00E3    9600.0   26.00E3
   10800.0   23.90E3    12000.   23.30E3   13140.0   23.50E3
   13200.0   40.00E3    14400.   34.00E3   16800.0   31.40E3
*
*==========
*==========
*====== METAL PHASE :
*INITIAL MASS OF METALS IN KG :
*     FE |      ZR |      CR |      NI |      SI |
       0.    16.9237        0.       0.0       0.
*
*INITIAL TEMP. OF METAL / OMIT METAL AFTER ZR BURNOUT / REACTION ZR-SIO2
* KELVIN |  1=YES  |  1=YES  |  1=YES  | METAL DISPERSED INTO OXIDE
     2600.         0         1         1
*==== POWER IN THE METAL PHASE :
*NUMBER OF COUPLE : (TIME IN SEC. ; INTERNAL POWER IN WATT )
*---| IF THIS NUMBER IS 0,GOTO THE CARD : TIME STEP AND FINAL TIME.
    0
*==========
*==========
*=== TIME CHARACTERISTICS :  TIME STEP , FINAL TIME, MIN/MAX TIME STEP:
*  SEC.  |   SEC.  |   SEC.  |   SEC.  |
      0.05     8400.  0.010000       1.0
*==========
*==========
*=======  PRINTOUT :
*NUMBER OF PRINTOUT COUPLES :
    5
*COUPLES ( START PRINTOUT TIME,S ; PRINTOUT INTERVAL,S) ( 3 COUPLES/CARD
*   TIME |    STEP |    TIME |    STEP |    TIME |    STEP |
        0.       10.      100.      100.     1000.      200.
     5000.      500.    10000.      500.
*==========
*==========
*=======  AMBIENT ATMOSPHERIC PRESSURE:
*NUMBER OF COUPLES ( TIME, S ; PRESSURE,BAR )
*---|
    2
*COUPLES (TIME IN SEC. ; PRESSURE, BAR ) ( 3 COUPLES/CARD )
*   TIME | PRESSURE|    TIME | PRESSURE|---------|---------|
    7800.0     1.000      1.E6     1.000
*==========
*==========
```

```
*=======  AMBIENT TEMPERATURE FOR RADIATION ON THE TOP OF CORIUM :
*NUMBER OF COUPLES ( TIME, S ; TEMPERATURE, K )
*---|
    9
*COUPLES (TIME IN SEC. ; TEMPERATURE, K ) ( 3 COUPLES/CARD )
*   TIME | TEMPERA.|    TIME | TEMPERA.|---------|---------|
     7800.      450.     8100.      550.     8400.     1000.
     9000.      900.     9600.      900.    13800.     1250.
    15900.     1620.    16200.     1550.    16800.     1600.
*===========
*===========
*=======  INITIAL CAVITY SHAPE :
*NUMBER OF CAVITY POINTS : 1000<NB<1499 : CYLINDER WITH ROUNDED CORNER:
*ONE-DIMENSIONAL CALCULATION DESIRED ( 1=YES )
*---|----|
 1032    1
*NUMBER OF POINTS ON FLOOR AND CORNER, RADIUS OF CYLINDER AND CORNER,
*INTERVAL BETWEEN POINTS ON CYLINDER, CYLINDER HEIGHT.
*LO.|COR.|RADIUS,M |CORNER,M |INTERV.,M| HEIGHT,M|
   40   10      0.20     0.002     0.015      1.80
*===========
*== INTERVAL BETWEEN CAVITY POINTS DURING PROGRAM RUN.
*  METER |
      .010
*===========
* RADIUS SUMP WATER INGRESSION , BASEMAT THICKNESS ,TIME FOR SUMP WATER
*  METER |   METER |   SEC.  |
     1000.     1000.      1.E7
*===========
*===========
*=======  PRINTOUT OPTIONS: ( 0 = NO   ,  1 = YES ) (FORMAT I10 )
*TEMPERAT/ PROPERT./ INTERFA./ MASS BAL/
         1         1         1         1
*ENER.BAL/ GAS REL./  CAVITY /DIAGNOST./ 1D-TAB
         1         1         1         1        0
*===========
*===========
*=======  PLOT FILE OPTIONS: ( 0 = NO   ,  1 = YES ) (FORMAT I10 )
*DO YOU WANT PLOTS (CAVITY NOT INCLU.)? ; DO YOU WANT THE CAVITY SHAPE ?
* PLOTS  /  CAVITY /
         1         1
* START TIME AND INTERVAL TO WRITE PLOT FILE, SEC.(THIS CARD MUST STAY)
* WARNING ! FOR KFK PLOT PROGRAM, NO MORE THAN 500 TIMES CAN BE WRITTEN!
* SWITCH TO 3600 S AFTER 1 HOUR
* START  | INTERVAL|  1=YES   |
        0.       20.         0
*START TIME AND INTERVAL TO WRITE CAVITY PLOT, S (THIS CARD MUST STAY)
* START  | INTERVAL|
        0.      180.
*===========
*CALL CALTHER ? ( YES=1 )
        0
*========================= END OF WECHSL INPUT DATA ==================
*===========
```

A.2.2 Results

A.2.2.1 Print Output Example

```
*************************
*                       *
*  TIME =   8400.28 SEC  *        NEXT TIME STEP= 1.0000 SEC
*                       *
*************************    +++ METAL DISPERSED IN OXIDE PHASE +++


CAVITY DIMENSIONS, M :

       VERTICAL EROSION  :  -0.391
       MAXIMAL RADIUS    :   0.200
       ZERO LEVEL RADIUS :   0.200

TEMPERATURES, K :

       MELT            : 1742.0
       MELT/CONCRETE   : 1652.5
       MELT/SURFACE    : 1534.5
       LIQUIDUS        : 2187.7
       SOLIDUS         : 1710.6
       LEAVING GAS     : 1723.9
       WATER GAS REACT.: 1200.0

PROPERTIES OF THE MELT :

       DENSITY, KG/M3            : 4363.
       HEAT CONDUCTIVITY, W/(M.K):    2.848
       HEAT CAPACITY , J/(KG.K)  :  821.
       SURFACE TENSION, KG/S2    :    3.239
       VISCOSITY , KG/(S.M)      :    0.3111E+02

POOL-CONCRETE INTERFACE :
                                BOTTOM          MELT/WALL       MELT/SURFACE
       EROSION SPEED, CM/S :  0.4415E-02      0.0000E+00
       EROSION SPEED, CM/H :    15.89           0.00
       ENERGY FLUX,   W/M2 :  0.2061E+06      0.0000E+00      0.1388E+06
       ENERGY FLUX,  KW/M2 :     206.           0.              139.

       HEAT TRANSFER FOR BOTTOM/CONCRETE MIXED MODE

INTEGRATED MASS BALANCE IN THE MELT, TONS :

       INITIAL MELT MASS:    0.204    ACTUAL MASS OF MELT  :    0.316
       ERODED (CONC.+FE):    0.114    MASS OF LEAVING GASES:    0.002

       SUM OF LEFT TERMS:    0.318    SUM OF RIGHT TERMS   :    0.318
       THE DIFFERENCE BETWEEN THE 2 SUMS IS  0.410E-06 TONS, I.E   0.129E-03 %

MASSES ,VOLUMES AND HEIGHTS :
                                                    METAL       OXIDE
       MASS ,TONS                                :     0.001       0.315
       VOLUME, (INCLUDING VOID FRACTION), M3 :           0.08
       VOLUME, (WITHOUT VOID FRACTION), M3   :           0.07
       VOID FRACTION , IN PERCENT            :           4.60
       DEPTH, M                              :           0.60
       POOL HEIGHT FROM INITIAL BOTTOM, M    :           0.21
       VOLUME OF ERODED CONCRETE, M3         :           0.05
       MASS OF ERODED CONCRETE, TONS         :           0.114
```

WEIGHT FRACTION AND WEIGHT OF SPECIES IN THE MELT (315.76 KG) :

METALS :	KG	%	OXIDES :	KG	%
ZR :	0.00	0.000	UO2 :	140.89	44.621
SI :	0.57	0.179	ZRO2 :	68.94	21.833
CR :	0.00	0.000	FEO :	0.00	0.000
FE :	0.00	0.000	CAO :	10.05	3.183
NI :	0.00	0.000	SIO2 :	78.74	24.936
			AL2O3 :	16.57	5.248
			CR2O3 :	0.00	0.000

CRUST THICKNESS IN THE MELT, CM :

MELT/CONCRETE:	0.13
MELT/SURFACE :	0.36

HEAT FLUX BALANCE IN THE MELT , WATT :

POWER DUE TO DECAY HEAT	:	0.3205E+05
POWER ENTERING DUE TO GAS AND OXIDES	:	0.2423E+05
POWER LEAVING DUE TO GAS AND OXIDES	:	-0.1666E+04
POWER DUE TO OXIDATION REACTIONS	:	0.8828E+04
POWER DUE TO CONCRETE DECOMPOSITION	:	-0.2681E+05
CONDUCTION BETWEEN PHASES	:	--
RADIATION OR EVAPORATED AT SURFACE	:	-0.1744E+05
SPLASHOUT	:	0.0000E+00
SENSIBLE HEAT	:	0.1920E+05

INTEGRATED ENERGY BALANCE IN THE MELT, JOULE :

INITIAL ENTHALPIE	0.2917E+09	INTEGRATED ENTHALPIE	0.3824E+09
DECAY HEAT	0.2495E+09	CONCRETE DECOMPOSITION	0.2370E+09
ENTERING(GAS,OX.)	0.2138E+09	LEAVING (GASES)	0.1777E+08
OXIDAT. REACTIONS	0.1147E+09	RADIATION OR TO WATER	0.1878E+09
		SPLASHOUT	0.4473E+08
SUM OF LEFT TERMS	0.8697E+09	SUM OF RIGHT TERMS	0.8697E+09

THE DIFFERENCE BETWEEN THE 2 SUMS IS 0.3792E-05 J., I.E 0.4360E-12 %

GASES GOING IN THE CONTAINMENT, AT THE TEMPERATURE T= 1724. K.
AFTER THAT THE WATER-GAS REACTION OCCURED AT THE SURFACE :

	CO2	CO	H2O	H2
HEAT FLUX, WATT	0.1127E-12	0.3395E+03	0.3605E-12	0.1326E+04
MASS FLUX, KG/S	0.6776E-19	0.2053E-03	0.6437E-19	0.6064E-04
MOL. FLUX, MOL/S	0.1540E-17	0.7331E-02	0.3574E-17	0.3017E-01
WEIGHT FRACTION	0.2548E-15	0.7720E+00	0.2420E-15	0.2280E+00
MOLAR FRACTION	0.4106E-16	0.1955E+00	0.9532E-16	0.8045E+00
TOTAL MASS, KG	0.3263E-15	0.1815E+01	0.1172E-14	0.5359E+00
TOT.MOLS, MOL	0.7415E-14	0.6481E+02	0.6505E-13	0.2666E+03

THE CAVITY SHAPE HAS BEEN CALCULATED USING 82 POINTS, COORDINATES IN CM :
R=RADIUS ; Z=DEPTHNESS ; Z-REFERENCE: INITIAL BOTTOM OF THE CAVITY

R	Z	R	Z	R	Z	R	Z
0.0	-39.1	1.0	-39.1	2.0	-39.1	3.0	-39.1
4.0	-39.1	5.0	-39.1	6.0	-39.1	7.0	-39.1
8.0	-39.1	9.0	-39.1	10.0	-39.1	11.0	-39.1
12.0	-39.1	13.0	-39.1	14.0	-39.1	15.0	-39.1
16.0	-39.1	17.0	-39.1	18.0	-39.0	19.0	-38.8
19.7	-38.1	20.0	-37.1	20.0	-36.1	20.0	-35.1
20.0	-34.1	20.0	-33.1	20.0	-32.1	20.0	-31.1
20.0	-30.1	20.0	-29.1	20.0	-28.1	20.0	-27.1
20.0	-26.1	20.0	-25.1	20.0	-24.1	20.0	-23.1
20.0	-22.1	20.0	-21.1	20.0	-20.1	20.0	-19.1
20.0	-18.1	20.0	-17.1	20.0	-16.1	20.0	-15.1
20.0	-14.1	20.0	-13.1	20.0	-12.1	20.0	-11.1
20.0	-10.1	20.0	-9.1	20.0	-8.1	20.0	-7.1
20.0	-6.1	20.0	-5.1	20.0	-4.1	20.0	-3.1
20.0	-2.1	20.0	-1.1	20.0	-0.1	20.0	0.9
20.0	1.9	20.0	2.9	20.0	3.9	20.0	4.9
20.0	5.9	20.0	6.9	20.0	7.9	20.0	8.9
20.0	9.9	20.0	10.9	20.0	11.9	20.0	12.9
20.0	13.9	20.0	14.9	20.0	15.9	20.0	16.9
20.0	17.9	20.0	18.9	20.0	19.9	20.0	20.9
20.0	21.4	20.0	22.9	20.0	23.9	20.0	24.9
20.0	25.9	20.0	26.9	20.0	30.1	20.0	33.0
20.0	34.6	20.0	37.5	20.0	40.2	20.0	41.5
20.0	42.7	20.0	43.7	20.0	44.8	20.0	45.8
20.0	46.9	20.0	47.9	20.0	49.0	20.0	50.0
20.0	51.0	20.0	52.1	20.0	53.1	20.0	54.1
20.0	55.1	20.0	56.1	20.0	57.2	20.0	58.2
20.0	59.2	20.0	60.2	20.0	61.2	20.0	62.2
20.0	63.2	20.0	64.2	20.0	65.2	20.0	66.2
20.0	67.2	20.0	68.2	20.0	69.2	20.0	70.2
20.0	71.2	20.0	72.2	20.0	73.2	20.0	74.2
20.0	75.2	20.0	76.2	20.0	77.2	20.0	78.2
20.0	79.2	20.0	80.2	20.0	81.2	20.0	82.2
20.0	83.2	20.0	84.2	20.0	85.2	20.0	86.2
20.0	87.2	20.0	88.2	20.0	89.2	20.0	90.2
20.0	91.2	20.0	92.2	20.0	93.2	20.0	94.2
20.0	95.2	20.0	96.2	20.0	97.2	20.0	98.2
20.0	99.2	20.0	100.2	20.0	101.2	20.0	102.2
20.0	103.2	20.0	104.2	20.0	105.2	20.0	106.2
20.0	107.2	20.0	108.2	20.0	109.2	20.0	110.2
20.0	111.2	20.0	112.2	20.0	113.2	20.0	114.2
20.0	115.2	20.0	116.2	20.0	117.2	20.0	118.2
20.0	119.2	20.0	120.2	20.0	121.2	20.0	122.2
20.0	123.2	20.0	124.2	20.0	125.2	20.0	126.2
20.0	127.2	20.0	128.2	20.0	129.2	20.0	130.2
20.0	131.2	20.0	132.2	20.0	133.2	20.0	134.2
20.0	135.2	20.0	136.2	20.0	137.2	20.0	138.2
20.0	139.2	20.0	140.2	20.0	141.2	20.0	142.2
20.0	143.2	20.0	144.2	20.0	145.2	20.0	146.2
20.0	147.2	20.0	148.2	20.0	149.2	20.0	150.2
20.0	151.2	20.0	152.2	20.0	153.2	20.0	154.2
20.0	155.2	20.0	156.2	20.0	157.2	20.0	158.2
20.0	159.2	20.0	160.2	20.0	161.2	20.0	162.2
20.0	163.2	20.0	164.2	20.0	165.2	20.0	166.2
20.0	167.2	20.0	168.2	20.0	169.2	20.0	170.2
20.0	171.2	20.0	172.2	20.0	173.2	20.0	174.2
20.0	175.2	20.0	176.2	20.0	177.2	20.0	178.2

PREDEFINED STOP BECAUSE TIME= 0.8400E+04 SEC. REACHES THE TIME LIMIT
TF= 0.8400E+04 SEC. GIVEN IN THE INPUT DATA.

A.2.2.2 Cavity Shape

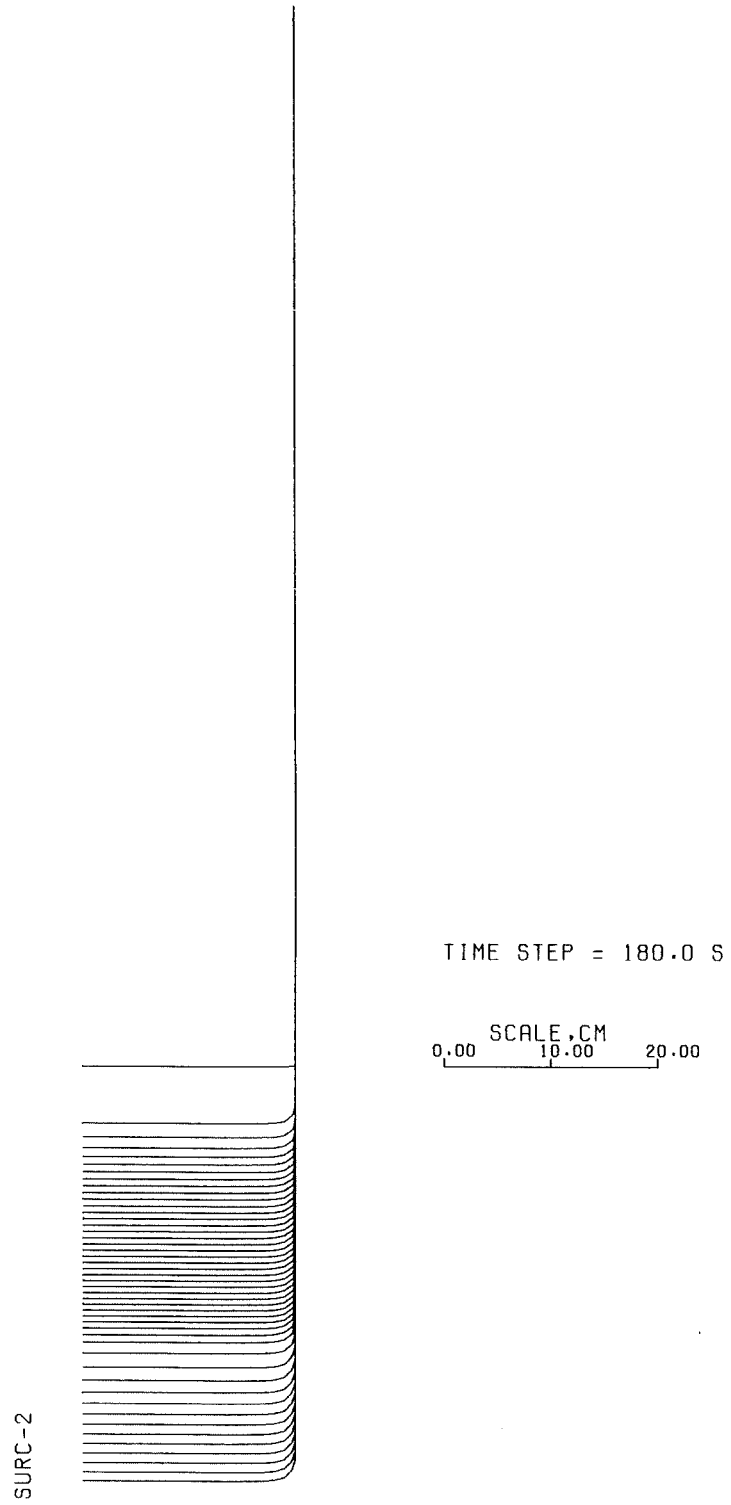

Fig. 33: Cavity shape (SURC test)

A.2.2.3 Selected Diagrams

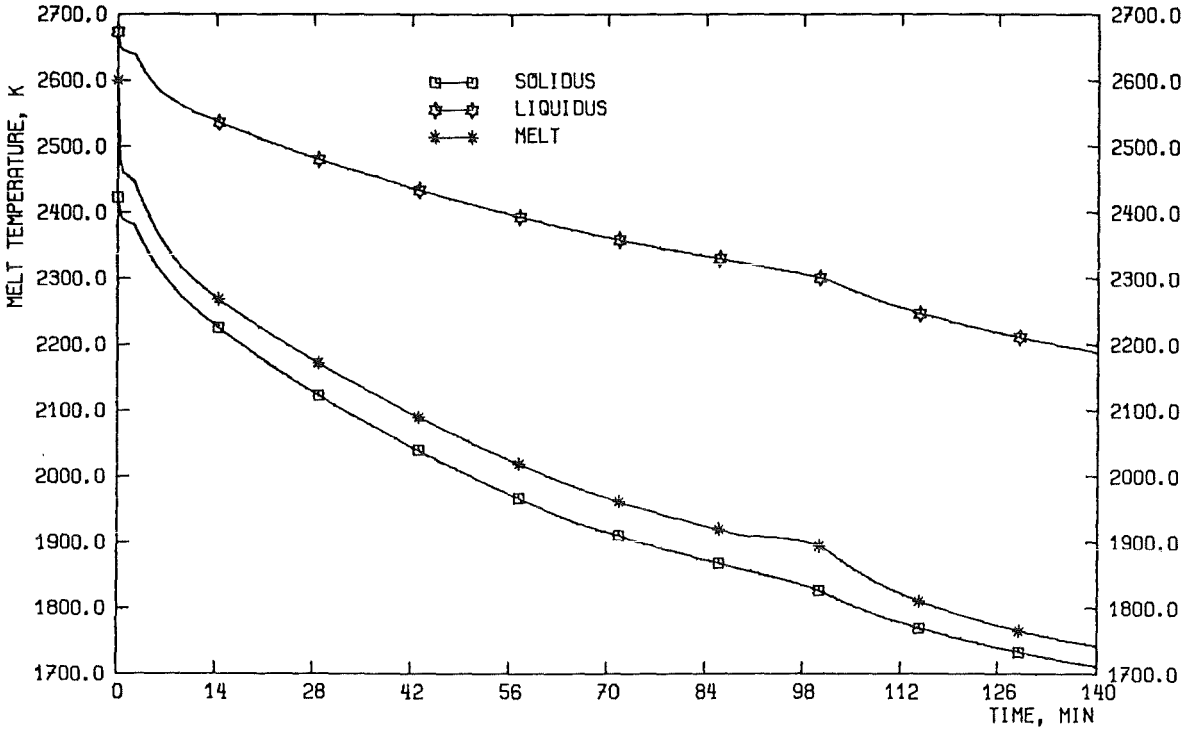

Fig. 34: Melt temperature (SURC test)

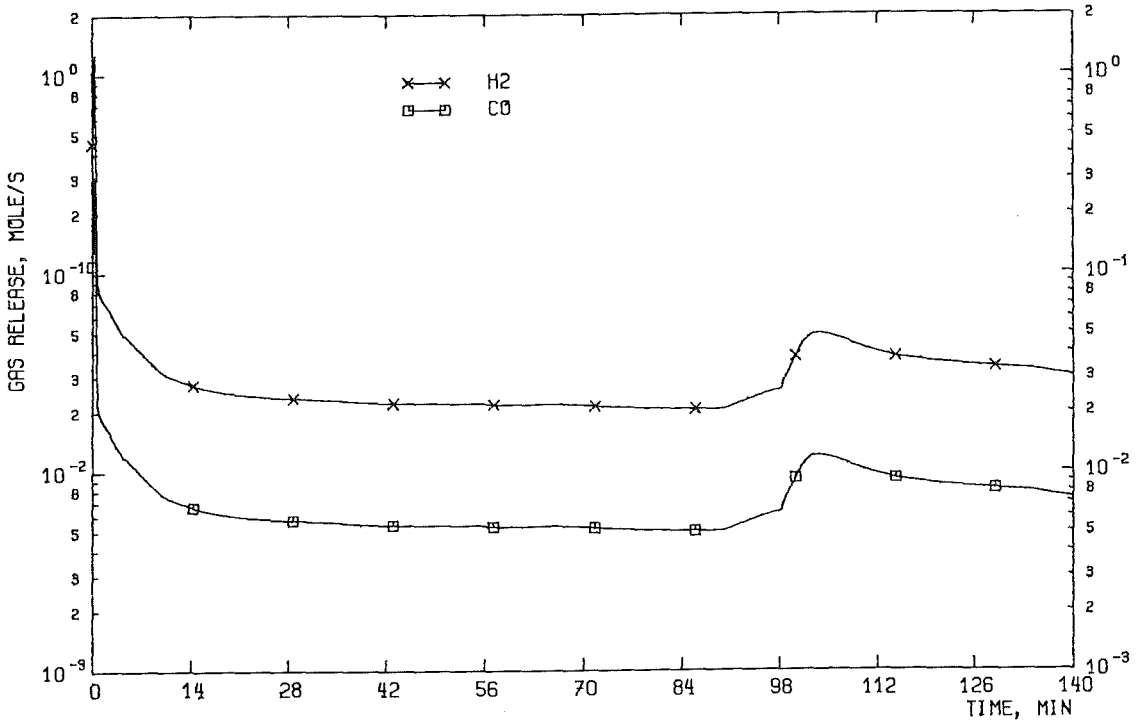

Fig. 35: Gas release rates (SURC test)

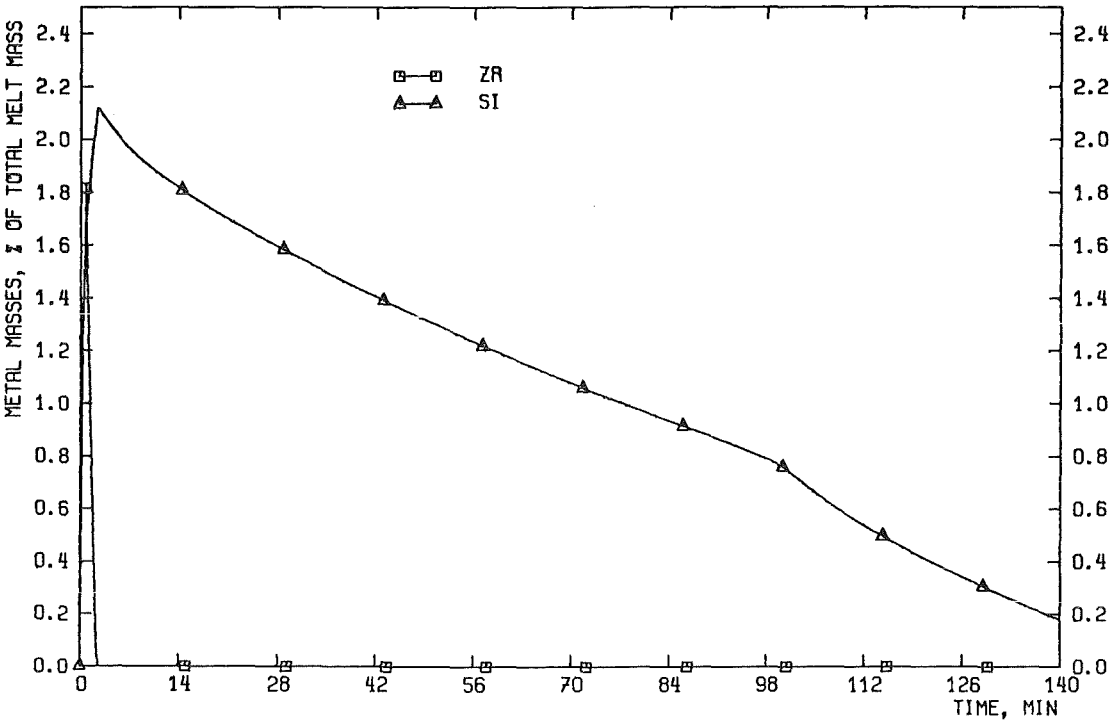

Fig. 36: Fraction of Zr and Si in the melt (SURC test)

A.3 Reactor Calculation

In the low pressure accident sequence the core melt is expected to relocate into a cylindrical reactor cavity with an inner radius of 3.2 m. If the 0.9 thick self-supporting concrete cylinder fails, the molten pool will be flooded by sump water. The initial melt temperature is estimated to be 2673 K. The reactor cavity and the 6 m thick basemat consists of siliceous type of concrete.

A.3.1 Input Data

```
 DRS-B10, 40% ZR OXIDE
*
*
*-------  THERMITE ADDITION:  RATE AND TIME OF REACTION
*  KG/S  |  SEC.   |
        0.        0.
*
*--------  ADDITION OF OTHER MATERIALS  -------------------------------
*  NUMBER OF ADDITIONS :
        0
*
*
*-------  CHARACTERISTICS OF CONCRETE WITHOUT STEEL --------------------
*
*WEIGHT FRACTION OF THE COMPONENTS : (AL2O3 IS THE COMPLEMENT)
*  CACO3 | CA(OH)2 |    SIO2 | FREE H2O|
     .0663     .0728     .7655     .0422
*   STEEL; MELT TEMP.; DECOMP. ENTH. ; DENSITY (ALL WITHOUT STEEL)
*KG/KGCON|  KELVIN |    J/KG |   KG/M3 |
      .065     1573.   2.075E6     2.3E3
*
*
*------ CHARACTERISTICS OF THE LIQUIDUS/SOLIDUS CURVE OF THE OXIDE PHASE
*       TABLE INPUT; NUMBER OF TABLE POINTS IMAT
*MAT|
   11
*    LOW TEMPERATURE GROUP :
*NUMBER OF SPECIES; SPECIES:1=UO2; 2=ZRO2; 3=FEO; 4=CAO; 5=SIO2; 6=AL2O3
*---|----|----|----|----|----|----|
    4    3    4    5    6
*LIQUIDUS: CCL,TLL (3 COUPLES PER CARD)
*     CCL|      TLL|      CCL|      TLL|      CCL|      TLL|
        .0     1573.        .1     1773.        .2     1893.
        .3     2073.        .4     2193.        .5     2293.
        .6     2373.        .7     2453.        .8     2523.
        .9     2583.        1.     2673.
*    HIGH TEMPERATURE GROUP :
*NUMBER OF SPECIES; SPECIES:1=UO2; 2=ZRO2; 3=FEO; 4=CAO; 5=SIO2; 6=AL2O3
*---|----|----|----|----|----|----|----|
    2    1    2
*SOLIDUS: CCL,TLL (3 COUPLES PER CARD)
*     CCS|      TSS|      CCS|      TSS|      CCS|      TSS|
        .0     1423.        .1     1483.        .2     1543.
        .3     1615.        .4     1715.        .5     1815.
        .6     1930.        .7     2073.        .8     2201.
        .9     2313.        1.     2423.
*
*
*------ CHARACTERISTICS OF THE OXIDE PHASE ----------------------------
*
* INITIAL MASS OF OXIDES IN KG :
*    UO2 |    ZRO2 |     FEO |     CAO |    SIO2 |   AL2O3 |   CR2O3 |
   103000.    16486.        0.        0.        0.        0.        0.
*INITIAL TEMP. OF OXIDE / VISCOSITY INCREASE DURING FREEZING (LIMESTONE)
* KELVIN |  1=YES  |
     2673.         0
*
```

```
* POWER IN THE OXIDE PHASE :
* NUMBER OF COUPLES : (TIME IN SEC. ; INTERNAL POWER IN WATT )
*---| IF THIS NUMBER IS 0,GOTO METAL PHASE(NO CARDS FOR SHIFT AND POWER)
   23
*SHIFT TIME AND FACTOR FOR INTERNAL HEAT GENERATION (OXIDE AND METAL)
*  SEC.  |---------|
    25200.        1.
*COUPLES (TIME IN SEC. ; INTERNAL POWER IN WATT ) ( 3 COUPLES/CARD )
*   TIME |    POWER |    TIME |    POWER |    TIME |    POWER |
        0.  13.177E7       60.  6.9754E7      360.  5.1946E7
      600.  4.6950E7     1080.   4.069E7     2700.  3.1046E7
     3600.  2.8560E7     7800.  2.3744E7    10800.  2.2232E7
    14400.  2.0944E7    15000.  2.0754E7    15600.  2.0586E7
    16200.  2.0418E7    18000.  1.9947E7    25200.  1.8458E7
    36000.  1.6912E7    72000.  1.4146E7    86400.  1.3496E7
   172800.  1.1200E7   259800.  9.9792E6   432000.  8.5456E6
   864000.  6.7872E6  1730000.  5.1856E6
*
*
*------ CHARACTERISTICS OF THE METAL PHASE ----------------------------
*
* INITIAL MASS OF METALS IN KG :
*     FE |      ZR |      CR |      NI |      SI |
    53000.    18000.    11000.     6400.        0.
*INITIAL TEMP. OF METAL / OMIT METAL AFTER ZR BURNOUT /
*REACTION ZR-SIO2       / METAL DISPERSED IN OXIDE PHASE
* KELVIN |  1=YES  |  1=YES  |  1=YES  |
     2673.        0         0         0
* POWER IN THE METAL PHASE :
* NUMBER OF COUPLES : (TIME IN SEC. ; INTERNAL POWER IN WATT )
*---| IF THIS NUMBER IS 0,GOTO THE CARD : TIME STEP AND FINAL TIME.
   23
*COUPLES (TIME IN SEC. ; INTERNAL POWER IN WATT ) ( 3 COUPLES/CARD )
*   TIME |    POWER |    TIME |    POWER |    TIME |    POWER |
        0.  17.965E6       60.  9.5088E6      360.  7.0784E6
      600.  6.4064E6     1080.  5.5440E6     2700.  4.2336E6
     3600.  3.8976E6     7800.  3.2368E6    10800.  3.0240E6
    14400.  2.8560E6    15000.  2.8336E6    15600.  2.8000E6
    16200.  2.7776E6    18000.  2.7104E6    25200.  2.5200E6
    36000.  2.3072E6    72000.  1.9264E6    86400.  1.8368E6
   172800.  1.5232E6   259800.  1.3552E6   432000.  1.1648E6
   864000.  0.9184E6  1730000.  0.7056E6
*
*
*------ TIME CHARACTERISTICS ------------------------------------------
*TIME STEP, FINAL TIME, MIN  /  MAX TIME STEP:
*  SEC.  |   SEC.  |   SEC.  |   SEC.  |
       1.0  1000000.       0.4       15.
*
* PRINTOUT :
* NUMBER OF PRINTOUT COUPLES :
    2
*COUPLES ( START PRINTOUT TIME,S ; PRINTOUT INTERVAL,S ; 3 COUPLES/CARD)
*   TIME |    STEP |    TIME |    STEP |    TIME |    STEP |
        0.    10000.   150000.    10000.
*
*------ AMBIENT ATMOSPHERIC PRESSURE ----------------------------------
*
*NUMBER OF COUPLES ( TIME, S ; PRESSURE,BAR )
*---|
    2
```

```
*COUPLES (TIME IN SEC. ; PRESSURE, BAR ) ( 3 COUPLES/CARD )
*   TIME | PRESSURE|    TIME | PRESSURE|    TIME | PRESSURE|
        0.        4.      1.E7        4.
*
*
*------ AMBIENT TEMPERATURE FOR RADIATION ON THE TOP OF CORIUM ---------
*
* NUMBER OF COUPLES ( TIME, S ; TEMPERATURE, K )
*---|
    4
*COUPLES (TIME IN SEC. ; TEMPERATURE, K ) ( 3 COUPLES/CARD )
*   TIME | TEMPERA.|    TIME | TEMPERA.|    TIME | TEMPERA.|
        0.     1700.     1000.     1500.   345600.     1000.
      1.E7     1000.
*
*
*------ CAVITY CHARACTERISTICS -----------------------------------------
*
* OPTION FOR INITIAL SHAPE : 1000<NB<1499 : CYLINDER WITH ROUNDED CORNER
*  ONE-DIMENSIONAL CALCULATION DESIRED ( 1=YES)
*---|----|
 1032    0
* NUMBER OF POINTS ON FLOOR AND CORNER, RADIUS OF CYLINDER AND CORNER,
* INTERVAL BETWEEN POINTS ON CYLINDER, CYLINDER HEIGHT.
*FLO| COR|RADIUS,M |CORNER,M |INTERV.,M| HEIGHT,M|
   40   10       3.2        .2      .075       11.
*
* INTERVAL BETWEEN CAVITY POINTS DURING PROGRAM RUN.
*  METER |
      .070
*
* RADIUS SUMP WATER INGRESSION ; BASEMAT THICKNESS ; TIME SUMP WATER
*  METER |   METER |   SEC   |
       4.1        6.      1.E7
*
*
*------ PRINTOUT OPTIONS: ( 0 = NO  ,  1 = YES ) -----------------------
*
*TEMP.   / PROPERT./ INTERFA./ MASS BAL/
         1         1         1         1
*ENER.BAL/ GAS REL./  CAVITY /DIAGNOST./ 1D-TAB  /
         1         1         1         1         1
*
*------  PLOT FILE OPTIONS: ( 0 = NO  ,  1 = YES )
*DO YOU WANT PLOTS (CAVITY NOT INCLU.)? ; DO YOU WANT THE CAVITY SHAPE ?
* PLOTS  /  CAVITY /
         1         1
*START TIME AND INTERVAL TO WRITE PLOT FILE, SEC. (THIS CARD MUST STAY)
* WARNING ! FOR KFK PLOT PROGRAM, NO MORE THAN 500 TIMES CAN BE WRITTEN!
* SWITCH TO 3600 S AFTER 1 HOUR
* START   | INTERVAL|  1=YES  |
        0.      100.         1
*START TIME AND INTERVAL TO WRITE CAVITY PLOT, SEC (THIS CARD MUST STAY)
* START   | INTERVAL|
        0.     3600.
*
*------  CALTHER CALCULATION DESIRED  (1=YES)
    0
*------  END OF WECHSL INPUT DATA  ----------------------------------
```

A.3.2 Results

A.3.2.1 Print Output Example

```
*************************
*                       *
*  TIME = 431042.59 SEC  *        NEXT TIME STEP=10.1620 SEC
*                       *
*************************


CAVITY DIMENSIONS, M :

       VERTICAL EROSION  :  -6.000
       MAXIMAL RADIUS    :   6.678
       ZERO LEVEL RADIUS :   6.559

TEMPERATURES, K :

       POOL -      METAL     : 1703.0   OXIDE    :  1608.3
       SURFACES -  MET./CONC.: 1573.0   OX./CONC.:  1589.9
                   MET./OX.  : 1661.7   OX./SURF.:   419.3
       LIQUIDUS -  METAL     : 1793.4   OXIDE    :  1624.7
       SOLIDUS  -  METAL     : 1783.4   OXIDE    :  1438.5
       GAS LEAVING THE MELT  :  416.9
       WATER GAS REACTION    : 1200.0

PROPERTIES:
                                      METAL            OXIDE
       DENSITY, KG/M3              :    7269.            2542.
       HEAT CONDUCTIVITY, W/(M.K):  45.947             2.325
       HEAT CAPACITY , J/(KG.K)    :     746.            1310.
       SURFACE TENSION, KG/S2      :   1.803             7.051
       VISCOSITY , KG/(S.M)        : 0.1000E+04       0.2496E+04

POOL-CONCRETE INTERFACE :
                              BOTTOM     METAL/WALL  OXIDE/WALL  OXIDE/SURFACE
       EROSION SPEED, CM/S :  0.7918E-03     --       0.2799E-03
       EROSION SPEED, CM/H :     2.85        --          1.01
       ENERGY FLUX,   W/M2 :  0.3853E+05     --       0.1362E+05  0.1979E+05
       ENERGY FLUX,  KW/M2 :      39.        --           14.         20.

       HEAT TRANSFER FOR BOTTOM/CONCRETE FILM MODE

INTEGRATED MASS BALANCE IN THE MELT, TONS :

       INITIAL MELT MASS:  207.886    ACTUAL MASS OF MELT  : 1946.228
       ERODED (CONC.+FE): 1873.890    MASS OF LEAVING GASES:  135.545

       SUM OF LEFT TERMS: 2081.776    SUM OF RIGHT TERMS   : 2081.772
       THE DIFFERENCE BETWEEN THE 2 SUMS IS  0.395E-02 TONS, I.E   0.190E-03 %

MASSES ,VOLUMES AND HEIGHTS :
                                                    METAL       OXIDE
       MASS ,TONS                                :   139.745    1806.483
       VOLUME, (INCLUDING VOID FRACTION), M3 :      19.23       711.96
       VOLUME, (WITHOUT VOID FRACTION), M3   :      19.23       710.76
       VOID FRACTION , IN PERCENT            :       0.00         0.17
       TOTAL DEPTH, M                        :            6.37
       POOL HEIGHT FROM INITIAL BOTTOM, M    :            0.37
       VOLUME OF ERODED CONCRETE, M3         :          779.58
       MASS OF ERODED CONCRETE, TONS         :         1873.890
```

WEIGHT FRACTION AND WEIGHT OF SPECIES IN EACH PHASE :

METAL: (SUM: 139745.07) KG		%	OXIDE: (SUM: 1806482.51) KG		%
ZR :	0.00	0.000	UO2 :	103000.00	5.702
SI :	0.00	0.000	ZRO2 :	40796.46	2.258
CR :	0.00	0.000	FEO :	43771.02	2.423
FE :	133345.07	95.420	CAO :	162317.93	8.985
NI :	6400.00	4.580	SIO2 :	1346913.64	74.560
			AL2O3 :	93606.54	5.182
			CR2O3 :	16076.92	0.890

CRUST THICKNESS IN EACH PHASE, CM :

IN THE METAL PHASE:		IN THE OXIDE PHASE:	
COMPLETELY SOLID		OXIDE/METAL:	0.00
HEIGHT :	34.27	OXIDE/CONCRETE:	0.00
		OXIDE/SURFACE:	14.16

HEAT FLUX BALANCE IN EACH PHASE, WATT :

		METAL	OXIDE
POWER DUE TO DECAY HEAT	:	0.1151E+07	0.8447E+07
POWER ENTERING DUE TO GAS AND OXIDES	:	0.1000E+07	0.7230E+07
POWER LEAVING DUE TO GAS AND OXIDES	:	-0.9016E+06	-0.1099E+07
POWER DUE TO OXIDATION REACTIONS	:	-0.1251E+04	0.0000E+00
POWER DUE TO CONCRETE DECOMPOSITION	:	-0.7266E+06	-0.6327E+07
CONDUCTION BETWEEN PHASES	:	-0.3873E+06	0.3873E+06
RADIATION OR EVAPORATED AT SURFACE	:	0.0000E+00	-0.2494E+07
SPLASHOUT	:	0.0000E+00	0.0000E+00
SENSIBLE HEAT	:	0.1345E+06	0.6143E+07

INTEGRATED ENERGY BALANCE IN THE MELT, JOULE :

INITIAL ENTHALPIE	0.3497E+12	INTEGRATED ENTHALPIE	0.3726E+13
DECAY HEAT	0.5383E+13	CONCRETE DECOMPOSITION	0.3793E+13
ENTERING(GAS,OX.)	0.3823E+13	LEAVING (GASES)	0.5761E+12
OXIDAT. REACTIONS	0.1646E+12	RADIATION OR TO WATER	0.1617E+13
		SPLASHOUT	0.7203E+10
SUM OF LEFT TERMS	0.9720E+13	SUM OF RIGHT TERMS	0.9720E+13

THE DIFFERENCE BETWEEN THE 2 SUMS IS 0.2002E+01 J., I.E 0.2060E-10 %

GASES GOING IN THE CONTAINMENT, AT THE SATURATION TEMPERATURE TSAT= 417. K.
OF THE SUMP WATER FLOODING THE SURFACE OF THE CORIUM :

	CO2	CO	H2O	H2
HEAT FLUX, WATT	0.9162E+04	0.9311E+03	0.4247E+07	0.3719E+04
MASS FLUX, KG/S	0.8371E-01	0.7431E-02	0.1643E+01	0.2168E-02
MOL. FLUX, MOL/S	0.1902E+01	0.2653E+00	0.9120E+02	0.1079E+01
WEIGHT FRACTION	0.4822E-01	0.4281E-02	0.9462E+00	0.1249E-02
MOLAR FRACTION	0.2014E-01	0.2809E-02	0.9656E+00	0.1142E-01
TOTAL MASS, KG	0.4034E+05	0.6970E+04	0.8608E+05	0.2155E+04
TOT.MOLS, MOL	0.9167E+06	0.2488E+06	0.4779E+07	0.1072E+07

THE SUMP WATER FLOODS THE CORIUM SURFACE AND IS EVAPORATED.
THIS WATER EVAPORATES AT TSAT= 417. K WITH A MASS FLOW OF 1.466 KG/S.
THE EVAPORATION ENTHALPIE OF THIS WATER IS 2737.2 KJ/KG
THE TOTAL MASS OF THE EVAPORATED WATER IS NOW: 829755. KG.

THE CAVITY SHAPE HAS BEEN CALCULATED USING 187 POINTS, COORDINATES IN CM :
R=RADIUS ; Z=DEPTHNESS ; Z-REFERENCE: INITIAL BOTTOM OF THE CAVITY

R	Z	R	Z	R	Z	R	Z
0.0	-527.7	7.0	-527.7	14.0	-527.7	21.0	-527.7
28.0	-527.7	35.0	-527.7	42.0	-527.7	49.0	-527.7
56.0	-527.7	63.0	-527.7	70.0	-527.7	77.0	-527.7
84.0	-527.7	91.0	-527.7	98.0	-527.7	105.0	-527.7
112.0	-527.7	119.0	-527.7	126.0	-527.7	133.0	-527.7
140.0	-527.7	147.0	-527.7	154.0	-527.7	161.0	-527.7
168.0	-527.7	175.0	-527.7	182.0	-527.7	189.0	-527.7
196.0	-527.7	203.0	-527.7	210.0	-527.7	217.0	-527.7
224.0	-527.7	231.0	-527.7	238.0	-527.7	245.0	-527.7
252.0	-527.7	259.0	-527.7	266.0	-527.7	273.0	-527.7
280.0	-527.7	287.0	-527.7	294.0	-527.7	300.9	-526.7
307.6	-524.6	313.8	-521.3	319.3	-517.1	324.4	-512.2
329.0	-506.9	333.2	-501.3	337.5	-495.8	339.3	-493.5
246.6	-527.7	249.9	-533.9	254.6	-539.1	259.6	-544.0
264.7	-548.8	269.7	-553.6	274.8	-558.4	279.9	-563.2
285.0	-568.0	290.2	-572.7	295.5	-577.3	300.8	-581.8
306.3	-586.2	311.9	-590.4	317.6	-594.5	323.4	-598.4
330.3	-599.6	337.3	-599.9	344.3	-600.0	351.3	-599.8
358.3	-599.1	364.1	-595.3	369.8	-591.2	375.1	-586.6
380.2	-581.8	385.3	-577.1	390.6	-572.4	395.9	-567.9
401.4	-563.5	406.9	-559.2	412.5	-555.0	418.1	-550.8
423.8	-546.8	429.5	-542.7	435.3	-538.7	441.0	-534.8
446.8	-530.9	452.7	-527.0	458.5	-523.1	464.3	-519.2
470.1	-515.3	476.0	-511.5	481.8	-507.6	487.6	-503.7
493.5	-499.9	499.3	-496.0	505.1	-492.1	510.9	-488.2
516.7	-484.3	522.5	-480.3	528.2	-476.2	533.9	-472.1
539.5	-468.0	545.0	-463.7	550.5	-459.4	556.0	-454.9
561.3	-450.4	566.5	-445.8	571.7	-441.1	576.8	-436.2
581.7	-431.3	586.6	-426.2	591.3	-421.0	595.9	-415.8
600.4	-410.4	604.7	-404.9	608.9	-399.3	613.0	-393.6
616.9	-387.8	620.7	-381.9	624.3	-375.9	627.8	-369.8
631.1	-363.7	634.3	-357.4	637.3	-351.1	640.1	-344.7
642.8	-338.3	645.4	-331.7	647.8	-325.2	650.0	-318.5
652.1	-311.8	654.0	-305.1	655.8	-298.3	657.4	-291.5
658.9	-284.7	660.2	-277.8	661.4	-270.9	662.5	-264.0
663.5	-257.1	664.3	-250.1	665.0	-243.2	665.6	-236.2
666.2	-229.2	666.6	-222.2	666.9	-215.2	667.2	-208.2
667.4	-201.2	667.6	-194.2	667.7	-187.2	667.7	-180.2
667.8	-173.2	667.8	-166.2	667.8	-159.2	667.8	-152.2
667.7	-145.2	667.7	-138.2	667.6	-131.2	667.6	-124.2
667.4	-117.2	667.3	-110.2	667.1	-103.3	666.9	-96.3
666.7	-89.3	666.4	-82.3	666.1	-75.3	665.7	-68.3
665.3	-61.3	664.8	-54.3	664.2	-47.3	663.6	-40.4
662.9	-33.4	662.1	-26.4	661.2	-19.5	660.1	-12.6
658.9	-5.7	657.5	1.2	655.9	8.0	653.9	14.7
651.4	21.2	648.1	27.4	643.6	32.8	637.2	35.7
633.4	36.9	623.8	39.7	617.1	41.7	610.4	43.6
603.6	45.5	593.9	48.2	388.1	98.6	371.4	106.4
365.2	109.7	358.8	114.4	352.5	120.9	347.9	126.2
343.3	131.5	338.7	136.7	334.1	142.0	329.5	147.3
329.1	154.8	329.0	161.9	329.0	169.0	329.0	176.0
329.0	183.0	329.0	190.0	329.0	197.0	328.9	204.0
328.8	211.0	328.7	218.0	328.6	225.0	328.5	232.0
328.4	241.1	328.3	249.8	328.1	265.0	328.0	273.4
327.8	282.1	327.7	290.6	327.5	298.9	327.4	307.5
327.3	316.0	327.2	324.4	327.2	332.7	327.1	340.9
327.1	349.0	327.0	357.0	327.0	365.1	326.9	373.1
326.9	381.1	326.9	389.1	326.8	397.0	326.8	405.0
326.8	412.8	326.7	420.7	326.7	428.6	326.7	436.4
326.7	444.1	326.6	451.6	326.6	459.1	326.6	466.6

326.6	474.1	326.6	481.5	326.5	488.9	326.4	496.4
326.4	503.8	326.2	511.2	326.0	518.6	325.8	526.0
325.5	533.3	325.2	540.7	324.7	548.0	324.2	555.4
323.7	562.8	323.1	570.2	322.6	577.5	322.1	585.1
321.6	592.4	321.2	599.9	320.8	607.4	320.5	614.9
320.3	622.5	320.1	630.1	320.0	637.7	320.0	645.3
320.0	652.9	320.0	661.6	320.0	668.6	320.0	675.6
320.0	682.6	320.0	689.6	320.0	696.6	320.0	703.6
320.0	710.6	320.0	717.6	320.0	724.6	320.0	731.6
320.0	738.6	320.0	745.6	320.0	752.6	320.0	759.6
320.0	766.6	320.0	773.6	320.0	780.6	320.0	787.6
320.0	794.6	320.0	801.6	320.0	808.6	320.0	815.6
320.0	822.6	320.0	829.6	320.0	836.6	320.0	843.6
320.0	850.6	320.0	857.6	320.0	864.6	320.0	871.6
320.0	878.6	320.0	885.6	320.0	892.6	320.0	899.6

STOP BECAUSE OF BASEMAT PENETRATION AT TIME = 0.4310E+06 SEC

A.3.2.2 Cavity Shape

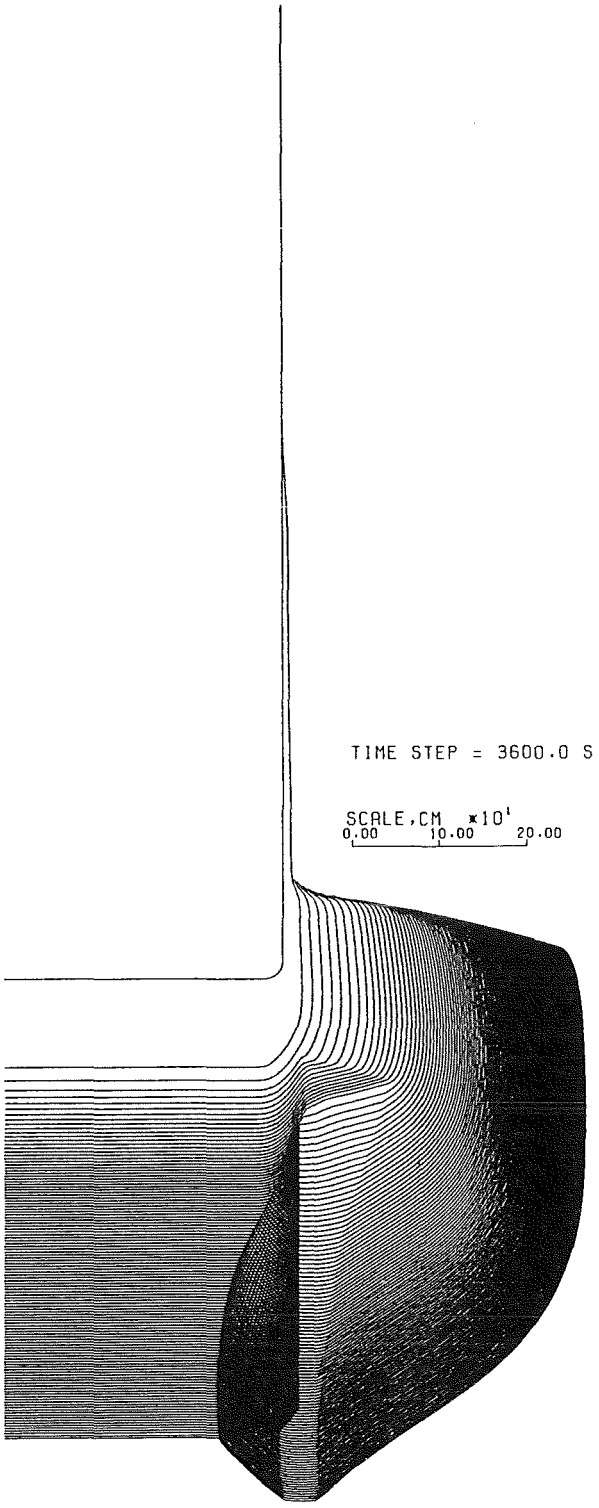

Fig. 37: Cavity shape (reactor calculation)

A.3.2.3 Selected Diagrams

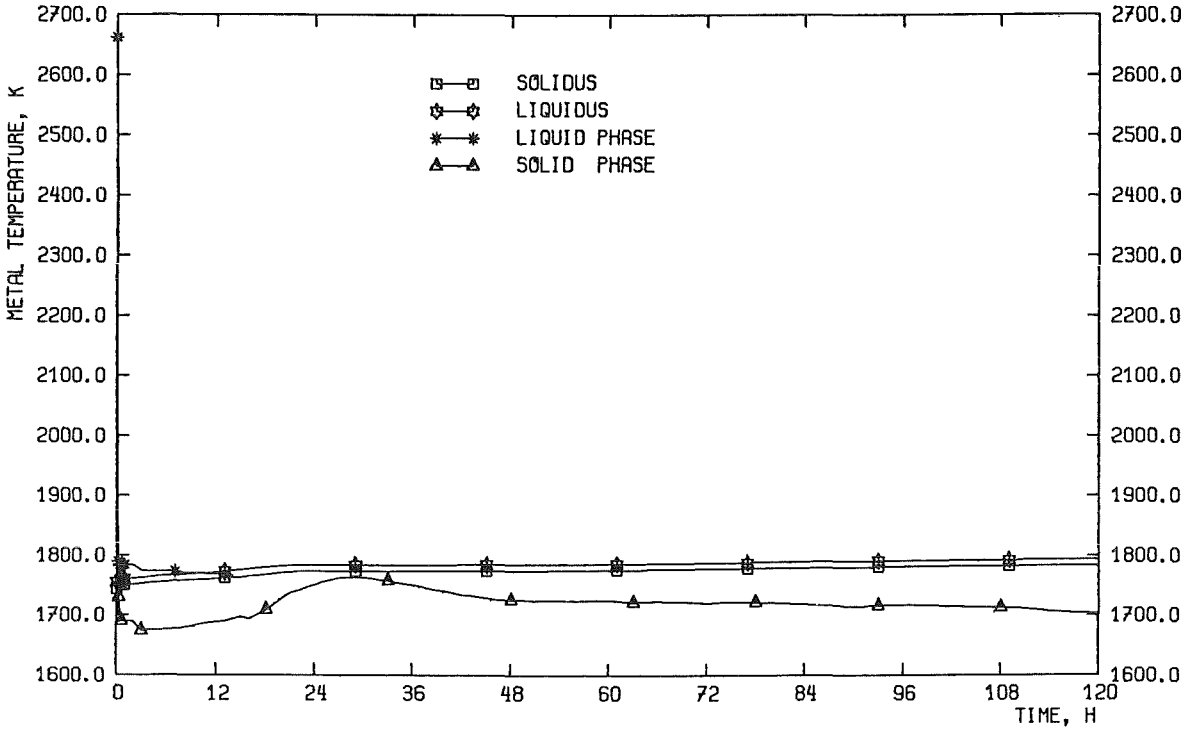

Fig. 38: Temperatures of metallic phase (reactor calculation)

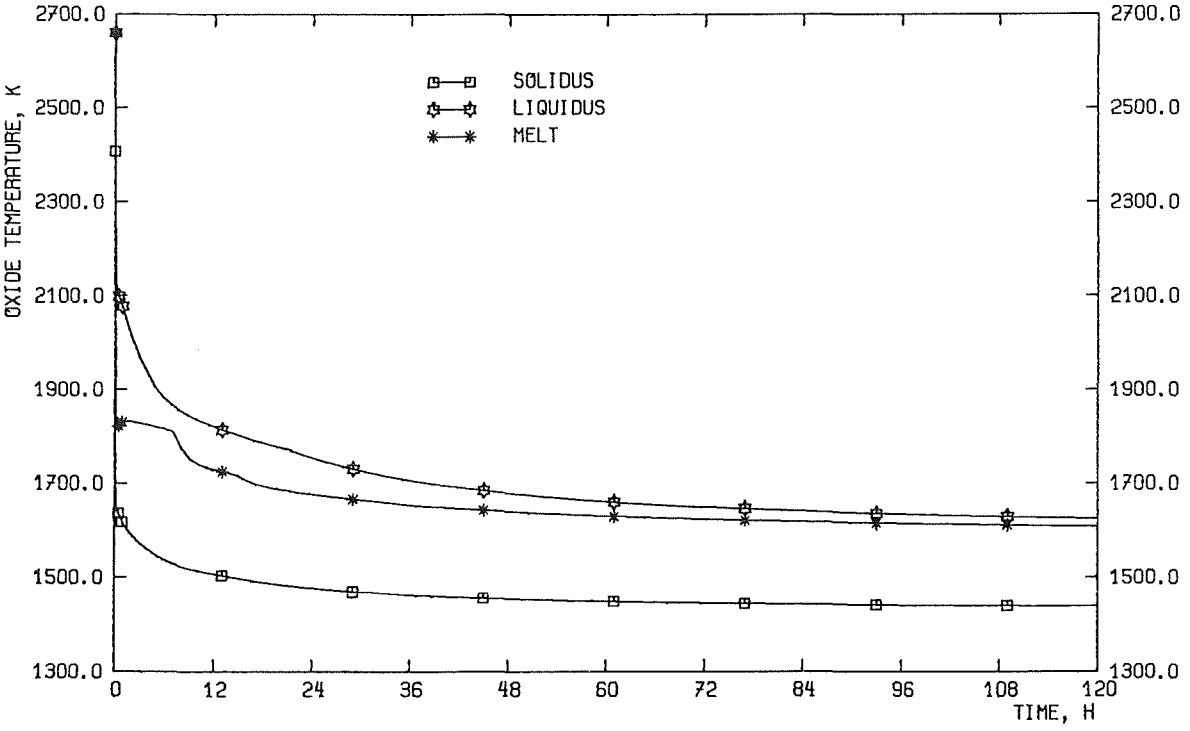

Fig. 39: Temperature of oxidic phase (reactor calculation)

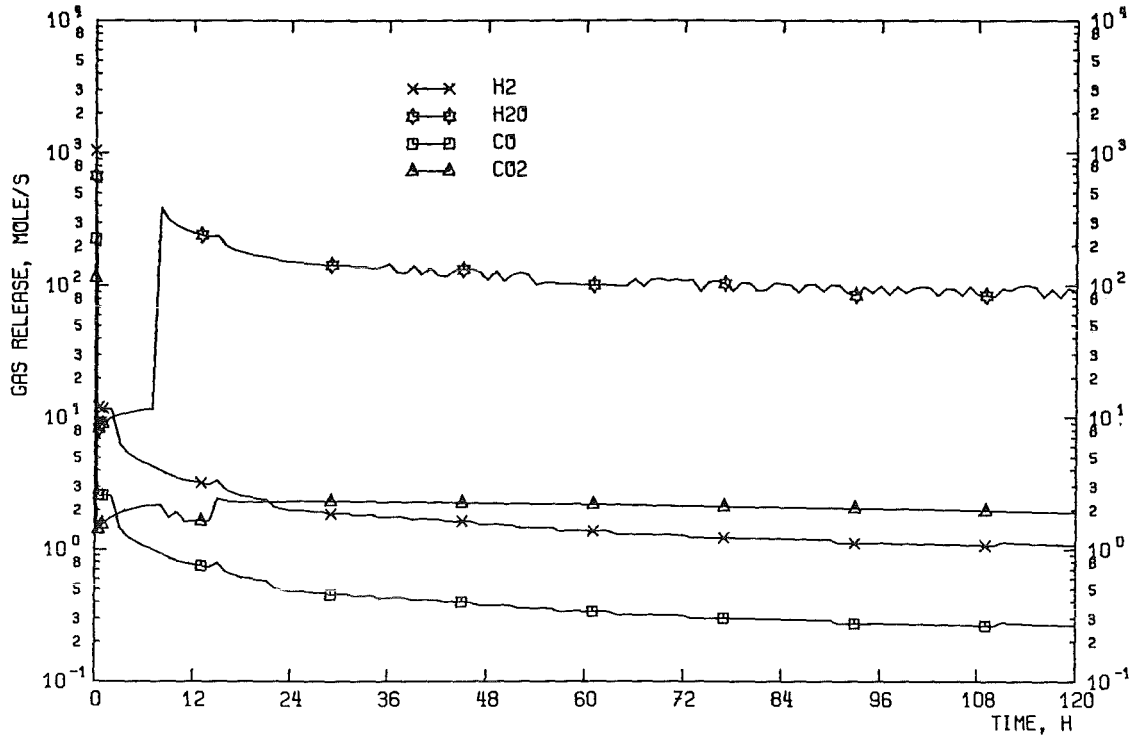

Fig. 40: Gas release (reactor calculation)

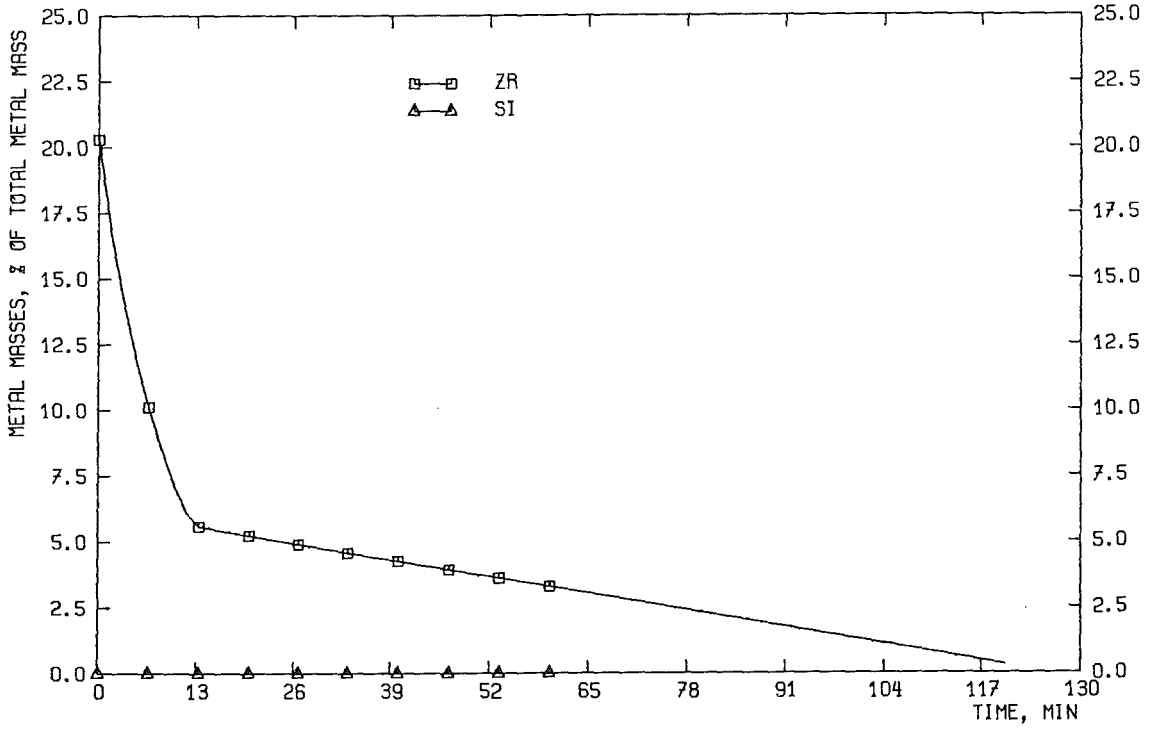

Fig. 41: Fraction of Zr and Si in the metal (reactor calculation)

Appendix B: Sample Calculation with WECHSL + CALTHER

In the following WECHSL calculation the CALTHER module is activated in order to determine the heat flux from the upper surface of the corium to the surrounding reactor cavity during MCCI. The walls heat up and are allowed to melt. The molten products are added to the corium mass, and the resulting gases to the gases originating from the corium.

B.1 Input Data

```
  WECHSL-MOD3 with CALTHER option: example
*=======  THERMITE ADDITION:  RATE AND TIME OF REACTION
*  KG/S  |  SEC.   |
        0.        0.
*
*-------  ADDITION OF OTHER MATERIALS   --------------------------------
*
*  NUMBER OF ADDITIONS : ( MAX. 10; IF 0, NO FURTHER CARDS )
        0
*-------  CHARACTERISTICS OF CONCRETE WITHOUT STEEL --------------------
*
*WEIGHT FRACTION OF THE COMPONENTS : (AL2O3 IS THE COMPLEMENT)
*  CACO3 | CA(OH)2 |    SIO2 | FREE H2O|
     0.008    0.0200     0.809     0.057
*REINFORCED STEEL; MELT TEMP.; DECOMPOSITION ENTH. ; DENSITY (NO STEEL):
*KG/KGCON|  KELVIN |    J/KG |   KG/M3 |
     0.000     1423.   2.186E6     2390.
*===========
*===========
*====== CHARACTERISTICS OF THE LIQUIDUS/SOLIDUS CURVE OF THE OXIDE PHASE
*==  TABLE INPUT; NUMBER OF TABLE POINTS IMAT
*MAT|
   11
*==  LOW TEMPERATURE GROUP :
*NUMBER OF SPECIES; SPECIES:1=UO2; 2=ZRO2; 3=FEO; 4=CAO; 5=SIO2; 6=AL2O3
*---|----|----|----|----|----|----|
    4    3    4    5    6
*LIQUIDUS: CCL,TLL (3 COUPLES PER CARD)
*     CCL|      TLL|      CCL|      TLL|      CCL|      TLL|
        .0     1573.        .1     1773.        .2     1893.
        .3     2073.        .4     2193.        .5     2293.
        .6     2373.        .7     2453.        .8     2523.
        .9     2583.        1.     2673.
*==  HIGHT TEMPERATURE GROUP :
*NUMBER OF SPECIES; SPECIES:1=UO2; 2=ZRO2; 3=FEO; 4=CAO; 5=SIO2; 6=AL2O3
*---|----|----|----|----|----|----|
    2    1    2
*SOLIDUS: CCL,TLL (3 COUPLES PER CARD)
*     CCS|      TSS|      CCS|      TSS|      CCS|      TSS|
        .0     1423.        .1     1483.        .2     1543.
        .3     1615.        .4     1715.        .5     1815.
        .6     1930.        .7     2073.        .8     2201.
        .9     2313.        1.     2423.
*===========
*===========
*====== OXIDE PHASE :
*INITIAL MASS OF OXIDES IN KG :
*    UO2 |    ZRO2 |     FEO |     CAO |    SIO2 |   AL2O3 |   CR2O3 |
    80000.    20000.        0.        0.        0.        0.        0.
*INITIAL TEMPERATURE OF OXIDE :and viscosity option
* KELVIN |  1=YES  |
     2673.        0
*==== POWER IN THE OXIDE PHASE :
*NUMBER OF COUPLE : (TIME IN SEC. ; INTERNAL POWER IN WATT )
*---| IF THIS NUMBER IS 0,GOTO METAL PHASE(NO CARDS FOR SHIFT AND POWER)
   11
*SHIFT TIME FOR INTERNAL HEAT GENERATION; MULTIPLICATION FACTOR
*  SEC.  |---------|
        0.        1.
```

```
*COUPLES (TIME IN SEC. ; INTERNAL POWER IN WATT ) ( 3 COUPLES/CARD )
*   TIME |   POWER |    TIME |   POWER |    TIME |   POWER |
       0.   13.40E6    40776.   12.06E6    72000.   10.31E6
   86400.    9.83E6   172800.    8.16E6   259800.    7.27E6
  432000.    6.23E6   864000.    4.94E6  1728000.    3.78E6
 2592000.    3.12E6  5814000.    2.12E6
*===========
*===========
*====== METAL PHASE :
*INITIAL MASS OF METALS IN KG :
*     FE |      ZR |      CR |      NI |
        0.        0.        0.        0.
*INITIAL TEMPERATURE OF METAL , IMEND, IZRCH, I
* imend=0 after Zr burnout, metal taken into account; =1 not taken
* izrch=1 reaction Zr/SiO2  ;  izrch=0 no Zr/SiO2 reaction
* I=1 only oxyde phase exists
* By default: imend=0 izrch=0 I=0
* KELVIN       IMEND   IZRCH   I
     2673.         0     0     1
*==== POWER IN THE METAL PHASE :
*NUMBER OF COUPLE : (TIME IN SEC. ; INTERNAL POWER IN WATT )
*---| IF THIS NUMBER IS 0,GOTO THE CARD : TIME STEP AND FINAL TIME.
    2
*COUPLES (TIME IN SEC. ; INTERNAL POWER IN WATT ) ( 3 COUPLES/CARD )
*   TIME |   POWER |    TIME |   POWER |    TIME |   POWER |
       0.        0.    2.12E6      0.
*===========
*===========
*=== TIME CHARACTERISTICS :  TIME STEP , FINAL TIME, MIN/MAX TIME STEP:
*  SEC.  |   SEC.  |   SEC.  |   SEC.  |
      0.4        4.        .1        4.
*===========
*===========
*=======  PRINTOUT :
*NUMBER OF PRINTOUT COUPLES :
    2
*COUPLES ( START PRINTOUT TIME,S ; PRINTOUT INTERVAL,S) ( 3 COUPLES/CARD
*   TIME |    STEP |    TIME |    STEP |    TIME |    STEP |
       0.        2.       10.       10.
*===========
*===========
*=======  AMBIENT ATMOSPHERIC PRESSURE:
*NUMBER OF COUPLES ( TIME, S ; PRESSURE,BAR )
*---|
    2
*COUPLES (TIME IN SEC. ; PRESSURE, BAR ) ( 3 COUPLES/CARD )
*   TIME | PRESSURE|    TIME | PRESSURE|---------|---------|
       0.      2.5    864000.      2.5
*===========
*===========
*=======  AMBIENT TEMPERATURE FOR RADIATION ON THE TOP OF CORIUM :
*NUMBER OF COUPLES ( TIME, S ; TEMPERATURE, K )
*---|
    2
*COUPLES (TIME IN SEC. ; TEMPERATURE, K ) ( 3 COUPLES/CARD )
*   TIME | TEMPERA.|    TIME | TEMPERA.|---------|---------|
       0.      773.   864000.      773.
*===========
*===========
*=======  INITIAL CAVITY SHAPE :
*NUMBER OF CAVITY POINTS : 1000<NB<1499 : CYLINDER WITH ROUNDED CORNER:
*---|--I1DIM  (default=0  ; =1 means 1D cavity - no vertical walls)
 1032    0
*NUMBER OF POINTS ON FLOOR AND CORNER, RADIUS OF CYLINDER AND CORNER,
```

```
*INTERVAL BETWEEN POINTS ON CYLINDER, CYLINDER HEIGHT.
*FLO| COR|RADIUS,M |CORNER,M |INTERV.,M| HEIGHT,M|
   30    5       3.0        .5       0.5        8.
*===========
*== INTERVAL BETWEEN CAVITY POINTS DURING PROGRAM RUN.
*  METER |
      0.07
*===========
*== CAVITY RADIUS FOR SUMP WATER INGRESSION :
*== BASEMAT THICKNESS
*== TIME FOR FOR SUMP WATER INGRESSION :
* RADIUS | BASEMAT | TIME     |
*  METER |  METER  | WATER S  |
     1000.        2.      1.E9
*===========
*===========
*=======  PRINTOUT OPTIONS: ( 0 = NO  ,  1 = YES ) (FORMAT I10 )
*TEMP.   / PROPERT./ INTERFA./ MASS BAL/
         1         1         1         1
*ENER.BAL/ GAS REL./  CAVITY /DIAGNOST./         /
         1         1         1         1         0
*===========
*===========
*=======  PLOT FILE OPTIONS: ( 0 = NO  ,  1 = YES ) (FORMAT I10 )
*DO YOU WANT PLOTS (CAVITY NOT INCLU.)? ; DO YOU WANT THE CAVITY SHAPE ?
* PLOTS  |  CAVITY |
         1         1
*START TIME AND INTERVAL TO WRITE PLOT FILE, IN SEC.(THIS CARD MUST STAY)
* WARNING ! FOR KFK PLOT PROGRAM, NO MORE THAN 500 TIMES CAN BE WRITTEN!
* START  | INTERVAL|  IPLINT (=1 means after 1 h, each hour)
        0.        2.         1
*TART TIME AND INTERVAL TO WRITE CAVITY PLOT, SEC. (THIS CARD MUST STAY)
* START  | INTERVAL|
        0.     3600.
*===========
*JPDC : FLAG FOR THE CAVITY MODEL  - FREE FORMAT -
*       =1 CAVITY MODEL
*       =0 NO CAVITY MODEL
   1
*======================== END OF WECHSL INPUT DATA
*========== IF JPDC=1 THE FOLLOWING DATA MUST BE DEFINED
*=========================CALTHER DATA INPUT (CAVITY MODEL)
*==========================  FREE  FORMAT
* TITLE CARD
  TEST WECHSL-MOD3 with CALTHER OPTION
* ICALC    =1 FOR TRANSIENT COMPUTATION (ALWAYS =1 IN WECHSL/CALTHER)
*          =0 FOR STATIONARY COMP. (ALLOWED ONLY FOR THE STAND ALONE VERSION)
   1
* TDEB           ;BEGINNING OF CALCULATION (S)
   0.
* GAZ     MODEL  ;GAS     KIND OF GAS MIXTURE (TRANSPA , GRIS ,REEL )
*                        TRANSPA  FOR A TRANSPARENT GAS MIXTURE
*                        GRIS     FOR A MEAN ABSORBING GAS MIXTURE (GRAY CASE)
*                        REEL     FOR A REAL ABSORBING GAS MIXTURE WITH NBA
*                                 DIFFERENT TRANSMITTANCE BANDS
*                ;MODEL  MODEL OF BAND ABSORPTION (LEBOURG,THOMSON)
*                        LEBOURG  (RECOMENDED)
TRANSPA LEBOURG
* NBA ;NUMBER OF INDEPENDENT BAND OF TRANSMITTANCE CONSIDERED IN THE CALCULATION
*      OF THE RADIATIVE HEAT EXCHANGE IN THE CAVITY ( =1 IS RECOMMENDED)
*  NBA=1 (FOR GAS=GRIS) A MEAN TRANSMITTANCE IS CALCULATED
*  NBA>1 (FOR GAS=REEL) TRANSMITTANCE IS CALCULATED FOR EACH TRANSMITTANCE BAND
*      FOR H2O THE 5 ABSORBING BANDS DEFINE NBA=11 DIFFERENT TRANSMITTANCE BANDS
*      (IF NBA>1 ,THE GOOD VALUE OF NBA IS CALCULATED BY CALTHER)
```

```
   1
********** TIME STEP TABLES FOR CALTHER CALCULATIONS
* NTT      NUMBER OF POINTS IN THE TABLES
   2
* DTT    TPST    ; TIME STEP DTT (S) UNTIL TIME TPST ( S)
* ===============> IF (TIME .LE. 86400.)  DTT = DT OF WECHSL
   1.   86400.
  60.  864000.
********** TIME STEP TABLES FOR CALTHER PRINT RESULTS
* NTI      NUMBER OF POINTS IN THE TABLES
   5
* DTI    TPSI    ; TIME STEP DTI (S) UNTIL TIME TPSI ( S)
    2.     100.
  100.    1000.
  1000.  80000.
  6400.  86400.
 43200. 864000.
*
*******************************GEOMETRY*****************************************
** NCOMP         NUMBER OF COMPONANTS INCLUDING THE GAS MIXTURE AND THE UPPER
*               SURFACE OF CORIUM
    6
** DIAM HCUV     INNER DIAMETER AND HEIGHT OF THE CAVITY SPACE (M)
   5.2   4.
*
**************** DESCRIPTION AND MESHING OF THE CAVITY WALLS ******************
*--LOOP L1 ON EACH "WALL COMPONENT" ( JC=1,NPAMU   WITH NPAMU=NCOMP-2 )
*      ( THE GAS MIXTURE AND THE TOP SURFACE OF CORIUM ARE NOT CONSIDERED HERE)
*  IALFC(JC) NMIC(JC) ;IALFC  GEOMETRY INDEX (0 FOR PLANE,1 FOR CYLINDRIC )
*                     ;NMIC   NUMBER OF DIFFERENT MATERIALS IN EACH WALL COMP.
*                     ;NMIC  =1 IS RECOMENDED FOR THIS VERSION
       1         1
*----*LOOP L2 ON EACH MATERIAL I INSIDE EACH WALL COMPONENT
* NC(I,JC)  RIC(I,JC)  REC(I,JC)  TOTAL NBR OF MESHES ,INTERNAL RADIUS (M),
*                                                      EXTERNAL  RADIUS (M)
* IF  NC(I,JC)>0  CONSTANT MESHES IN THE COMPONENT DEFINED ONLY BY RIC,REC
* IF  NC(I,JC)<0  VARIABLE MESHES IN THE COMPONENT DEFINED BY ADDITIONAL
*                 PARAMETERS IXM,NDX,DXC
*                 IXM     NBR OF COUPLES( NDX , DXC)
*                 NDX     NBR OF DIFFERENT SPACE STEPS OF SIZE DXC (M)
    -60       2.6        4.4
     4         30   .01     10   .02     10  .04     10  .09
*   IXM       NDX   DXC    NDX   DXC    NDX  DXC    NDX  DXC ..............
*----*END L2
       1         1
    -60       2.6        4.4
     4         30   .01     10   .02     10  .04     10  .09
       1         1
    -60       2.6        4.4
     4         30   .01     10   .02     10  .04     10  .09
       0         1
     10       2.6        3.
*--*END L1
*
****************** RADIATIVE TRANFER CHARACTERISTICS ************************
*--LOOP L3 ON EACH BOUNDARY CAVITY COMPONENT ( JC=1,NPAR  WITH NPAR =NCOMP-1 )
*         JC=1        FOR TOP SURFACE OF CORIUM
*         JC=2,3,..   FOR LATERAL WALL COMPONENTS
*         JC=..,NPAR  FOR TIP WALL COMPONENTS (REATOR VESSEL)
*A(JC)    EMI(JC)   ; A=AREA (M**2)   EMI=EMISSIVITY OF THE WALL COMPONENT
 21.237    0.7
*FVU(JC+(J-1)*NPAR),J=1,NPAR)  VIEW FACTOR BETWEEN TWO WALL COMPONENTS
  0.00000  0.39792  0.22875  0.13087  0.24246  F(1,1) F(1,2)...F(N,N)
 21.782    0.7                                 A(1)    EMI(1)
```

```
  0.38796  0.22408  0.16493  0.09544  0.12759  F(2,1) F(2,2)...F(2,N)
 21.782    0.7                                 A(2)    EMI(2)
  0.22300  0.16500  0.22408  0.16493  0.22303
 21.782    0.7
  0.12700  0.09600  0.16500  0.22408  0.38796
 21.237    0.8
  0.24200  0.13100  0.22900  0.39800  0.00000  F(N,1) F(N,2)...F(N,N)
*--END L3
* FCGA  CORRECTION COEFFICIENT FOR MEAN BEAM LENGTH (.9 IS RECOMMENDED)
  0.9
*--LOOP L4 ON EACH BOUNDARY CAVITY COMPONENT ( JC=1,NPAR  WITH NPAR =NCOMP-1 )
* CGA(JC+(J-1)*NPAR),J=1,NPAR  MEAN BEAM LENGTH BETWEEN TWO BOUNDARY CAV. COMP.
  0.000  2.684  3.280  4.227  4.000
  2.684  5.200  5.368  5.844  4.227
  3.280  5.368  5.200  5.368  3.280
  4.227  5.844  5.368  5.200  2.684
  4.000  4.227  3.280  2.684  0.000
*--END L4
*****************THERMAL EXCHANGE ON EACH INTERFACE OF A WALL COMPONENT ********
*--LOOP L5 ON EACH WALL COMPONENT ( JC=1,NPAMU  WITH NPAMU =NCOMP-2 )
*                       THE CORIUM SURFACE IS NOT CONSIDERED HERE
*                       THE GAS MIXTURE    IS NOT CONSIDERED HERE
*----LOOP L6 I=1,IMF ON EACH WALL INTERFACE (SEE COMMENTS IN THE SUBR. CAVREAD)
*                IMF=NMIC(JC)+1: NBR OF INTERFACES PER WALL COMP.
* STEFAN CST. ,COND.COEF. ,CONV. COEF.,LEFT EMITTANCE,RIGHT EMITTANCE,SHAPE COEF
*  W/(M*2/K*4),W/M/K      , W/M*2/K   ,              ,               ,
  0.              0.          0.       0.80          0.85             1.
  0.              0.        200.       1.            1.               1.
*----END  L6
  0.              0.          0.       0.80          0.85             1.
  0.              0.        200.       1.            1.               1.
  0.              0.          0.       0.80          0.85             1.
  0.              0.        200.       1.            1.               1.
  0.              0.          0.       0.80          0.85             1.
  0.              0.        100.       1.            1.               1.
*--END  L5
*
*****************MATERIAL IDENTIFICATION IN EACH WALL COMPONENT ***************
*--LOOP L7 ON EACH WALL COMPONENT ( JC=1,NPAMU  WITH NPAMU =NCOMP-2 )
*----LOOP L8 I=1,IM ON THE MATERIALS OF EACH WALL COMP.  IM=NMIC(JC)
*IDC(I,JC),SC(I,JC)      ,MATERIAL INDEX IDC   ,VOLUMETRIC HEAT SOURCE W/M*3
*                         IDC =1 SILICATE CONCRETE
*                         IDC =2 LCS CONCRETE
*                         IDC =3 INOX
*                         IDC =4 STAINLESS STEEL
  1         0.
*----END  L8
  1         0.
  1         0.
  4         0.
*--END  L7
*
***************THERMAL BOUNDARY CONDITIONS ON EACH WALL COMP. **************
*--LOOP L9 ON EACH WALL COMPONENT ( JC=1,NPAMU  WITH NPAMU =NCOMP-2 )
*----JC=1-----------------------------------
* N2(JC),RC(NN,JC)    ; N2:NBR OF POINTS IN THE TABLE (TS2,CL2)
*                     ; RC:RADIUS WHERE THE EXTERNAL TEMPERATURE IS IMPOSED (M)
  3      5.0
*----LOOP L10 I=1,N2(JC)
*TS2(I,JC),CL2(I,JC)  ; TIME (S)   ,TEMPERATURE (K)
  0.        400.
  45000.    400.
  999000.   400.
*NS(JC)               ; NS:NBR OF POINTS IN THE SOURCE POWER TABLE (TS,FS)
```

```
  3
*TS(I,JC),FS(I,JC)    ; TIME (S)     ,NORMALIZED POWER   (FS(I,JC).LE.1.))
  0.        0.
  10000.    0.
  999000.   0.
*----END L10
*----JC=2-----------------------------------
  3      5.0        (N2  ,  RC)
  0.         400.
  45000.     400.
  999000.    400.
  3                 (NS)
  0.         0.
  10000.     0.
  999000.    0.
*----JC=3-----------------------------------
  3      5.0
  0.         400.
  45000.     400.
  999000.    400.
  3
  0.         0.
  10000.     0.
  999000.    0.
*----JC=4-----------------------------------
  4      6.0
  0.          800.
  86500.      800.
  432000.     800.
  999000.     800.
  3
  0.         0.
  10000.     0.
  999000.    0.
*--END L9
*
***************** INITIAL TEMPERATURE INSIDE EACH WALL COMP.
*
*--LOOP L11 ON EACH WALL COMPONENT ( JC=1,NPAMU  WITH NPAMU =NCOMP-2 )
*----LOOP L12 J=1,IM ON THE MATERIALS OF THE WALL   IM=NMIC(JC) =1 RECOMENDED
*           INIT=1  TEMPERATURE=CONSTANT = TO
*           INIT=2  LINEAR TEMPERATURE FROM TI (INNER) TO TE (OUTER) IN EACH
*                   MATERIAL SLAB OF A WALL COMP.
*           INIT=3  TEMPERATURE VERSUS RADIUS. TC(I,JC),I=K1,K2
*  INIT
    1
*  TO
    400.0
*----END  L12
    1
    400.0
    1
    400.0
    2
*   TI      TE
    600.0    800.
*----END  L11
*
************* GAS MIXTURE DESCRIPTION *****
*
* NTG   : NBR OF POINTS IN THE GAS TEMPERATURE TABLE (TTG(I),TG(I))
  -3
*   IF NTG>0  THE FOLLOWING TABLE IS GIVEN
*--LOOP L13 I=1,NTG
```

```
*   TTG(I)   TG(I)  ;TIME(S)  ,GAS TEMPERATURE (K)
*--END  L13
*   IF NTG<0  THE TABLE IS NOT GIVEN AND THE GAS TEMP. IS CALCULATED
* NTP   : NBR OF POINTS IN THE GAS PRESSURE TABLE (TTP(J),PGAZ(J))
   3
*--LOOP L14 I=1,NTG
*TTP(J)    PGAZ(J)   ; TIME (S)   ,PRESSURE (PA)
  0.      300000.
  3000.   300000.
  10000.  300000.
*--END  L14
*============= MASS FRACTION OF H20 IN THE GAS MIXTURE
* NH20  : NBR OF POINTS IN THE H20 MASS FRACTION TABLE (TH20(J),YYH20(J))
  2
*--LOOP L15 I=1,NH20
*TH20(J)   YYH20(J)  ;TIME (S)   ,MASS FRACTION
  0.        0.50
  999000.   0.50
*--END  L15
*============= MASS FRACTION OF CO2 IN THE GAS MIXTURE
*/////// NOT TAKEN INTO ACCOUNT IN THE VERSION OF MAY 89
*/////// BUT THE FOLLOWING VALUES MUST BE GIVEN BY THE USER
* NCO2  : NBR OF POINTS IN THE CO2 MASS FRACTION TABLE (TCO2(J),YYCO2(J))
  2
*--LOOP L16 I=1,NCO2
*TCO2(J)    YYCO2(J)  ;TIME (S)   ,MASS FRACTION
  0.         0.15
  999000.    0.15
*--END  L16
*============= MASS FRACTION OF CO  IN THE GAS MIXTURE
*/////// NOT TAKEN INTO ACCOUNT IN THE VERSION OF MAY 89
*/////// BUT THE FOLLOWING VALUES MUST BE GIVEN BY THE USER
* NCO   : NBR OF POINTS IN THE CO  MASS FRACTION TABLE (TCO(J),YYCO(J))
  2
*--LOOP L17 I=1,NCO
*TCO(J)    YYCO(J)  ;TIME (S)   ,MASS FRACTION
  0.         0.15
  999000.    0.15
*--END  L17
*
*********CHARACTERISTICS OF THE CONCRETE OF THE CAVITY WALLS ****
* RHOB, RHOE,    CPB,     CPE ;
  2390.  950.  1.9928E6  2.1420E6
*TSAT,DTSAT,TFUS,    HB,  XSIO2, XCAO, XAL203
 420.  2.   1600.  0.27E6  .80  .0440  .0960
* CK1, CK2,   CK3
  3.2  2.4  -0.0012
*
****************** CONCRETE GAS RELEASE **************************
*--LOOP L18 L=1,3  ON THE THREE GAS RELEASES
*XW(L),     HV(L),   AK(L),  EK(L),  RK(L), TINF(L),TSUP(L)
 0.04000   2.26E6     0.      0.       0.      0.      0.
 0.01000   5.52E6   3.3E10  1.709E8   8314.   523.    973.
 0.01000   3.76E6   1.1E04  1.888E8   8314.   873.   1300.
*--END  L18
*
********** CHARACTERISTICS OF REACTOR VESSEL STAINLESS STEEL ******
*RHOC,    HBC,    TFUSC
 7800.   289000.   1800.
*************************** END OF CALTHER DATA
```

B.2 Print Output Example

```
*************************
*                       *
*  TIME =      2.01 SEC  *        NEXT TIME STEP= 0.11 SEC
*                       *
*************************


CAVITY DIMENSIONS, M :

       VERTICAL EROSION  :  -0.002
       MAXIMAL RADIUS    :   3.002
       ZERO LEVEL RADIUS :   2.720

TEMPERATURES, K :

       POOL -           METAL:   --     OXIDE    :  2658.4
       SURFACES -  MET./CONC.:   --     OX./CONC.:  2425.1
                   MET./OX.  :   --     OX./SURF.:  2654.8
       LIQUIDUS -  METAL     :   --     OXIDE    :  2663.9
       SOLIDUS  -  METAL     :   --     OXIDE    :  2411.9
       GAS LEAVING THE MELT  : 2420.5
       WATER GAS REACTION    : 1200.0

PROPERTIES:
                                      METAL             OXIDE
       DENSITY, KG/M3              :     --               8251.
       HEAT CONDUCTIVITY, W/(M.K):     --               2.997
       HEAT CAPACITY , J/(KG.K)  :     --                523.
       SURFACE TENSION, KG/S2    :     --               0.477
       VISCOSITY , KG/(S.M)      :     --            0.8660E-02

POOL-CONCRETE INTERFACE :
                              BOTTOM     METAL/WALL  OXIDE/WALL  OXIDE/SURFACE
       EROSION SPEED, CM/S :  0.9835E-01     --       0.9562E-01
       EROSION SPEED, CM/H :   354.06        --        344.23
       ENERGY FLUX,   W/M2 :  0.5138E+07     --       0.4996E+07  0.1377E+07
       ENERGY FLUX,  KW/M2 :    5138.        --         4996.       1377.

       HEAT TRANSFER FOR BOTTOM/CONCRETE MIXED MODE

INTEGRATED MASS BALANCE IN THE MELT, TONS :

       INITIAL MELT MASS:  100.000    ACTUAL MASS OF MELT  :  100.295
       ERODED (CONC.+FE):    0.315    MASS OF LEAVING GASES:    0.021

       SUM OF LEFT TERMS:  100.315    SUM OF RIGHT TERMS   :  100.315
       THE DIFFERENCE BETWEEN THE 2 SUMS IS -0.284E-13 TONS, I.E  -0.283E-13 %

MASSES ,VOLUMES AND HEIGHTS :
                                                  METAL       OXIDE
       MASS ,TONS                                :    0.000    100.295
       VOLUME, (INCLUDING VOID FRACTION), M3 :    0.00        81.07
       VOLUME, (WITHOUT VOID FRACTION), M3   :    0.00        12.16
       VOID FRACTION , IN PERCENT            :    0.00        85.00
       DEPTH, M                              :    0.00         2.90
       POOL HEIGHT FROM INITIAL BOTTOM, M    :         2.90
       VOLUME OF ERODED CONCRETE, M3         :         0.13
       MASS OF ERODED CONCRETE, TONS         :         0.315

WEIGHT FRACTION AND WEIGHT OF SPECIES IN EACH PHASE  :

    METAL: (SUM:       0.00) KG   %       OXIDE: (SUM:  100294.80) KG   %
          ZR :         0.00     0.000          UO2 :     80000.00    79.765
```

SI :	0.00	0.000	ZRO2 :	20000.00	19.941
CR :	0.00	0.000	FEO :	0.00	0.000
FE :	0.00	0.000	CAO :	6.19	0.006
NI :	0.00	0.000	SIO2 :	255.17	0.254
			AL2O3 :	33.43	0.033
			CR2O3 :	0.00	0.000

HEAT FLUX BALANCE IN THE MELT , WATT :

POWER DUE TO DECAY HEAT	:	0.1340E+08
POWER ENTERING DUE TO GAS AND OXIDES	:	0.2814E+09
POWER LEAVING DUE TO GAS AND OXIDES	:	-0.1544E+09
POWER DUE TO OXIDATION REACTIONS	:	0.0000E+00
POWER DUE TO CONCRETE DECOMPOSITION	:	-0.3491E+09
CONDUCTION BETWEEN PHASES	:	--
RADIATION OR EVAPORATED AT SURFACE	:	-0.3896E+08
SPLASHOUT	:	-0.6545E+07
SENSIBLE HEAT	:	-0.2542E+09

INTEGRATED ENERGY BALANCE IN THE MELT, JOULE :

INITIAL ENTHALPIE	0.1596E+12	INTEGRATED ENTHALPIE	0.1591E+12
DECAY HEAT	0.2694E+08	CONCRETE DECOMPOSITION	0.6895E+09
ENTERING(GAS,OX.)	0.5558E+09	LEAVING (GASES)	0.3047E+09
OXIDAT. REACTIONS	0.0000E+00	RADIATION OR TO WATER	0.8036E+08
		SPLASHOUT	0.1170E+08
SUM OF LEFT TERMS	0.1602E+12	SUM OF RIGHT TERMS	0.1602E+12

THE DIFFERENCE BETWEEN THE 2 SUMS IS 0.2339E+08 J., I.E 0.1460E-01 %

GASES GOING IN THE CONTAINMENT, AT THE TEMPERATURE T= 2421. K.
AFTER THAT THE WATER-GAS REACTION OCCURED AT THE SURFACE :

	CO2	CO	H2O	H2
HEAT FLUX, WATT	0.1493E+07	0.0000E+00	0.7529E+08	0.0000E+00
MASS FLUX, KG/S	0.5618E+00	0.0000E+00	0.9880E+01	0.0000E+00
MOL. FLUX, MOL/S	0.1277E+02	0.0000E+00	0.5486E+03	0.0000E+00
WEIGHT FRACTION	0.5380E-01	0.0000E+00	0.9462E+00	0.0000E+00
MOLAR FRACTION	0.2274E-01	0.0000E+00	0.9773E+00	0.0000E+00
TOTAL MASS, KG	0.1110E+01	0.0000E+00	0.1951E+02	0.0000E+00
TOT.MOLS, MOL	0.2521E+02	0.0000E+00	0.1083E+04	0.0000E+00

THE CAVITY SHAPE HAS BEEN CALCULATED USING 83 POINTS, COORDONATES IN CM :
R=RADIUS ; Z=DEPTHNESS ; Z-REFERENCE: INITIAL BOTTOM OF THE CAVITY

R	Z	R	Z	R	Z	R	Z
0.0	-0.2	7.0	-0.2	14.0	-0.2	21.0	-0.2
28.0	-0.2	35.0	-0.2	42.0	-0.2	49.0	-0.2
56.0	-0.2	63.0	-0.2	70.0	-0.2	77.0	-0.2
84.0	-0.2	91.0	-0.2	98.0	-0.2	105.0	-0.2
112.0	-0.2	119.0	-0.2	126.0	-0.2	133.0	-0.2
140.0	-0.2	147.0	-0.2	154.0	-0.2	161.0	-0.2
168.0	-0.2	175.0	-0.2	182.0	-0.2	189.0	-0.2
196.0	-0.2	203.0	-0.2	210.0	-0.2	217.0	-0.2
224.0	-0.2	231.0	-0.2	238.0	-0.2	245.0	-0.2
252.0	0.1	258.9	1.2	265.8	2.4	272.0	5.6
278.3	8.8	283.5	13.4	288.5	18.4	292.4	24.2
295.6	30.4	298.0	37.0	299.2	43.9	300.1	50.8
300.1	57.8	300.1	64.8	300.1	71.8	300.1	78.8
300.1	85.8	300.1	92.8	300.1	99.8	300.1	106.8
300.1	113.8	300.1	120.8	300.2	127.8	300.2	134.8
300.2	141.8	300.2	148.8	300.2	155.8	300.2	162.8
300.2	169.8	300.2	176.8	300.2	183.8	300.2	190.8
300.2	197.8	300.2	204.8	300.2	211.8	300.2	218.8
300.2	225.8	300.2	232.8	300.2	239.8	300.2	246.8
300.2	253.8	300.2	260.8	300.2	267.8	300.2	274.8
300.2	281.8	300.1	289.8	300.0	295.8		

TOO RAPID HEAT FRONT: EAULIB TEM 0.201E+01IS 3ISA 2IFLAG 1

***TIME = 2. JC 1 TPA = 428.6 T(2)= 428.6 T(N)= 400.0 PHIO=1645416.8 PPN= 0.00 ICLIM= 0 ; 0MOLTEN MESHES
TRELAX 1600.0QSUP 0.183E+07 QGAZ 0.375E-10SOMQ 0.186E-08 TGAZ 0.163E+04 TSUR 2654.8 TAMB 0.146E+04
SLAB 1 MATERIAL 1 RI= 2.600 RE= 4.400 IALF 1

J	R (M)	T(K)	FLUX(W)	FCP	FCF	SO(W/M3)	ROFREE	RO(BOUN)	RO(CO2)	RO(CONC.)	S1KG/M1/S	S2KG/M3/S	S3KG/M3/S	S4
1	0.000	428.6	0.165E+07	1.	1.	0.000E+00	0.000E+00	0.000E+00	0.000E+00	0.000E+00	0.000E+00	0.000E+00	0.000E+00	0.000E+00
2	2.600	428.6	0.270E+05******	1.	1.	0.000E+00	0.323E+02	0.239E+02	0.239E+02	0.225E+04	-0.551E+02	0.000E+00	0.000E+00	0.000E+00
3	2.610	400.6	0.618E+03	1.	1.	0.000E+00	0.956E+02	0.239E+02	0.239E+02	0.225E+04	0.000E+00	0.000E+00	0.000E+00	0.000E+00
4	2.620	400.0	0.799E+01	1.	1.	0.000E+00	0.956E+02	0.239E+02	0.239E+02	0.225E+04	0.000E+00	0.000E+00	0.000E+00	0.000E+00
5	2.630	400.0	0.767E-01	1.	1.	0.000E+00	0.956E+02	0.239E+02	0.239E+02	0.225E+04	0.000E+00	0.000E+00	0.000E+00	0.000E+00
6	2.640	400.0	0.611E-03	1.	1.	0.000E+00	0.956E+02	0.239E+02	0.239E+02	0.225E+04	0.000E+00	0.000E+00	0.000E+00	0.000E+00
7	2.650	400.0	0.428E-05	1.	1.	0.000E+00	0.956E+02	0.239E+02	0.239E+02	0.225E+04	0.000E+00	0.000E+00	0.000E+00	0.000E+00
8	2.660	400.0	0.274E-07	1.	1.	0.000E+00	0.956E+02	0.239E+02	0.239E+02	0.225E+04	0.000E+00	0.000E+00	0.000E+00	0.000E+00
9	2.670	400.0	0.620E-09	1.	1.	0.000E+00	0.956E+02	0.239E+02	0.239E+02	0.225E+04	0.000E+00	0.000E+00	0.000E+00	0.000E+00

	FREE	ISA	EVAP (KG/M2/S)	FRONT VEL (M/S)	X FRONT (M)	KG/M2 LOST BY MELTING	KG/M2 TOTAL LOST	
FREEH2O	1	2	0.276E+00	0.288E-02	0.331E-02	0.000E+00	0.316E+00	0.000E+00
BOUNDH2O	2	1	0.000E+00	0.000E+00	0.000E+00	0.000E+00	0.000E+00	0.000E+00
CO2	2	1	0.000E+00	0.000E+00	0.000E+00	0.000E+00	0.000E+00	0.000E+00
CONCRETE	2	2	0.000E+00	0.000E+00	0.000E+00	0.000E+00	0.000E+00	0.000E+00

***TIME = 2. JC 2 TPA = 418.5 T(2)= 418.5 T(N)= 400.0 PHIO=1063336.5 PPN= 0.00 ICLIM= 0 ; 0MOLTEN MESHES
TRELAX 1600.0QSUP 0.183E+07 QGAZ 0.375E-10SOMQ 0.186E-08 TGAZ 0.163E+04 TSUR 2654.8 TAMB 0.146E+04
SLAB 1 MATERIAL 1 RI= 2.600 RE= 4.400 IALF 1

J	R (M)	T(K)	FLUX(W)	FCP	FCF	SO(W/M3)	ROFREE	RO(BOUN)	RO(CO2)	RO(CONC.)	S1KG/M1/S	S2KG/M3/S	S3KG/M3/S	S4
1	0.000	418.5	0.106E+07	1.	1.	0.000E+00	0.000E+00	0.000E+00	0.000E+00	0.000E+00	0.000E+00	0.000E+00	0.000E+00	0.000E+00
2	2.600	418.5	0.175E+05******	1.	1.	0.000E+00	0.547E+02	0.239E+02	0.239E+02	0.225E+04	-0.356E+02	0.000E+00	0.000E+00	0.000E+00
3	2.610	400.4	0.400E+03	1.	1.	0.000E+00	0.956E+02	0.239E+02	0.239E+02	0.225E+04	0.000E+00	0.000E+00	0.000E+00	0.000E+00
4	2.620	400.0	0.517E+01	1.	1.	0.000E+00	0.956E+02	0.239E+02	0.239E+02	0.225E+04	0.000E+00	0.000E+00	0.000E+00	0.000E+00
5	2.630	400.0	0.496E-01	1.	1.	0.000E+00	0.956E+02	0.239E+02	0.239E+02	0.225E+04	0.000E+00	0.000E+00	0.000E+00	0.000E+00
6	2.640	400.0	0.395E-03	1.	1.	0.000E+00	0.956E+02	0.239E+02	0.239E+02	0.225E+04	0.000E+00	0.000E+00	0.000E+00	0.000E+00
7	2.650	400.0	0.276E-05	1.	1.	0.000E+00	0.956E+02	0.239E+02	0.239E+02	0.225E+04	0.000E+00	0.000E+00	0.000E+00	0.000E+00
8	2.660	400.0	0.176E-07	1.	1.	0.000E+00	0.956E+02	0.239E+02	0.239E+02	0.225E+04	0.000E+00	0.000E+00	0.000E+00	0.000E+00
9	2.670	400.0	0.620E-09	1.	1.	0.000E+00	0.956E+02	0.239E+02	0.239E+02	0.225E+04	0.000E+00	0.000E+00	0.000E+00	0.000E+00

	FREE	ISA	EVAP (KG/M2/S)	FRONT VEL (M/S)	X FRONT (M)	KG/M2 LOST BY MELTING	KG/M2 TOTAL LOST	
FREEH2O	1	2	0.178E+00	0.186E-02	0.214E-02	0.000E+00	0.204E+00	0.000E+00
BOUNDH2O	2	1	0.000E+00	0.000E+00	0.000E+00	0.000E+00	0.000E+00	0.000E+00
CO2	2	1	0.000E+00	0.000E+00	0.000E+00	0.000E+00	0.000E+00	0.000E+00
CONCRETE	2	2	0.000E+00	0.000E+00	0.000E+00	0.000E+00	0.000E+00	0.000E+00

TOO RAPID HEAT FRONT: EAULIB TEM 0.201E+01IS 3ISA 2IFLAG 1

***TIME = 2. JC 3 TPA = 420.1 T(2)= 420.1 T(N)= 400.0 PHIO= 708632.7 PPN= 0.00 ICLIM= 0 ; 0MOLTEN MESHES
TRELAX 1600.0QSUP 0.183E+07 QGAZ 0.375E-10SOMQ 0.186E-08 TGAZ 0.163E+04 TSUR 2654.8 TAMB 0.146E+04
SLAB 1 MATERIAL 1 RI= 2.600 RE= 4.400 IALF 1

J	R (M)	T(K)	FLUX(W)	FCP	FCF	SO(W/M3)	ROFREE	RO(BOUN)	RO(CO2)	RO(CONC.)	S1KG/M1/S	S2KG/M3/S	S3KG/M3/S	S4
1	0.000	420.1	0.709E+06	1.	1.	0.000E+00	0.000E+00	0.000E+00	0.000E+00	0.000E+00	0.000E+00	0.000E+00	0.000E+00	0.000E+00
2	2.600	420.1	0.190E+05******	1.	1.	0.000E+00	0.773E+02	0.239E+02	0.239E+02	0.225E+04	-0.235E+02	0.000E+00	0.000E+00	0.000E+00
3	2.610	400.4	0.380E+03	1.	1.	0.000E+00	0.956E+02	0.239E+02	0.239E+02	0.225E+04	0.000E+00	0.000E+00	0.000E+00	0.000E+00
4	2.620	400.0	0.443E+01	1.	1.	0.000E+00	0.956E+02	0.239E+02	0.239E+02	0.225E+04	0.000E+00	0.000E+00	0.000E+00	0.000E+00
5	2.630	400.0	0.395E-01	1.	1.	0.000E+00	0.956E+02	0.239E+02	0.239E+02	0.225E+04	0.000E+00	0.000E+00	0.000E+00	0.000E+00
6	2.640	400.0	0.298E-03	1.	1.	0.000E+00	0.956E+02	0.239E+02	0.239E+02	0.225E+04	0.000E+00	0.000E+00	0.000E+00	0.000E+00
7	2.650	400.0	0.201E-05	1.	1.	0.000E+00	0.956E+02	0.239E+02	0.239E+02	0.225E+04	0.000E+00	0.000E+00	0.000E+00	0.000E+00
8	2.660	400.0	0.122E-07	1.	1.	0.000E+00	0.956E+02	0.239E+02	0.239E+02	0.225E+04	0.000E+00	0.000E+00	0.000E+00	0.000E+00
9	2.670	400.0	0.563E-09	1.	1.	0.000E+00	0.956E+02	0.239E+02	0.239E+02	0.225E+04	0.000E+00	0.000E+00	0.000E+00	0.000E+00

	FREE	ISA	EVAP (KG/M2/S)	FRONT VEL (M/S)	X FRONT (M)	KG/M2 LOST BY MELTING	KG/M2 TOTAL LOST	
FREEH2O	1	2	0.117E+00	0.123E-02	0.955E-03	0.000E+00	0.913E-01	0.000E+00
BOUNDH2O	2	1	0.000E+00	0.000E+00	0.000E+00	0.000E+00	0.000E+00	0.000E+00
CO2	2	1	0.000E+00	0.000E+00	0.000E+00	0.000E+00	0.000E+00	0.000E+00
CONCRETE	2	2	0.000E+00	0.000E+00	0.000E+00	0.000E+00	0.000E+00	0.000E+00

TOTAL MASS ERODED KG H2OLB= 0.133E+02 H2OLE= 0.000E+00 CO2= 0.000E+00 MOLTEN CONC= 0.000E+00 TOTO= 0.133E+02 OCO2= 0.133E+02
EVTO= 0.124E+02EVTC= 0.000E+00EVTB= 0.000E+00EVMTO= 0.000E+00EVMTC= 0.000E+00EVTMB= 0.000E+00

```
***TIME  =      2.  JC 4 TPA =   609.8  T(2)=  610.4  T(N)=  800.0  PHIO= 486316.2     PPN= 0.00  ICLIM= 0 ;  0MOLTEN MESHES
                    TRELAX 1800.0QSUP 0.183E+07 QGAZ 0.375E-10SOMQ 0.186E-08 TGAZ 0.163E+04 TSUR 2654.8 TAMB 0.146E+04
     SLAB    1  MATERIAL 4  RI= 2.600  RE= 3.000  IALF 0

 J    R (M)  T(K)   FLUX(W)   FCF   SO(W/M3)    RO(STEAL   S1KG/M1/S
 1    0.000  609.8 0.486E+06    1.  0.000E+00 0.000E+00 0.000E+00
 2    2.600  610.4-0.924E+04    1.  0.000E+00 0.780E+04 0.000E+00
 3    2.640  620.1-0.194E+05    1.  0.000E+00 0.780E+04 0.000E+00
 4    2.680  640.0-0.199E+05    1.  0.000E+00 0.780E+04 0.000E+00
 5    2.720  660.0-0.202E+05    1.  0.000E+00 0.780E+04 0.000E+00
 6    2.760  680.0-0.206E+05    1.  0.000E+00 0.780E+04 0.000E+00
 7    2.800  700.0-0.210E+05    1.  0.000E+00 0.780E+04 0.000E+00
 8    2.840  720.0-0.214E+05    1.  0.000E+00 0.780E+04 0.000E+00
 9    2.880  740.0-0.218E+05    1.  0.000E+00 0.780E+04 0.000E+00
           FREE  ISA      EVAP    FRONT VEL    X FRONT  KG/M2 LOST    KG/M2 TOTAL
                        (KG/M2/S)     (M/S)        (M)     BY  MELTING   LOST
             2    2   0.000E+00   0.000E+00   0.000E+00   0.000E+00   0.000E+00   0.000E+00


TOTAL MASS ERODED  KG      AMTCV= 0.000E+00 EVTCV= 0.000E+00EVMTCV= 0.000E+00
 TOO RAPID HEAT FRONT: EAULIB TEM 0.212E+01IS 3ISA 2IFLAG 1
 TOO RAPID HEAT FRONT: EAULIB TEM 0.212E+01IS 3ISA 2IFLAG 1
 TOO RAPID HEAT FRONT: EAULIB TEM 0.223E+01IS 3ISA 2IFLAG 1
 TOO RAPID HEAT FRONT: EAULIB TEM 0.223E+01IS 3ISA 2IFLAG 1
 TOO RAPID HEAT FRONT: EAULIB TEM 0.234E+01IS 3ISA 2IFLAG 1
 TOO RAPID HEAT FRONT: EAULIB TEM 0.234E+01IS 3ISA 2IFLAG 1
 TOO RAPID HEAT FRONT: EAULIB TEM 0.246E+01IS 3ISA 2IFLAG 1
 TOO RAPID HEAT FRONT: EAULIB TEM 0.246E+01IS 3ISA 2IFLAG 1
 TOO RAPID HEAT FRONT: EAULIB TEM 0.257E+01IS 3ISA 2IFLAG 1
 TOO RAPID HEAT FRONT: EAULIB TEM 0.257E+01IS 3ISA 2IFLAG 1
 TOO RAPID HEAT FRONT: EAULIB TEM 0.269E+01IS 3ISA 2IFLAG 1
 TOO RAPID HEAT FRONT: EAULIB TEM 0.269E+01IS 3ISA 2IFLAG 1
 TOO RAPID HEAT FRONT: EAULIB TEM 0.281E+01IS 3ISA 2IFLAG 1
 TOO RAPID HEAT FRONT: EAULIB TEM 0.292E+01IS 3ISA 2IFLAG 1
 TOO RAPID HEAT FRONT: EAULIB TEM 0.304E+01IS 3ISA 2IFLAG 1
 TOO RAPID HEAT FRONT: EAULIB TEM 0.316E+01IS 3ISA 2IFLAG 1
 TOO RAPID HEAT FRONT: EAULIB TEM 0.329E+01IS 3ISA 2IFLAG 1
 TOO RAPID HEAT FRONT: EAULIB TEM 0.341E+01IS 3ISA 2IFLAG 1
 TOO RAPID HEAT FRONT: EAULIB TEM 0.353E+01IS 3ISA 2IFLAG 1
 TOO RAPID HEAT FRONT: EAULIB TEM 0.363E+01IS 3ISA 2IFLAG 1
 TOO RAPID HEAT FRONT: EAULIB TEM 0.373E+01IS 3ISA 2IFLAG 1
```